A model of the effect of moisture on the pyrolysis of wood

Moerman, E.

Award date:
1997

A model of the effect of moisture on the pyrolysis of wood

E. Moerman

R-1444-A

Begeleider: K. Krishna Prasad
Afstudeerdocent: G.J.F. van Heijst

Abstract

Cooking in developing countries is mostly done on open wood fires. Problems like the scarcity of fuel wood and a negative impact of wood smoke on the users health lead to a wide interest in wood fired cookstoves. However most work limited itself to developing stoves using a 'trial and error' method. One of the few institutes that studied theory behind woodstoves was the Woodburning Stoves Group. Results are described by Bussmann (1988). An important limitation of that work is that the power output of the stove cannot be predicted. Changes in stove geometry, fuel composition, charge size or charge period require a new experimental determination of what Bussmann calls the fire penetration rate. The study in this report tries to reduce this limitation of Bussmann's model and predict the power output after at most a handful of experiments for each serious change in stove geometry. In order to do that the pyrolysis and moisture evaporation of a thermally irradiated piece of wood is studied. Pyrolysis studies have been done before, however never with moist wood.

To see if results are useful only a simple one-dimensional model for a single piece of wood is used and it does not incorporate combustion of the charred part of the wood. The model consists of rate equations that use Arrhenius type reaction rates for the primary pyrolysis reactions WOOD->CHAR+TAR+GAS and the secondary reaction TAR->GAS. The continuity equations for all gas components (N_2, O_2, water vapour, TAR and GAS) are used, where all gas components are assumed to be ideal gases. The moisture evaporation is governed by the combined Clausius-Clapeyron-Kelvin equation. Since wood is a porous medium the Darcy equation is used as momentum equation. Finally the energy equation includes a source term, due to evaporation and pyrolysis, and energy convection by the gases. The inclusions of the moisture requires the use of a generalized Newton-Raphson method for the solution of the continuity equations. For a large permeability (about 10^{-12} m^2) even the Newton-Raphson method does not result in super-linear convergence, however convergence is obtained.

The simulation results can be described by a pyrolysis front and an evaporation front. At such a front unreacted wood or the moisture is zero on the hot side of the front and equal to the initial value on the other side of the front. The position of these fronts can mostly be described by an equation of the from $x = a_0 + a_1\sqrt{t} + a_2 t$ (x = position of front, a_i is i-th coefficient and t = time). The coefficients in this equation depend on thermal radiation and the wood bulk density according to simple equations. Bad fits only occur for thermal radiation smaller than 2 kW m^{-2}, because the temperature obtained for thermal radiation smaller than 2 kW m^{-2} is insufficient for pyrolysis. The effect of moisture on the coefficients is not easy to determine. A few exponential functions result and they often lead to a poor match between a simulation and simple equations for the fronts. For the evaporation front the match is usually not too bad, but no acceptable fits could be found that describe the position of the pyrolysis front as a function of moisture content and time. The simple equations for the position of the pyrolysis and evaporation fronts provide a simple and fast way for calculating the power output provided by the volatile gases and the energy used for the evaporation of the moisture. This easy description is ideal for stove development work in the field since a quick determination of volatile power output and energy loss due to moisture evaporation is possible without the use of complicated mathematical models.

Contents

1 Introduction

Wood fires have been used for thousands of years for heating, lighting and food preparation. In spite of the long use of wood fires the understanding of small open wood fires remains insufficient. Hardly any research has ever been done on the subject, this while billions of people are still cooking on these small open wood fires. The Woodburning Stove Group has been one of the very few institutes trying to describe the processes occurring in a wood fired cook stove. At the Woodburning Stove Group a model was developed to describe the heat and mass transfer in a cook stove, see Bussmann and Krishna Prasad (1986) and Bussmann (1988). The efficiency it predicts is in most cases not sufficiently correct. Probably this is due to the model used for power output as provided by the pyrolysis of the wood. Every newly added batch of wood is assumed to start pyrolysing at once. This is obviously incorrect as can be seen when observing an actual wood fire. Actually predicting the pyrolysis rate of the wood was still impossible. Trying to describe this requires knowledge of the pyrolysis process in a single piece of wood. Studies and experiments regarding the pyrolysis of wood have been done in the past, but the results are not very consistent. Used parameters like activation energies and frequency factors can differ by several magnitudes among different studies. The reason for this is the large number of reactions and components (thousands of reactions and hundreds of components, see Emmons and Atreya (1983)) occurring during the pyrolysis and combustion of wood. Usually models limit themselves to only a few global reactions and components. The global reactions are apparently very sensitive to the actual situation of the problem (temperature, airflows, etc.) while different values for volatile properties, activation energy and frequency factor can produce about the same porosity profiles. Obviously it is not possible with the present technology to measure concentrations of hundreds of components, temperature and gas velocities on a microscopic scale. Therefore it is not very useful to use reaction parameters found in one study to describe a situation that is not exactly the same. As a result we will not study reaction parameters in this report as is done in some other pyrolysis studies. This study limits itself to the effects of initial wood density, thermal radiation and moisture content. The study leads to a model that can predict the power output of a piece of wood for given parameters like fuel type, fuel bed temperature and moisture content of the fuel. This power output can then be used to replace the power output Bussmann and Krishna Prasad (1986) and Bussmann (1988) used in their model. This would result in truly predictive possibilities of that model and probably a better prediction of the efficiency.

The effect of moisture content is extremely important for small scale wood fires, but as far as we know nobody ever included the moisture content in the pyrolysis model. It is not much of a surprise that modelling the effects of moisture was not done before since it complicates matters enormously and especially the stability of numerical methods is negatively affected. This report limits itself to the description of a single piece of wood. Apart from heat transfer, evaporation of the moisture and pyrolysis of the wood is included in the description. Other effects like char combustion and flaming combustion will be omitted here since they can only be studied together with processes in the fuel chamber, which depend critically on among others the geometry of the combustion chamber.

Even the description of just the processes occurring in a single piece of wood is a complicated task and requires quite a number of assumptions. The description of the evaporation of the moisture in the wood is obtained with the work of Whitaker (1977) as a starting point. Whitaker derived the equations describing the drying of porous solids like wood; however it is far too lengthy to repeat in detail in this report. His explanation of the fundamentals is very clear and a crude fundamental description will be repeated here to get a better idea of the principles at work. For the description of the pyrolysis process the work of Di Blasi (1993) is used. Although Moallemi *et al.* (1993) and Kailasanath and Zinn (1981) also described the pyrolysis of wood they only described the process as a one-step reaction. Di Blasi (1993) and some others too used a two-step reaction to describe the pyrolysis process. This two-step reaction scheme should solve the problem of the reaction energies for pyrolysis. The process of char combustion which follows on the pyrolysis is described in countless publications. A good review, although a bit old, was published by Laurendeau (1979) in which he discusses the reacting core model already described by Shen and Smith (1965) and Wen and Wei (1971). However the char combustion is not taken into account in this study.

To start with a description of the drying process in a porous medium is given in chapter 2. In this chapter the point equations governing the drying processes will be introduced. These point equations describe the problem in each point of space. The point equations require an exact description of the medium, which is usually impossible. Therefore chapter 3 introduces the concept of volume averaging and applies it to the previously derived point equations. This enables the derivation of a useful mathematical description for the drying problem. In chapter 4 the pyrolysis reactions will be introduced and the concepts from chapters 2 and 3 will be used to derive the equations describing a moist pyrolysing piece of wood. In chapter 5 this set of equations is converted to difference equations using the control volume method as described by for instance Patankar 1980. This description is used as the basis for the numerical simulations. In chapter 6 a number of simulation results are presented and discussed. The context in which this study is done is discussed in chapter 7. The narrow context of the improvement of an earlier model and the wider context of wood stove development for developing countries is discussed there. After this conclusions and recommendations will follow in chapter 8. Finally a reference list can be found in chapter 9.

2 Point equations for drying of a porous medium

To describe the situation at hand we turn to a description given by Whitaker (1977) who derives macroscopic equations from microscopic ones for drying of a porous medium. Although he only describes the drying process of a porous medium he introduces the concept forming the basis of the model presented here. In most other publications the governing equations are given without any derivation or explanation. Therefore it is not always clear how to interpret differences between governing equations. Following Whitaker the meaning of the equations used and possible differences between equations in different reports become clear. Whitaker considers a porous medium (in our case wood) with a fluid (water in this case) in the interior and the remainder filled with an inert gas and the vapour of the fluid. In Figure 1 a schematic sketch is given, it clearly shows the different phases; the solid (σ) phase, the liquid (β) phase and the gas (γ) phase. For each point in space the exact conservation equations can be written down as long as it is known to

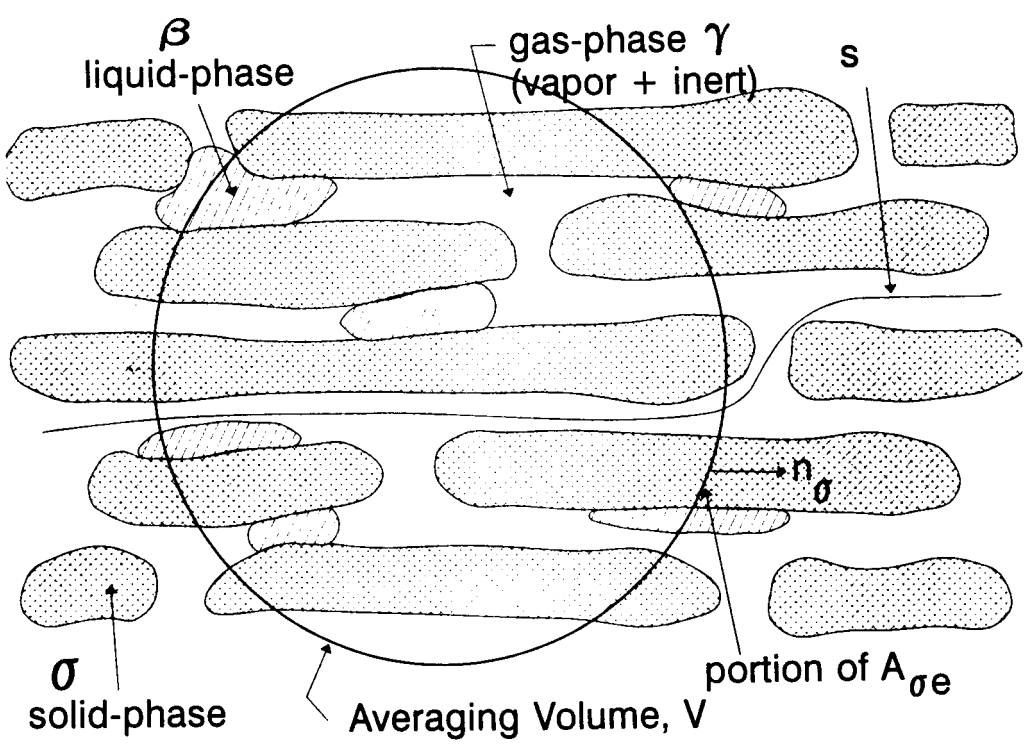

Figure 1 Sketch of a drying porous medium.

which phase the point belongs, Whitaker therefore uses the term point equations. Throughout the report the index β denote the liquid phase, γ the gas phase, σ the solid phase and n the n-th component of the gas phases. In this chapter the continuity equations for the different phases and gas components will be given first in section 2.1. In section 2.2 the energy equations for the

different phases are given, while a simplified momentum equation is derived for the gas phase in section 2.3. To complete the set of equations boundary conditions are presented in section 2.4.

2.1 Continuity equations

The solid phase is assumed to be a rigid, non-reacting matrix fixed in an inertial frame; the conservation of mass for the solid phase then reduces to $\rho_\sigma = 0$. For the liquid phase the usual continuity equation holds:

$$\frac{\partial \rho_\beta}{\partial t} + \nabla \cdot (\rho_\beta \boldsymbol{v}_\beta) = 0 \tag{1}$$

with ρ_β the liquid density and $\boldsymbol{v}_\beta$ the velocity of the liquid. A one-component liquid has been taken, therefore no additional continuity equations for the components are needed.

In the gas phase N components are considered and contrary to Whitaker first order reactions in the gas phase are taken into account. The continuity equation for the total gas-phase is the same as the resulting equation for the liquid phase:

$$\frac{\partial \rho_\gamma}{\partial t} + \nabla \cdot (\rho_\gamma \boldsymbol{v}_\gamma) = 0 \tag{2}$$

Since the vapour component does not take part in any chemical reaction neither as reactant nor as product the same equation as for the total gas phase can be written down for the vapour. In fact this equation also applies to all other components not involved in reactions. To obtain the continuity equation for any of these non-involved component just replace the index γ in equation (2) by the appropriate index for that component.

For the gas components that are involved in reactions the continuity equation is written as:

$$\frac{\partial \rho_n}{\partial t} + \nabla \cdot (\rho_n \boldsymbol{v}_n) = \dot{\rho}_n \tag{3}$$

where the index n denotes the n-th component of the gas phase. The term on the right hand side denotes the production term of component n due to chemical reactions. In line with Di Blasi (1993) only first order reactions with Arrhenius type reaction rates are considered. For a reacting component n:

$$\dot{\rho}_n = -\sum_j K_j \rho_n = -\sum_j A_j \rho_n \exp(-E_{a,j}/RT_\gamma) \tag{4}$$

with K_j the reaction rate for reaction j, A_j the frequency factor for the reaction j of component n, $E_{a,j}$ the activation energy for the reaction j of component n, R the universal gas constant and T_γ the temperature of the gas phase. From the conservation of mass it follows immediately that:

$$\dot{\rho}_k = -\dot{\rho}_n = \sum_j K_j \rho_n \tag{5}$$

for a component k which is a product of a first order reaction j of component n. The situation that we will try to describe is more complicated than this, but the principle is the same. A more detailed discussion will be given in chapter 4.

Since diffusive processes in the interior of fuel particles in a burning stove are expected to be negligible, diffusion effects will not be considered in this report and $\boldsymbol{v}_n$ in (3) can be replaced by $\boldsymbol{v}_\gamma$. Also the effect of electromagnetic radiation on the interior of the piece of wood is neglected since these effects are only assumed to occur at the surface of the slab of wood. This simplifies the original derivation given by Whitaker (1977) considerably.

2.2 Energy equation

The energy equation for the solid phase can be written as:

$$\frac{\partial}{\partial t}(\rho_\sigma h_\sigma) = -\nabla \cdot \boldsymbol{q}_\sigma \tag{6}$$

Here h_σ denotes the enthalpy of the σ phase and $\boldsymbol{q}_\sigma$ is the heat flux in the σ phase due to heat conduction. The solid phase velocity $\boldsymbol{v}_\sigma$ is zero, since the solid matrix is assumed to be fixed and rigid. This appears to be a reasonable assumption, although shrinking of the solid phase does occur. The enthalpy is commonly expressed as:

$$h_\sigma = c_{p,\sigma}(T_\sigma - T_\sigma^0) + h_\sigma^0 \tag{7}$$

where T_σ^0 is a reference temperature of the solid phase and h_σ^0 the enthalpy of the solid phase at this reference temperature. With the specific heat for constant pressure of the solid phase $c_{p,\sigma}$ being constant and using Fourier's law the following familiar expression for heat conduction in a solid is obtained:

$$\rho_\sigma c_{p,\sigma} \frac{\partial T_\sigma}{\partial t} = k_\sigma \nabla^2 T_\sigma \tag{8}$$

k_σ the thermal conductivity for the σ-phase is assumed to be constant. However for convenience this temperature equation is not considered, but an enthalpy equation like equation (6) will be used instead.

The energy equation for the liquid (β) phase is different from the energy equation for the σ phase since the convection term has to be included. The compressional work and the viscous dissipation are assumed to be negligible, resulting in:

$$\frac{\partial(\rho_\beta h_\beta)}{\partial t} + \nabla \cdot (\rho_\beta h_\beta \boldsymbol{v}_\beta) = -\nabla \cdot \boldsymbol{q}_\beta \tag{9}$$

The energy equation for the gas phase differs from this one since the gas density is not constant and there is more than one gas component. Again compressional work and viscous dissipation are neglected, so the resulting energy equation for the gas phase is:

$$\frac{\partial}{\partial t}\left(\sum_{n=1}^{n=N} \rho_n h_n\right) + \nabla \cdot \left(\sum_{n=1}^{n=N} \rho_n \boldsymbol{v}_n h_n\right) = -\nabla \cdot \boldsymbol{q}_\gamma \tag{10}$$

With N number of components present in the gas and h_n defined in such a way that the total enthalpy of the gas can be expressed in terms of the enthalpy of its components as:

$$\rho_\gamma h_\gamma = \sum_{n=1}^{n=N} \rho_n h_n \tag{11}$$

In this equation the total density of the gas phase and the densities of the gas components are used. Conservation of mass in the gas phase within a fixed unit volume leads to the relation:

$$\rho_\gamma = \sum_{n=1}^{n=N} \rho_n \tag{12}$$

This equation leads to the well-known concept of partial pressures.

2.3 Momentum equation

Since the inertial frame is chosen in such a way that the solid matrix is fixed in that frame the momentum of the solid phase is zero. So only the momentum equations for the liquid and gas phase have to be considered. The momentum equation for the gas phase is the familiar relation:

$$\rho_\gamma \frac{D}{Dt} \boldsymbol{v}_\gamma = -\nabla p_\gamma + \rho_\gamma \boldsymbol{g} + \mu_\gamma \nabla^2 \boldsymbol{v}_\gamma \tag{13}$$

with $\boldsymbol{g}$ the gravity vector. It is assumed that the viscosity μ_γ is constant. The gravity term on the right-hand side of (13) will be neglected. This is allowed since the magnitude of the pressure difference is expected to be 1000 Pa over a typical length of 0.01 m, thus making the pressure gradient term of the order 10^5 kg m^{-2} s^{-2}. On the other hand the magnitude of the gas density is 1 kg m^{-3} and the gravity vector is almost 10 m s^{-2} along the z-axis, so the gravity term is of magnitude 10 kg m^{-2} s^{-2}. Since this is much smaller than the pressure gradient the gravity can be neglected. The term on the left-hand side represents the total derivative and it can also be neglected since the magnitude here is much smaller than the pressure gradient. With a velocity that is of magnitude 0.1 m s^{-1} and a typical time step of 0.1 s the term of the partial time derivative is of the order 1 kg m^{-2} s^{-2}. The convective term of the total derivative has a magnitude 1 kg m^{-2} s^{-2}. Clearly both these terms are negligible when compared to the pressure gradient. Wood consists of gas (water) filled channels with a diameter of the magnitude 10^{-4} m, therefore the viscosity term cannot be neglected. What remains are the pressure gradient and the viscous term. Obviously these terms are now equal in size and determined by equation (13):

$$\nabla p_\gamma = \mu_\gamma \nabla^2 \boldsymbol{v}_\gamma \tag{14}$$

Again this will be converted to a more useful form in the next chapter.

2.4 Boundary conditions

The differential equations derived so far require appropriate boundary conditions in order to describe the problem completely. The boundary conditions are to be described for the interfaces

between different phases. The interface between the liquid and vapour phase is a moving surface due to the liquid evaporation process. The evaporation process at the $A_{\beta\gamma}$ surface requires energy causing a jump condition for the thermal energy equation. $A_{\beta\gamma}$ means the interface between the liquid (β) phase and the gas (γ) phase and equivalent for other combinations of the indices. The interface between the liquid (β) and the gas (γ) phase has a surface area denoted by $A_{\beta\gamma}$ and there is a unit vector $n_{\beta\gamma}$ associated with this surface. This vector is perpendicular to the surface $A_{\beta\gamma}$ and points from the surface into gas phase γ (from β into γ). Obviously $A_{\beta\gamma}=A_{\gamma\beta}$ and $n_{\beta\gamma}=-n_{\gamma\beta}$. To determine the jump condition a material volume $V_m(t)$ containing both the β and γ phase as shown in figure 2 is considered. The volume of the β phase contained in the total volume V_m is called $V_\beta(t)$ and that of the γ phase $V_\gamma(t)$. Since the material volume is chosen in such a way that it contains no other phases it is obvious that $V_m(t)=V_\beta(t)+V_\gamma(t)$. The notation V(t) shows that the volumes can change in time. The surface A_β is the surface of the volume $V_\beta(t)$ that is in contact with the β

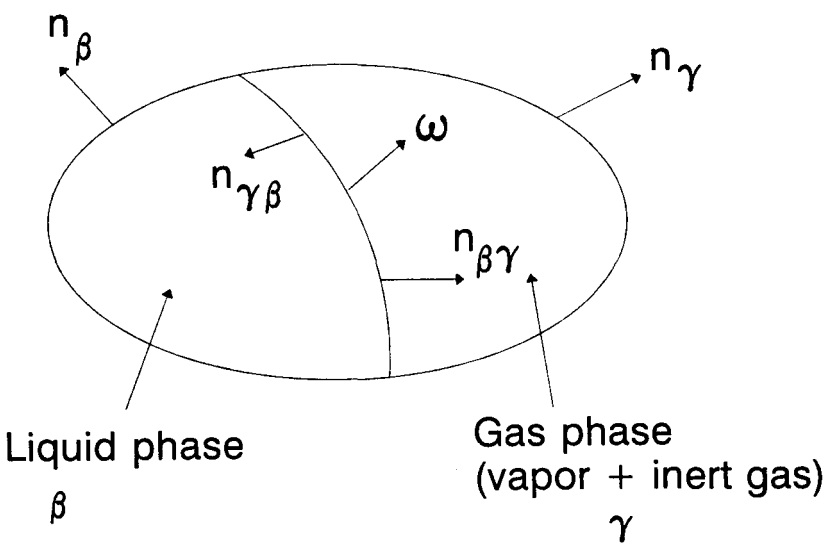

Figure 2 Sketch of the boundaries between different phases in a volume $V_m(t)$.

phase outside $V_m(t)$, while $A_{\beta\gamma}$ is the surface of the volume $V_\beta(t)$ that is in contact with the γ phase inside $V_m(t)$. These two surfaces together form the total surface of the volume $V_\beta(t)$. In the following it is assumed that the surface tension is negligible for all surfaces, so the surfaces have negligible energy. For highly porous media like wood this assumption might not be valid for the β-γ interface and the boundary conditions described by for instance Slattery (1967) should be applied. Since we are only exploring the possibilities of the inclusion of moisture evaporation in the pyrolysis of wood we will not consider surface tensions of the liquid. The velocity of the interface $A_{\beta\gamma}$ with unit vector $\boldsymbol{n}_{\beta\gamma}$ is denoted by $\boldsymbol{w}$. Since diffusion processes are neglected $\boldsymbol{v}_n=\boldsymbol{v}_\gamma$ in equation (10) and using equation (11) leads to:

$$\frac{\partial}{\partial t}(\rho_\gamma h_\gamma) + \nabla\cdot(\rho_\gamma h_\gamma \boldsymbol{v}_\gamma) = -\nabla\cdot\boldsymbol{q}_\gamma \qquad (15)$$

The energy equation for the volume $V_m(t)$ can be written as:

$$\frac{d}{dt}\int_{V_m(t)}(\rho h)\,dV = -\int_{A_m(t)}\boldsymbol{q}\cdot\boldsymbol{n}\,dA \qquad (16)$$

The left hand side represents the rate at which the energy of the volume $V_m(t)$ changes, while the right hand side represents the energy flux through the surface of $V_m(t)$ due to heat conduction. This equation applies to any volume $V_m(t)$ even when it contains surfaces where (ρh) and $\boldsymbol{q}$ are discontinuous. Obviously in the β phase we get:

$$\rho h = \rho_\beta h_\beta \qquad \text{and} \qquad \boldsymbol{q} = \boldsymbol{q}_\beta \tag{17}$$

while substituting β by γ gives the expressions for the γ phase. Integrating equation (9) over V_β results in:

$$\int_{V_\beta(t)} \frac{\partial}{\partial t}(\rho_\beta h_\beta)\,dV + \int_{V_\beta(t)} \nabla\cdot(\rho_\beta h_\beta \boldsymbol{v}_\beta)\,dV = -\int_{V_\beta(t)} \nabla\cdot\boldsymbol{q}_\beta\,dV = -\int_{A_\beta} \boldsymbol{q}_\beta\cdot\boldsymbol{n}_\beta\,dA - \int_{A_{\beta\gamma}} \boldsymbol{q}_\beta\cdot\boldsymbol{n}_{\beta\gamma}\,dA \tag{18}$$

where Gauss's theorem was used to equate the volume integral of the heat flux gradient to the surface integrals of the heat flux on the right hand side. Taking an infinitesimal small element fixed in space as a basis for the derivation of a partial differential equation for a fluid property and applying Gauss's theorem leads to what Whitaker calls the general transport theorem. Applied to the energy of the volume it becomes:

$$\frac{d}{dt}\int_{V_\beta(t)} (\rho_\beta h_\beta)\,dV = \int_{V_\beta(t)} \frac{\partial}{\partial t}(\rho_\beta h_\beta)\,dV + \int_{A_\beta} \rho_\beta h_\beta \boldsymbol{v}_\beta\cdot\boldsymbol{n}_\beta\,dA + \int_{A_{\beta\gamma}} \rho_\beta h_\beta \boldsymbol{w}\cdot\boldsymbol{n}_{\beta\gamma}\,dA \tag{19}$$

Like equation (16) the left hand side denotes the rate at which the total energy of the volume $V_\beta(t)$ changes. The first term on the right hand side represents the rate of change in energy content of the material contained by the volume $V_\beta(t)$. The second term on the right-hand side is due to the convection of enthalpy from V_β to the liquid phase bordering on V_β, see figure 2. The third term is the change in energy content due to the movement of the interface $A_{\beta\gamma}$; due to shrinking or extending of the volume V_β there is either less or more material contained by the volume. The theorem of Gauss is used again, but this time to express the volume integral of the convective term (second term on the left hand side of equation (18)) into surface integrals of the convection term. Also using equation (19) to eliminate the first term on the left hand side of equation (18) and rearranging all surface integrals leads to:

$$\frac{d}{dt}\int_{V_\beta(t)} (\rho_\beta h_\beta)\,dV + \int_{A_{\beta\gamma}} \rho_\beta h_\beta(\boldsymbol{v}_\beta - \boldsymbol{w})\cdot\boldsymbol{n}_{\beta\gamma}\,dA = -\int_{A_\beta} \boldsymbol{q}_\beta\cdot\boldsymbol{n}_\beta\,dA - \int_{A_{\beta\gamma}} \boldsymbol{q}_\beta\cdot\boldsymbol{n}_{\beta\gamma}\,dA \tag{20}$$

The velocity at which the interface between the β and the γ phase moves is denoted by $\boldsymbol{w}$. The above derivation can be repeated for the gas phase; interchanging the β and γ indices in equation (20) gives the result for the gas phase:

$$\frac{d}{dt}\int_{V_\gamma(t)} (\rho_\gamma h_\gamma)\,dV + \int_{A_{\gamma\beta}} \rho_\gamma h_\gamma(\boldsymbol{v}_\gamma - \boldsymbol{w})\cdot\boldsymbol{n}_{\gamma\beta}\,dA = -\int_{A_\gamma} \boldsymbol{q}_\gamma\cdot\boldsymbol{n}_\gamma\,dA - \int_{A_{\gamma\beta}} \boldsymbol{q}_\gamma\cdot\boldsymbol{n}_{\gamma\beta}\,dA \tag{21}$$

Adding equations (20) and (21) and using $A_{\beta\gamma} = A_{\gamma\beta}$ and $\boldsymbol{n}_{\beta\gamma} = -\boldsymbol{n}_{\gamma\beta}$ leads to:

$$\frac{d}{dt}\int_{V_m(t)}(\rho h)\,dV + \int_{A_{\beta\gamma}}[\rho_\beta h_\beta(\boldsymbol{v}_\beta-\boldsymbol{w})\cdot\boldsymbol{n}_{\beta\gamma} + \rho_\gamma h_\gamma(\boldsymbol{v}_\gamma-\boldsymbol{w})\cdot\boldsymbol{n}_{\gamma\beta}]\,dA = -\int_{A_m(t)}\boldsymbol{q}\cdot\boldsymbol{n}\,dA - \int_{A_{\beta\gamma}}(\boldsymbol{q}_\beta\cdot\boldsymbol{n}_{\beta\gamma} + \boldsymbol{q}_\gamma\cdot\boldsymbol{n}_{\gamma\beta})\,dA \tag{22}$$

where the definition:

$$\frac{d}{dt}\int_{V_m(t)}(\rho h)\,dV = \frac{d}{dt}\int_{V_\beta(t)}(\rho_\beta h_\beta)\,dV + \frac{d}{dt}\int_{V_\gamma(t)}(\rho_\gamma h_\gamma)\,dV \tag{23}$$

was used together with the definition:

$$\int_{A_m(t)}\boldsymbol{q}\cdot\boldsymbol{n}\,dA = \int_{A_\beta(t)}\boldsymbol{q}_\beta\cdot\boldsymbol{n}_\beta\,dA + \int_{A_\gamma(t)}\boldsymbol{q}_\gamma\cdot\boldsymbol{n}_\gamma\,dA \tag{24}$$

which hold because $A_m(t) = A_\beta(t) + A_\gamma(t)$. Since equation (22) has to equal equation (16) for arbitrary interface $A_{\beta\gamma}$ it follows that:

$$\rho_\beta h_\beta(\boldsymbol{v}_\beta-\boldsymbol{w})\cdot\boldsymbol{n}_{\beta\gamma} + \rho_\gamma h_\gamma(\boldsymbol{v}_\gamma-\boldsymbol{w})\cdot\boldsymbol{n}_{\gamma\beta} = -\boldsymbol{q}_\beta\cdot\boldsymbol{n}_{\beta\gamma} - \boldsymbol{q}_\gamma\cdot\boldsymbol{n}_{\gamma\beta} \tag{25}$$

This is the required jump condition for the interface between the liquid and the gas (vapour) phase. The boundary conditions for the interfaces $A_{\sigma\beta}$ and $A_{\sigma\gamma}$ follow easily using the same methods as just described. In fact those cases are simpler since $\boldsymbol{v}_\sigma = 0$ and the interfaces are fixed. For the $A_{\sigma\beta}$ interface the result is:

$$\boldsymbol{q}_\sigma\cdot\boldsymbol{n}_{\sigma\beta} + \boldsymbol{q}_\beta\cdot\boldsymbol{n}_{\beta\sigma} = 0 \tag{26}$$

and replacing the indices β with γ gives the boundary condition for the $A_{\sigma\gamma}$ interface.

A similar derivation can be made for the continuity equation. The continuity equation for the volume $V_m(t)$ can be represented as:

$$\frac{d}{dt}\int_{V_m(t)}\rho\,dV = 0 \tag{27}$$

since no source term is present. It is also possible to integrate the liquid continuity equation (1) over the volume $V_\beta(t)$ resulting in:

$$\int_{V_\beta(t)}\frac{\partial\rho_\beta}{\partial t}dV + \int_{V_\beta(t)}\nabla\cdot(\rho_\beta\boldsymbol{v}_\beta)\,dV = 0 \tag{28}$$

Rewriting the second term into a surface integral and using the general transport theorem:

$$\frac{d}{dt}\int_{V_\beta(t)}\rho_\beta\,dV = \int_{V_\beta(t)}\frac{\partial\rho_\beta}{\partial t}dV + \int_{A_\beta}\rho_\beta\boldsymbol{v}_\beta\cdot\boldsymbol{n}_\beta\,dA + \int_{A_{\beta\gamma}}\rho_\beta\boldsymbol{w}\cdot\boldsymbol{n}_{\beta\gamma}\,dA \tag{29}$$

results in:

$$\frac{d}{dt}\int_{V_\beta(t)}\rho_\beta\,dV + \int_{A_{\beta\gamma}}\rho_\beta(\boldsymbol{v}_\beta-\boldsymbol{w})\cdot\boldsymbol{n}_{\beta\gamma}\,dA = 0 \tag{30}$$

Exchanging β and γ in equation (30) gives the result for the gas phase γ:

$$\frac{d}{dt}\int_{V_\gamma(t)} \rho_\gamma dV + \int_{A_{\gamma\beta}} \rho_\gamma (\boldsymbol{v}_\gamma - \boldsymbol{w}) \cdot \boldsymbol{n}_{\gamma\beta} dA = 0 \tag{31}$$

Adding equation (30) and (31) results in:

$$\frac{d}{dt}\int_{V_m(t)} \rho dV + \int_{A_{\beta\gamma}} [\rho_\beta (\boldsymbol{v}_\beta - \boldsymbol{w}) \cdot \boldsymbol{n}_{\beta\gamma} + \rho_\gamma (\boldsymbol{v}_\gamma - \boldsymbol{w}) \cdot \boldsymbol{n}_{\gamma\beta}] dA = 0 \tag{32}$$

Since the first term is according to equation (27) zero and the equation should hold for arbitrary $A_{\beta\gamma}$ this yields:

$$\rho_\beta (\boldsymbol{v}_\beta - \boldsymbol{w}) \cdot \boldsymbol{n}_{\beta\gamma} + \rho_\gamma (\boldsymbol{v}_\gamma - \boldsymbol{w}) \cdot \boldsymbol{n}_{\gamma\beta} = 0 \tag{33}$$

The same can be repeated for the vapour component (n = 1) of the gas the result of which can be obtained from (33) by replacing the index γ in ρ_γ and $\boldsymbol{v}_\gamma$ by 1 or V both denoting the vapour component. For the other gas components the situation is different since those components only occur in the gas phase. Consequently the density ρ_n is zero in the liquid phase and it is possible to write for $n \neq 1$:

$$\frac{d}{dt}\int_{V_\gamma(t)} \rho_n dV = 0 \tag{34}$$

Using this in equation (31) with the index γ in ρ_γ and $\mathbf{v}_\gamma$ changed into n with $n \neq 1$ immediately yields:

$$\rho_n (\boldsymbol{v}_n - \boldsymbol{w}) \cdot \boldsymbol{n}_{\gamma\beta} = 0 \tag{35}$$

Since the solid matrix is fixed and the density of the solid phase is constant, the boundary condition for the other boundaries reduce to the very simple form $\boldsymbol{v}_\sigma = 0$, $\boldsymbol{v}_\beta = 0$ on $A_{\sigma\beta}$ and $\boldsymbol{v}_\gamma = 0$ on $A_{\sigma\gamma}$.

3 Volume averaged equations for drying of a porous medium

The quantities occurring in the point equations of the previous chapter are difficult to determine, for instance the place of the interfaces and the velocity at which the interfaces are moving are usually not known. To solve this problem volume averaged equations will be introduced. These equations should for a small control volume around every point in space tell us what on the average the behaviour of the relevant quantities are. The derivation given by Whitaker (1977) will be followed, but with the simpler equations obtained in chapter 2 and with reacting gas components. First the different averages are explained in section 3.1. Then averaging is applied to the continuity equations from chapter 2 in section 3.2, to the energy equations in section 3.3, the momentum equations in section 3.4 and finally in section 3.5 to the thermodynamic equations.

3.1 Basics of averaging

The averaging volume is denoted by V, see figure 1. Although the volume in this figure is spherical any shape of the volume will do since the shape of the volume doesn't enter the equations. Regarding the averaging procedure for multi-phase problems there are three possible ways to calculate a volume average:

1. the spatial average of some function f defined everywhere in the averaging volume V:

$$<f> \doteq \frac{1}{V}\int_V f\,dV \tag{36}$$

where $<f>$ denotes the space average of f;

2. the phase average of a quantity defined in some phase. For example with f_β a quantity solely defined in the phase β, with $<f_\beta>$ denoting the phase average of f_β this results in:

$$<f_\beta> \doteq \frac{1}{V}\int_V f_\beta\,dV = \frac{1}{V}\int_{V_\beta} f_\beta\,dV \tag{37}$$

3. the intrinsic phase average. With f_β again defined solely in the β phase the intrinsic phase average is defined as:

$$<f_\beta>^\beta \doteq \frac{1}{V_\beta}\int_V f_\beta\,dV = \frac{1}{V_\beta}\int_{V_\beta} f_\beta\,dV \tag{38}$$

The difference between phase average and intrinsic phase average can be shown by considering the density of the β phase. Denoting it as ρ_β and assuming it to be constant throughout the β phase and zero in the other phases the phase average density for the β phase is $(V_\beta/V)\rho_\beta$ while the intrinsic phase average density is $(V_\beta/V_\beta)\rho_\beta=\rho_\beta$. It is immediately clear that the intrinsic phase averaged density is a good measure for the actual density. However in a number of cases the phase average and the space average are equal and a macroscopic measurement of the relevant quantity actually determines its space average eg. temperature. Space averaged solid and liquid densities

are easily obtained by weighing the wet and the dry medium. Of course with the reasonable assumption that the gas density can be neglected compared to solid and liquid phase densities.

The volume fraction occupied by the β phase denoted as ϵ_β is defined by:

$$\epsilon_\beta \doteq \frac{V_\beta}{V} \tag{39}$$

The volume fractions for the other phases are defined in the same way. Since the sum of the volumes occupied by all the different phases equals the total volume V it follows that the sum of all the volume fractions is one, so

$$\epsilon_\beta + \epsilon_\gamma + \epsilon_\sigma = 1 \tag{40}$$

Furthermore the relation between the phase average and the intrinsic phase average follows from equations (37), (38) and (39):

$$<f_\beta>^\beta = \frac{1}{V_\beta}\int_{V_\beta} f_\beta dV = \frac{1}{\epsilon_\beta V}\int_{V_\beta} f_\beta dV = \frac{1}{\epsilon_\beta}<f_\beta> \tag{41}$$

while equivalent expressions hold for the other phases. For later use the averaging theorem as given by Slattery (1972) is presented here:

$$<\nabla f_\beta> = \nabla <f_\beta> + \frac{1}{V}\int_{A_{\beta\sigma}} f_\beta \boldsymbol{n}_{\beta\sigma} dA + \frac{1}{V}\int_{A_{\beta\gamma}} f_\beta \boldsymbol{n}_{\beta\gamma} dA \tag{42}$$

while again equivalent expressions hold for the other phases. The tools needed for deriving the volume averaged equations are now ready to be used in the rest of the sections of this chapter.

3.2 Continuity equations

First the continuity equation for the liquid phase will be averaged. The phase average is obtained by integrating equation (1) over V_β and dividing it by V. This results in:

$$\frac{1}{V}\int_{V_\beta} \frac{\partial \rho_\beta}{\partial t} dV + \frac{1}{V}\int_{V_\beta} \nabla \cdot (\rho_\beta \boldsymbol{v}_\beta) dV = 0 \tag{43}$$

Applying the general transport theorem equation (19) to the first term of this equation enables us to rewrite this term as:

$$\frac{1}{V}\int_{V_\beta(t)} \left(\frac{\partial \rho_\beta}{\partial t}\right) dV = \frac{d}{dt}\left[\frac{1}{V}\int_{V_\beta(t)} \rho_\beta dV\right] - \frac{1}{V}\int_{A_{\beta\gamma}} \rho_\beta \boldsymbol{w} \cdot \boldsymbol{n}_{\beta\gamma} dA - \frac{1}{V}\int_{A_{\beta\sigma}} \rho_\beta \boldsymbol{w} \cdot \boldsymbol{n}_{\beta\sigma} dA \tag{44}$$

while the second term can be rewritten using the averaging theorem equation (42) resulting in:

$$<\nabla \cdot (\rho_\beta \boldsymbol{v}_\beta)> = \nabla \cdot <\rho_\beta \boldsymbol{v}_\beta> + \frac{1}{V}\int_{A_{\beta\gamma}} \rho_\beta \boldsymbol{v}_\beta \cdot \boldsymbol{n}_{\beta\gamma} dA + \frac{1}{V}\int_{A_{\beta\sigma}} \rho_\beta \boldsymbol{v}_\beta \cdot \boldsymbol{n}_{\beta\sigma} dA \qquad (45)$$

Since the boundary conditions $\boldsymbol{v}_\beta = \boldsymbol{w} = 0$ on $A_{\beta\sigma}$ inserting equations (44) and (45) in equation (43) results in:

$$\frac{\partial}{\partial t}<\rho_\beta> + \nabla \cdot <\rho_\beta \boldsymbol{v}_\beta> + \frac{1}{V}\int_{A_{\beta\gamma}} \rho_\beta (\boldsymbol{v}_\beta - \boldsymbol{w}) \cdot \boldsymbol{n}_{\beta\gamma} dA = 0 \qquad (46)$$

The partial time derivative in the first term occurs because the average is associated with a volume fixed in space and as a result the total time derivative that would result from (44) can be replaced with the partial time derivative. The last term in (46) represents the mass rate of vaporization per unit volume:

$$\frac{1}{V}\int_{A_{\beta\gamma}} \rho_\beta (\boldsymbol{v}_\beta - \boldsymbol{w}) \cdot \boldsymbol{n}_{\beta\gamma} dA \equiv <\dot{\rho}_v> \qquad (47)$$

Volume averaging for the continuity equation of the gas phase can be done in the same way and exchanging the indices β and γ in (46) gives the result:

$$\frac{\partial <\rho_\gamma>}{\partial t} + \nabla \cdot <\rho_\gamma \boldsymbol{v}_\gamma> = <\dot{\rho}_v> \qquad (48)$$

Where the boundary condition in equation (33) was used and (47) was used to write the non-zero surface integral as a production term component for the vapour $<\dot{\rho}_v>$. Note that the sign of the production term is different from that in the β phase. This is because a sink in the liquid phase is a source in the gas phase. For the vapour component this equation becomes:

$$\frac{\partial <\rho_1>}{\partial t} + \nabla \cdot <\rho_1 \boldsymbol{v}_1> = <\dot{\rho}_v> \qquad (49)$$

For the components involved in reactions a term $\dot{\rho}_n$ has to be considered.

$$\frac{\partial <\rho_n>}{\partial t} + \nabla \cdot <\rho_n \boldsymbol{v}_n> = <\dot{\rho}_n> \qquad (50)$$

For the components $n \neq 1$ the term $<\dot{\rho}_v>$ doesn't occur due to the boundary condition (35). For components not involved in reactions the term with $<\dot{\rho}_n>$ doesn't appear either. From now on the production term $<\dot{\rho}_n>$ will be used for all n. This means that $<\dot{\rho}_n> = 0$ if a gas component is not involved in reactions neither as reactant nor as product. Diffusion effects are not taken into account in this study, so $\boldsymbol{v}_n = \boldsymbol{v}_\gamma$ in these equations. Details of these derivations can be found in Whitaker (1977) who also includes diffusion in the description.

The resulting volume averaged continuity equations are given in their phase averaged form which as we remember is not for all quantities as easy to interpret as the intrinsic phase average form. Therefore the continuity equations obtained so far will be rewritten in an intrinsic phase average form except for any velocities occurring. Velocities are written in a phase averaged form since this tends to be the form of the velocity common in other pyrolysis studies. The first term is most conveniently rewritten using the relation given in (41) for the γ phase resulting in:

$$\frac{\partial}{\partial t}(\epsilon_\gamma <\rho_\gamma>^\gamma) + \nabla \cdot <\rho_\gamma \boldsymbol{v}_\gamma> = <\dot{\rho}_v> \tag{51}$$

Treating the second term in the same way is useless since ρ_γ and $\boldsymbol{v}_\gamma$ are needed separately for the numerical simulation. Therefore this term will be treated a little differently; the representation scheme proposed by Gray (1975) will be used. He suggested to represent quantities as a constant value equal to the average of the quantity over the averaging volume and a small deviation from that average for a point inside the averaging volume. So in a way similar to what is done for turbulent flows. In this case it would mean:

$$\rho_\gamma = <\rho_\gamma>^\gamma + \tilde{\rho}_\gamma \quad \text{and} \quad \boldsymbol{v}_\gamma = <\boldsymbol{v}_\gamma> + \tilde{\boldsymbol{v}}_\gamma \quad \text{for the } \gamma \text{ phase} \tag{52}$$

where the tilde ($\sim$) denotes a small deviation from the average value. Of course the value, the average and the small deviation are all zero in a phase in which they are not defined. The argument of the second term of equation (51) is then easily rewritten as:

$$\begin{aligned} <\rho_\gamma \boldsymbol{v}_\gamma> &= \frac{1}{V}\int_{V_\gamma} \rho_\gamma \boldsymbol{v}_\gamma dV = \frac{1}{V}\int_{V_\gamma} (<\rho_\gamma>^\gamma + \tilde{\rho}_\gamma)\boldsymbol{v}_\gamma dV = <\rho_\gamma>^\gamma \frac{1}{V}\int_{V_\gamma} \boldsymbol{v}_\gamma dV + \\ \frac{1}{V}\int_{V_\gamma} \rho_\gamma (<\boldsymbol{v}_\gamma> + \tilde{\boldsymbol{v}}_\gamma) dV &= <\rho_\gamma>^\gamma <\boldsymbol{v}_\gamma> + <\boldsymbol{v}_\gamma> \frac{1}{V}\int_{V_\gamma} \tilde{\rho}_\gamma dV + <\tilde{\rho}_\gamma \tilde{\boldsymbol{v}}_\gamma> = \\ & <\rho_\gamma>^\gamma <\boldsymbol{v}_\gamma> + <\tilde{\rho}_\gamma \tilde{\boldsymbol{v}}_\gamma> \end{aligned} \tag{53}$$

where $<\rho_\gamma>^\gamma$ and $<\boldsymbol{v}_\gamma>$ can be carried through the integral sign because they are constant in the averaging volume V. Furthermore the average of a deviation is zero by definition in Gray's representation. Since the deviation of a quantity is assumed to be much smaller than its intrinsic phase average (e.g. $\rho_\gamma \ll <\rho_\gamma>^\gamma$) it follows that the last term on the right-most side of the equation is negligible. Therefore equation (51) can be written as:

$$\frac{\partial}{\partial t}(\epsilon_\gamma <\rho_\gamma>^\gamma) + \nabla \cdot (<\rho_\gamma>^\gamma <\boldsymbol{v}_\gamma>) = <\dot{\rho}_v> \tag{54}$$

The other continuity equations can be handled in a similar way which leads to:

$$\frac{\partial}{\partial t}(\epsilon_\beta <\rho_\beta>^\beta) + \nabla \cdot (<\rho_\beta>^\beta <\boldsymbol{v}_\beta>) = - <\dot{\rho}_v> \tag{55}$$

for the liquid phase. Remembering the convention for the notation of production terms it is possible to write:

$$\frac{\partial}{\partial t}(\epsilon_\gamma <\rho_n>^\gamma) + \nabla \cdot (<\rho_n>^\gamma <\boldsymbol{v}_n>) = <\dot{\rho}_n> \tag{56}$$

for the n-th component. Writing out the right-hand side for reactants using (4) gives:

$$<\dot{\rho}_n> = -A_j <\rho_n \exp(-E_{a,j}/RT_\gamma)> = -A_j <\rho_n \exp[-\alpha/(1+x)]> \tag{57}$$

where A_j is the frequency factor and $E_{a,j}$ the activation energy for reaction j which uses reactant n. Also the universal gas constant R is introduced here. All this is just using the Arrhenius expression for the reaction rate for reaction j using reactant n. In the previous equation the following expressions were used for brevity:

$$\alpha = \frac{E_{a,j}}{R<T_\gamma>^\gamma} \qquad \wedge \qquad x = \frac{\tilde{T}_\gamma}{<T_\gamma>^\gamma} \tag{58}$$

Also Gray's representation scheme was used to represent the temperature as:

$$T_\gamma = <T_\gamma>^\gamma + \tilde{T}_\gamma \qquad \text{and} \qquad \rho_n = <\rho_n>^\gamma + \tilde{\rho}_n \tag{59}$$

where ρ_n is given in the representation scheme for later use. The term between the averaging signs on the right hand side of equation (57) is written as a Taylor series in x to first order:

$$<\rho_n \exp[-\frac{\alpha}{(1+x)}]> = <\rho_n(1+\alpha x)\exp[-\alpha]> = \{<\rho_n> + \frac{\alpha}{<T_\gamma>^\gamma}<\rho_n \tilde{T}_n>\}\exp[-\alpha] \tag{60}$$

Again using Gray's representation scheme for ρ_n in the second term on the right hand side and using the relation between the phase average and the intrinsic phase average for the first term results in:

$$<\rho_n \exp[-\frac{\alpha}{(1+x)}]> = \{\epsilon_\gamma <\rho_n>^\gamma + \frac{\alpha}{<T_\gamma>^\gamma}(<\rho_n>^\gamma <\tilde{T}_\gamma> + <\tilde{\rho}_n \tilde{T}_n>\}\exp[-\alpha]$$
$$= \epsilon_\gamma <\rho_n>^\gamma \exp[-\alpha] \tag{61}$$

where the right-hand side results since the average of the temperature deviation in the second term in the middle is zero and the average of the two deviations, the third term in the middle, is negligible. Taking all these equations together results in:

$$<\dot{\rho}_n> = -A_n \epsilon_\gamma <\rho_n>^\gamma \exp[-\frac{E_{a,n}}{R<T_\gamma>^\gamma}] = -\epsilon_\gamma <\rho_n>^\gamma K_n \tag{62}$$

the quantities $<\boldsymbol{v}_\beta>$ and $<\boldsymbol{v}_\gamma>$ in the continuity equations are not given as intrinsic averages and will be discussed later in this chapter. The reaction rate K_n is introduced here to denote the Arrhenius reaction rate for reaction n, so $K_n = A_n \exp(-E_{a,n}/RT)$. Of course in this case the proper temperature expression would be $<T_\gamma>^\gamma$ instead of T.

3.3 Energy equation

The volume average of the energy equation for the gas phase will be determined next since this is the most general case. The volume averaged energy equations for the other phases follow easily from it. To obtain the volume averaged energy equation for the gas phase integrate (10) over V_γ and divide the result by the averaging volume V. This results in:

$$\frac{1}{V}\int_{V_\gamma} \sum_{n=1}^{n=N} \{\frac{\partial}{\partial t}(\rho_n h_n) + \nabla \cdot (\rho_n h_n \boldsymbol{v}_\gamma) + \nabla \cdot \boldsymbol{q}_\gamma\} dV =$$
$$\sum_{n=1}^{n=N} \{<\frac{\partial}{\partial t}\rho_n h_n> + <\nabla \cdot (\rho_n h_n \boldsymbol{v}_n)>\} + <\nabla \cdot \boldsymbol{q}_\gamma> = 0 \tag{63}$$

The first term between the equal signs can be rewritten using the general transport equation:

$$\frac{1}{V}\int_{V_\gamma}\frac{\partial}{\partial t}(\rho_n h_n)\,dV = \frac{d}{dt}\{\frac{1}{V}\int_{V_\gamma}\rho_n h_n\,dV\} - \frac{1}{V}\int_{A_{\gamma\sigma}}\rho_n h_n \boldsymbol{w}\cdot\boldsymbol{n}_{\gamma\sigma}\,dA - \frac{1}{V}\int_{A_{\gamma\beta}}\rho_n h_n \boldsymbol{w}\cdot\boldsymbol{n}_{\gamma\beta}\,dA =$$
$$\frac{\partial}{\partial t}<\rho_n h_n> - \frac{1}{V}\int_{A_{\gamma\beta}}\rho_n h_n \boldsymbol{w}\cdot\boldsymbol{n}_{\gamma\beta}\,dA \qquad (64)$$

The integral over $A_{\gamma\sigma}$ is zero because $\boldsymbol{v}_\gamma = \boldsymbol{w} = 0$ on $A_{\gamma\sigma}$, while:

$$\frac{1}{V}\frac{d}{dt}\int_{V_\gamma}\rho_n h_n\,dV = \frac{d}{dt}<\rho_n h_n> = \frac{\partial}{\partial t}<\rho_n h_n> \qquad (65)$$

since the average is determined at a fixed position and over a fixed volume V. The other terms can be rewritten using Slattery's averaging theorem equation (42) which gives for the convection term:

$$<\nabla\cdot(\rho_n h_n \boldsymbol{v}_n)> = \nabla\cdot<\rho_n h_n \boldsymbol{v}_n> + \frac{1}{V}\int_{A_{\gamma\sigma}}\rho_n h_n \boldsymbol{v}_n\cdot n_{\gamma\sigma}\,dA + \frac{1}{V}\int_{A_{\gamma\beta}}\rho_n h_n \boldsymbol{v}_n\cdot n_{\gamma\beta}\,dA =$$
$$\nabla\cdot<\rho_n h_n \boldsymbol{v}_n> + \frac{1}{V}\int_{A_{\gamma\beta}}\rho_n h_n \boldsymbol{v}_n\cdot n_{\gamma\beta}\,dA \qquad (66)$$

where the last equality holds since $\boldsymbol{v}_n = 0$ on $A_{\gamma\sigma}$. Treating the conduction term in the same way results in:

$$<\nabla\cdot\boldsymbol{q}_\gamma> = \nabla\cdot<\boldsymbol{q}_\gamma> + \frac{1}{V}\int_{A_{\gamma\sigma}}\boldsymbol{q}_\gamma\cdot n_{\gamma\sigma}\,dA + \frac{1}{V}\int_{A_{\gamma\beta}}\boldsymbol{q}_\gamma\cdot n_{\gamma\beta}\,dA \qquad (67)$$

Inserting equations 64 to 67 into equation (63) results in:

$$\sum_{n=1}^{n=N}\{\frac{\partial}{\partial t}<\rho_n h_n> + \nabla\cdot<\rho_n h_n \boldsymbol{v}_n> + \frac{1}{V}\int_{A_{\gamma\beta}}\rho_n h_n(\boldsymbol{v}_n-\boldsymbol{w})\cdot\boldsymbol{n}_{\gamma\beta}\,dA\} =$$
$$-\nabla\cdot<\boldsymbol{q}_\gamma> - \frac{1}{V}\int_{A_{\gamma\sigma}}\boldsymbol{q}_\gamma\cdot\boldsymbol{n}_{\gamma\sigma}\,dA - \frac{1}{V}\int_{A_{\gamma\beta}}\boldsymbol{q}_\gamma\cdot\boldsymbol{n}_{\gamma\beta}\,dA \qquad (68)$$

Taking the first two terms and expressing the enthalpy in temperature according to (7) yields:

$$\frac{\partial}{\partial t}<\rho_n h_n> + \nabla\cdot<\rho_n h_n \boldsymbol{v}_n> = (h_n^0 - c_{p,n}T_\gamma^0)(\frac{\partial}{\partial t}<\rho_n> + \nabla\cdot<\rho_n \boldsymbol{v}_n>) +$$
$$c_{p,n}(\frac{\partial}{\partial t}<\rho_n T_\gamma> + \nabla\cdot<\rho_n T_\gamma \boldsymbol{v}_n>) = (h_n^0 - c_{p,n}T_\gamma^0)<\dot{\rho}_n> + \qquad (69)$$
$$c_{p,n}(\frac{\partial}{\partial t}<\rho_n T_\gamma> + \nabla\cdot<\rho_n T_\gamma \boldsymbol{v}_n>)$$

Where the continuity equation (50) was used for the last equality. With Gray's representation scheme for the second term on the right-hand side:

$$<\rho_n T_\gamma> = <\rho_n><T_\gamma>^\gamma + <\tilde{\rho}_n\tilde{T}_\gamma> = <\rho_n><T_\gamma>^\gamma \qquad (70)$$

where the last equality results since the average of the product of two deviations is negligible. Gray's representation scheme for the third term on the right-hand side of (69) results in:

$$<f_n T_\gamma> = <f_n><T_\gamma>^\gamma = <\rho_n \boldsymbol{v}_n><T_\gamma>^\gamma = <\rho_n>^\gamma <\boldsymbol{v}_n><T_\gamma>^\gamma \tag{71}$$

where the function $f_n = \rho_n \boldsymbol{v}_n$ was used for typographic reasons. Using these last two expressions in (69) results in:

$$\frac{\partial}{\partial t}<\rho_n h_n> + \nabla \cdot <\rho_n h_n \boldsymbol{v}_n> = \frac{\partial}{\partial t}(c_{p,n}<\rho_n><T_\gamma>^\gamma) + \tag{72}$$
$$\nabla \cdot (c_{p,n}<\rho_n>^\gamma <T_\gamma>^\gamma <\boldsymbol{v}_n>) + (h_n^0 - c_{p,n}T_\gamma^0)<\dot{\rho}_n>$$

Inserting (72) into (68) and expressing the n-component density phase average in the intrinsic phase average results in:

$$\sum_{n=1}^{n=N}\{\frac{\partial}{\partial t}(c_{p,n}\epsilon_\gamma <\rho_n>^\gamma <T_\gamma>^\gamma) + \nabla \cdot (c_{p,n}<\rho_n>^\gamma <\boldsymbol{v}_n><T_\gamma>^\gamma) + (h_n^0 - c_{p,n}T_\gamma^0)<\dot{\rho}_n> + \tag{73}$$
$$\frac{1}{V}\int_{A_{n\beta}} \rho_n h_n (\boldsymbol{v}_n - \boldsymbol{w}) \cdot \boldsymbol{n}_{\gamma\beta} dA\} = -\nabla \cdot <\boldsymbol{q}_\gamma> - \frac{1}{V}\int_{A_{\gamma\sigma}} \boldsymbol{q}_\gamma \cdot \boldsymbol{n}_{\gamma\sigma} dA - \frac{1}{V}\int_{A_{n\beta}} q_\gamma \cdot \boldsymbol{n}_{\gamma\beta} dA$$

The energy equation for the liquid phase is easily written down by exchanging the indices γ and β and changing n into β in (73) while leaving out the sum since there is only one component in the β phase. The sign of the production term $<\dot{\rho}_1>$ has to be changed too, since a sink in the liquid phase is a source in the gas phase; it also follows from boundary condition (33) and the definition of the source term in equation (47). Therefore the energy equation for the liquid phase is:

$$\frac{\partial}{\partial t}(c_{p,\beta}\epsilon_\beta <\rho_\beta>^\beta <T_\beta>^\beta) + \nabla \cdot (c_{p,\beta}<\rho_\beta>^\beta <\boldsymbol{v}_\beta><T_\beta>^\beta) - (h_\beta^0 - c_{p,\beta}T_\beta^0)<\dot{\rho}_1> + \tag{74}$$
$$\frac{1}{V}\int_{A_{\beta\gamma}} \rho_\beta h_\beta (\boldsymbol{v}_\beta - \boldsymbol{w}) \cdot \boldsymbol{n}_{\beta\gamma} dA = -\nabla \cdot <\boldsymbol{q}_\beta> - \frac{1}{V}\int_{A_{\beta\sigma}} \boldsymbol{q}_\beta \cdot \boldsymbol{n}_{\beta\sigma} dA - \frac{1}{V}\int_{A_{\beta\gamma}} q_\beta \cdot \boldsymbol{n}_{\beta\gamma} dA$$

To obtain a volume averaged form for the solid phase energy equation the indices β and σ in (74) have to be exchanged. Furthermore $\boldsymbol{v}_\sigma = \boldsymbol{w} = 0$ and there is no source or sink for the solid phase. This results in:

$$\frac{\partial}{\partial t}(c_{p,\sigma}\epsilon_\sigma <\rho_\sigma>^\sigma <T_\sigma>^\sigma) = -\nabla \cdot <\boldsymbol{q}_\sigma> - \frac{1}{V}\int_{A_{\sigma\beta}} \boldsymbol{q}_\sigma \cdot \boldsymbol{n}_{\sigma\beta} dA - \frac{1}{V}\int_{A_{\sigma\gamma}} \boldsymbol{q}_\sigma \cdot \boldsymbol{n}_{\sigma\gamma} dA \tag{75}$$

The set of volume averaged energy equations is quite complicated and the intrinsic phase temperatures in the different phases cannot be determined without a lot more information obtained either from experiments or from a further theoretical discussion. Since there is no compelling reason to work with the separate intrinsic phase temperatures local thermal equilibrium will be assumed. This means that:

$$<T_\beta>^\beta = <T_\gamma>^\gamma = <T_\sigma>^\sigma \tag{76}$$

from this and the definitions at the start of this section it follows that for instance:

$$<T> = \frac{1}{V}\int_V T dV = \frac{1}{V}\{ \int_{V_\beta} T dV + \int_{V_\gamma} T dV + \int_{V_\sigma} T dV \} = <T_\beta> + <T_\gamma> + <T_\sigma>$$
$$= \epsilon_\beta <T_\beta>^\beta + \epsilon_\gamma <T_\gamma>^\gamma + \epsilon_\sigma <T_\sigma>^\sigma = (\epsilon_\beta + \epsilon_\gamma + \epsilon_\sigma) <T_\beta>^\beta = <T_\beta>^\beta \quad (77)$$

In order to simplify the energy equations for the different phases they will be added together. Adding equations (73), (74) and (75) and introducing the space averaged temperature leads to the following equation:

$$\frac{\partial}{\partial t}\{ [c_{p,\sigma}\epsilon_\sigma <\rho_\sigma>^\sigma + c_{p,\beta}\epsilon_\beta <\rho_\beta>^\beta + \epsilon_\gamma \sum_{n=1}^{n=N} c_{p,n} <\rho_n>^\gamma] <T> \} +$$
$$\nabla \cdot \{ \sum_{n=1}^{n=N} c_{p,n} <\rho_n>^\gamma <\boldsymbol{v}_n>] <T> \} - (h^0_\beta - c_{p,\beta} T^0) <\dot{\rho}_1> + \sum_{n=1}^{n=N} (h^0_n - c_{p,n} T^0) <\dot{\rho}_n> + \quad (78)$$
$$\frac{1}{V}\int_{A_{\beta\gamma}} \rho_\beta h_\beta (\boldsymbol{v}_\beta - \boldsymbol{w}) \cdot \boldsymbol{n}_{\beta\gamma} dA + \frac{1}{V}\int_{A_{\gamma\sigma}} \sum_{n=1}^{n=N} \rho_n h_n (\boldsymbol{v}_n - \boldsymbol{w}) \cdot \boldsymbol{n}_{\gamma\beta} dA = -\nabla \cdot (<\boldsymbol{q}_\sigma> + <\boldsymbol{q}_\beta> + <\boldsymbol{q}_\gamma>)$$
$$-\frac{1}{V}\int_{A_{\sigma\beta}} [\boldsymbol{q}_\sigma \cdot \boldsymbol{n}_{\sigma\beta} + \boldsymbol{q}_\beta \cdot \boldsymbol{n}_{\beta\sigma}] dA - \frac{1}{V}\int_{A_{\sigma\gamma}} [\boldsymbol{q}_\sigma \cdot \boldsymbol{n}_{\sigma\gamma} + \boldsymbol{q}_\gamma \cdot \boldsymbol{n}_{\gamma\sigma}] dA - \frac{1}{V}\int_{A_{\beta\gamma}} [\boldsymbol{q}_\beta \cdot \boldsymbol{n}_{\beta\gamma} + \boldsymbol{q}_\gamma \cdot \boldsymbol{n}_{\gamma\beta}] dA$$

where $A_{\sigma\gamma} = A_{\gamma\sigma}$ was used and similar identities for other index combinations. Also the second term on the left hand side of equation (74) was dropped since $\boldsymbol{v}_\beta = 0$. Other terms with $\boldsymbol{v}_\beta$ are not yet dropped because they occur in boundary conditions that will be used. Applying the boundary conditions for the interfaces between the σ and β phases (see equation (26)) and similar for the interface between the σ and γ phase allows us to drop the first and second integral on the right-hand side of equation (78). The last term on the left-hand side can be further rewritten since diffusion is neglected, so $\boldsymbol{v}_n = \boldsymbol{v}_\gamma$ resulting in:

$$\frac{1}{V}\int_{A_{\gamma\sigma}} \sum_{n=1}^{n=N} \rho_n h_n (\boldsymbol{v}_n - \boldsymbol{w}) \cdot \boldsymbol{n}_{\gamma\beta} dA = \frac{1}{V}\int_{A_{\gamma\sigma}} \sum_{n=1}^{n=N} \rho_n h_n (\boldsymbol{v}_\gamma - \boldsymbol{w}) \cdot \boldsymbol{n}_{\gamma\beta} dA = \frac{1}{V}\int_{A_{\gamma\sigma}} \rho_\gamma h_\gamma (\boldsymbol{v}_\gamma - \boldsymbol{w}) \cdot \boldsymbol{n}_{\gamma\beta} dA \quad (79)$$

where the equation (11) was used for the last equality. It is now possible to apply the boundary condition for the β-γ interface, equation (25), and get rid of the remaining surface integrals, resulting in:

$$\frac{\partial}{\partial t}(C_p <\rho> <T>) + \nabla \cdot (c_{p,\gamma} <\rho_\gamma>^\gamma <\boldsymbol{v}_\gamma> <T>) - (h^0_\beta - c_{p,\beta} T^0) <\dot{\rho}_1> +$$
$$\sum_{n=1}^{n=N} (h^0_n - c_{p,n} T^0) <\dot{\rho}_n> = -\nabla \cdot (<\boldsymbol{q}_\sigma> + <\boldsymbol{q}_\beta> + <\boldsymbol{q}_\gamma>) \quad (80)$$

where for convenience the total gas phase heat capacity $c_{p\gamma}$ was introduced:

$$c_{p,\gamma} <\rho_\gamma>^\gamma = \sum_{n=1}^{n=N} c_{p,n} <\rho_n>^\gamma \quad (81)$$

the total heat capacity for all phases C_p:

$$C_p <\rho> = c_{p,\sigma}\epsilon_\sigma <\rho_\sigma>^\sigma + c_{p,\beta}\epsilon_\beta <\rho_\beta>^\beta + c_{p,\gamma}\epsilon_\gamma <\rho_\gamma>^\gamma \quad (82)$$

and $<\rho>$ the space averaged density according to the definition in equation (36):

$$<\rho> = \epsilon_\sigma <\rho_\sigma>^\sigma + \epsilon_\beta <\rho_\beta>^\beta + \epsilon_\gamma <\rho_\gamma>^\gamma \tag{83}$$

Attention is now focused on the right-hand side of (80). To do this first consider the expression:

$$<\boldsymbol{q}_\sigma> = -k_\sigma <\nabla T_\sigma> = -k_\sigma \{ \nabla <T_\sigma> + \frac{1}{V}\int_{A_{\sigma\gamma}} T_\sigma \boldsymbol{n}_{\sigma\gamma} dA + \frac{1}{V}\int_{A_{\sigma\beta}} T_\sigma \boldsymbol{n}_{\sigma\beta} dA \} \tag{84}$$

which follows from the use of Slattery's averaging theorem. The phase average heat flow due to conduction for the other phases is obtained in the same way. Also introducing space averaged temperatures results for equation (80) in:

$$\begin{aligned} &\frac{\partial}{\partial t}(C_p <\rho><T>) + \nabla \cdot (c_{p,\gamma} <\rho_\gamma>^\gamma <\boldsymbol{v}_\gamma><T>) - (h^0_\beta - c_{p,\beta}T^0)<\dot{\rho}_1> \\ &+ \sum_{n=1}^{n=N} (h^0_n - c_{p,n}T^0)<\dot{\rho}_n> = \nabla \cdot \{ \nabla[(\epsilon_\sigma k_\sigma + \epsilon_\beta k_\beta + \epsilon_\gamma k_\beta)<T>] \\ &+ \frac{(k_\sigma - k_\gamma)}{V}\int_{A_{\sigma\gamma}} T_\sigma \boldsymbol{n}_{\sigma\gamma} dA + \frac{(k_\beta - k_\sigma)}{V}\int_{A_{\beta\sigma}} T_\beta \boldsymbol{n}_{\beta\sigma} dA + \frac{(k_\gamma - k_\beta)}{V}\int_{A_{\gamma\beta}} T_\gamma \boldsymbol{n}_{\gamma\beta} dA \} \end{aligned} \tag{85}$$

where $A_{\sigma\gamma} = A_{\gamma\sigma}$, $\boldsymbol{n}_{\sigma\gamma} = -\boldsymbol{n}_{\gamma\sigma}$ and similar relations for the other index combinations were used. At this point Whitaker (1977) suggests to incorporate the surface integrals on the right-hand side of equation (85) in an effective thermal conductivity tensor k_{eff}. He introduces this result after a lengthy derivation (however it is introduced here without delay). The final equation is:

$$\frac{\partial}{\partial t}(C_p <\rho><T>) + \nabla \cdot (c_{p,\gamma} <\rho_\gamma>^\gamma <\boldsymbol{v}_\gamma><T>) + S(T) = \nabla \cdot (k_{eff} \cdot \nabla <T>) \tag{86}$$

where the temperature dependent source term S(T) was used:

$$S(T) = -(h^0_\beta - c_{p,\beta}T^0)<\dot{\rho}_v> + \sum_{n=1}^{n=N} (h^0_n - c_{p,n}T^0)<\dot{\rho}_n> \tag{87}$$

Whitaker does present arguments to support the introduction of an effective conductivity tensor. However he is not able to give a useable form for the tensor. The problem is that it is apparently not possible to determine the tensor elements from a theoretical point of view while it is very difficult to determine the tensor experimentally, especially for the case of burning wood that is considered here. For a more detailed discussion see Whitaker (1977).

3.4 Momentum equation

It is assumed that the gas-phase is a connected region and that there exists an arbitrary curve entirely contained by the gas phase and which passes from one end to the other end of the piece of wood, see figure 1. A region is defined as connected if between any two points in the region a curve exists that connects these two points and which is contained entirely in that region. Note that connected regions of the gas-phase can be thought of that do not allow a curve through the gas-phase to pass from one end of the piece of wood to the other. So the second condition above is an entirely new condition. To summarise an arbitrary curve exists that can pass through

any point in the gas phase without ever passing an interface. The arc length along the arbitrary curve is denoted by s and the unit tangent vector by $\lambda(s)$. Then the scalar product of $\lambda(s)$ with the simplified momentum equation (14) results in:

$$\mu_\gamma \lambda \cdot (\nabla^2 \boldsymbol{v}_\gamma) = \lambda \cdot \nabla p_\gamma = \frac{dp_\gamma}{ds} \tag{88}$$

Whitaker (1969) gives in one of his publications arguments for the possibility of the following map:

$$\boldsymbol{v}_\gamma = M_\gamma \cdot \langle \boldsymbol{v}_\gamma \rangle \tag{89}$$

with M_γ a matrix that maps $\langle \boldsymbol{v}_\gamma \rangle$ linearly into $\boldsymbol{v}_\gamma$ under the assumption that spatial variations in M_γ are much larger than spatial variations in $\langle \boldsymbol{v}_\gamma \rangle$. Using this in (88) leads to:

$$\frac{dp_\gamma}{ds} = \mu_\gamma \lambda \cdot (\nabla^2 M_\gamma) \cdot \langle \boldsymbol{v}_\gamma \rangle \tag{90}$$

Integrating this along the curve from reference point $s=0$ to an arbitrary point $s(\boldsymbol{r})$ leads to:

$$p_\gamma(\boldsymbol{r}) = p_\gamma(0) + \mu_\gamma \{ \int_{\eta=0}^{\eta=s(r)} \lambda \cdot (\nabla^2 M_\gamma) d\eta \} \cdot \langle \boldsymbol{v}_\gamma \rangle = p_\gamma(0) - \mu_\gamma \boldsymbol{m}_\gamma \cdot \langle \boldsymbol{v}_\gamma \rangle \tag{91}$$

where the assumption was used that spatial variations in $\langle \boldsymbol{v}_\gamma \rangle$ are negligible compared to those in $\nabla^2 M_\gamma$ and $\boldsymbol{m}_\gamma$ was introduced for the integral. Taking the gradient of this equation results in:

$$\nabla \langle p_\gamma(r) - p_\gamma(0) \rangle = \frac{1}{V} \int_{A_{\gamma\sigma}} (p_\gamma - p_\gamma(0)) \boldsymbol{n}_\gamma dA = -\mu_\gamma \{ \frac{1}{V} \int_{A_{\gamma\sigma}} \boldsymbol{n}_\gamma \boldsymbol{m}_\gamma dA \} \cdot \langle \boldsymbol{v}_\gamma \rangle = -\mu_\gamma K_\gamma^{-1} \cdot \langle \boldsymbol{v}_\gamma \rangle \tag{92}$$

where equation (91) was used to obtain the second equality. To obtain the third equality it was again assumed that μ_γ and $\langle \boldsymbol{v}_\gamma \rangle$ are constant. For convenience the matrix K_γ^{-1} was introduced and it is assumed to have an inverse K_γ, therefore equation (92) can be written as[1]:

$$\langle \boldsymbol{v}_\gamma \rangle = -\frac{1}{\mu_\gamma} K_\gamma \cdot \nabla (\epsilon_\gamma \langle p_\gamma - p_\gamma(0) \rangle^\gamma) \tag{93}$$

where the phase average of the pressure is written as an intrinsic phase average and with K_γ the gas phase permeability matrix. Equation (93) is also known as the Darcy equation. The matrix K_γ has to be determined experimentally.

Although Whitaker provides the momentum equation for the liquid phase, $\boldsymbol{v}_\beta = 0$ is assumed here. He introduces more unknown parameters and his result depends on the number of β-γ interfaces in an averaging volume too. For a large number of interfaces, a low moisture content, the phase averaged gas velocity $\langle \boldsymbol{v}_\gamma \rangle$ goes to zero. For a small number of interfaces, a high moisture content, the expression is much more complicated. The number of interfaces is important, because each interface has a surface tension thus messing up the expressions for gas pressure and energy. Observations show that for large pieces of wood, eg. logs on a wood fire, moisture

[1] Actually this equation is incorrect, since a constant pressure and a gradient in the gas phase volume fraction would lead to an flow of the fluid. In the correct equation the volume fraction comes before the gradient sign and the reference pressure can be dropped, since its gradient is zero.

migration occurs on a macroscopic scale. However it is assumed that $<v_\beta>$ is zero and that moisture migration is caused by evaporation and condensation.

3.5 Thermodynamic relations

The required thermodynamic equations were too obvious to be discussed in chapter 2. Instead they are presented in this section and averaging will be applied to them. An assumption that can be applied to the gas components is that they are ideal gases in which case they satisfy the ideal gas law:

$$p_n = \rho_n R_n T_\gamma \qquad \text{for } n=1,2,.. \tag{94}$$

in which p_n is the partial pressure for the n-th gas component, $R_n = R/M_n$ is the specific gas constant, R the universal gas constant and M_n the molar mass for gas component n. Integrating this equation over V_γ, dividing by V_γ and using Gray's representation scheme results in the volume averaged form of the ideal gas law:

$$\begin{aligned}\frac{1}{V_\gamma}\int_{V_\gamma} p_n dV = <p_n>^\gamma = \frac{1}{V_\gamma}\int_{V_\gamma} \rho_n R_n T_\gamma dV = <\rho_n>^\gamma R_n \frac{1}{V_\gamma}\int_{V_\gamma} T_\gamma dV + R_n \frac{1}{V_\gamma}\int_{V_\gamma} \tilde{\rho}_n T_\gamma dV = \\ <\rho_n>^\gamma R_n <T_\gamma>^\gamma + R_n <T_\gamma>^\gamma \frac{1}{V_\gamma}\int_{V_\gamma} \tilde{\rho}_n dV + R_n \frac{1}{V_\gamma}\int_{V_\gamma} \tilde{\rho}_n \tilde{T}_\gamma dV = <\rho_n>^\gamma R_n <T_\gamma>^\gamma\end{aligned} \tag{95}$$

There are rate equations that connect the continuity equations with the energy equation for all n except for the vapour component. Therefore an equation is required that connects the continuity equation for the vapour to the energy equation. The evaporation process depends on the partial pressure of the vapour component in the gas phase. The equation describing the evaporation for a flat liquid-gas interface is called the Clausius-Clapeyron equation. However in this case the evaporation occurs in a porous medium with very small pores and as a result there is a considerable curvature of the liquid-vapour interface. It is therefore better to combine the Clausius-Clapeyron equation and the Kelvin equation, see Whitaker (1977) and Defay *et al.* (1966):

$$p_1 = p_1^{\circ} \exp\left[-\left(\frac{2\sigma_{\beta\gamma}}{r\rho_\beta R_1 T} + \frac{\Delta h_{vap}}{R_1}\left(\frac{1}{T}-\frac{1}{T_0}\right)\right)\right] = p_1^{\circ} \exp\left[-\left(\frac{C_{evap}}{T} + \frac{L}{R_1}\left(\frac{1}{T}-\frac{1}{T_0}\right)\right)\right] \tag{96}$$

where the first term in the argument of the exponential is due to the Kelvin equation which takes into account the surface tension and the curvature of the interface, while the second term describes the evaporation for the flat interface. Furthermore in this equation p_1° is the vapour pressure at reference temperature T_0, $\sigma_{\beta\gamma}$ is the surface tension of the interface between the β and γ phases and r is a characteristic length that has to be determined experimentally as a function of ϵ_β. The first term of the argument was redefined as a single unknown parameter C_{evap} and of course the energy needed for the evaporation of the liquid is its latent heat ($\Delta h_{vap} = L$). The volume average of the last equation is obtained in the same way that led from equation (57) to equation (62) for $<\dot{\rho}_n>$. Applying this results in:

$$< p_1 >^{\nu} = p_1{}^{\circ} \exp\left[-\left(\frac{C_{vap}}{< T >} + \frac{L}{R_1}\left(\frac{1}{< T >} - \frac{1}{T_o} \right) \right) \right] \tag{97}$$

where the space averaged temperature $< T >$ was introduced.

4 Modelling the pyrolysis of a piece of wood

In the previous chapter drying of a porous medium was described in order to introduce the concepts that help us to understand the description of porous media. What will be described in this chapter is the process of the pyrolysis of wet wood. The processes occurring in a piece of wood when it is thrown in a fire are of interest. The piece of wood will be irradiated by the flames and if present by parts of the combustion chamber. This radiation heats the surface of the piece of wood and due to heat conduction the interior of the wood is heated. As a result a pressure gradient of the gas phase forms and it results in a flow of the gas phase. At the same time the evaporation of the liquid phase starts. When the temperature rises even more (typically over 500 K) the wood starts pyrolysing and forms combustible gases and char. When a sufficient part of the wood is pyrolysed the edges of the remaining char will start to burn. The volatile gases leave the piece of wood entering the fuel bed where an airflow provides the oxygen to burn the volatile gases in a diffusion flame. In section 4.1 the global reactions that are supposed to occur are presented. Next the appropriate rate and continuity equations are given in section 4.2, while in section 4.3 the momentum and energy equations are obtained. Finally the thermodynamic and constitutional equations are discussed.

4.1 Global reactions

To model the pyrolysis process correctly the pyrolysis reactions have to be considered. Usually the pyrolysis is described by a single primary reaction, see for instance Kailasanath and Zinn (1981) and Moallemi *et al.* (1993). There is some controversy on this point since some experiments show that pyrolysis is endothermic (at low temperatures) while other experiments show that the process is exothermic (at high temperatures). Therefore Di Blasi (1993) also considers secondary reactions, with the primary reactions endothermic and the secondary reactions exothermic. He assumes that due to primary reactions two gas components are formed. In this way it should be possible to obtain endothermic reactions for low temperatures and exothermic reactions for high temperatures. The following primary reactions are assumed to occur:

$$\begin{aligned} \text{WOOD} &\xrightarrow{K_1} \text{GAS} \\ \text{WOOD} &\xrightarrow{K_2} \text{TAR} \\ \text{WOOD} &\xrightarrow{K_3} \text{CHAR} \end{aligned} \tag{98}$$

with K_n the reaction rate for the n-th reaction given by the Arrhenius factor defined as $K_n = A_n \exp(-E_{a,n}/RT)$. The TAR is supposed to decompose further in lighter gases denoted by GAS as a result of secondary reactions:

$$\text{TAR} \xrightarrow{K_4} \text{GAS} \tag{99}$$

Of course in reality far more products are formed and react further. However that is far too complex to model and therefore this simplified set of reactions is assumed to occur.

According to Whitaker (1977) it is possible to use the drying process presented in the previous chapter to describe a two-component solid with one component sublimating. The liquid phase then has to be replaced by the sublimating solid component. In order to describe the pyrolysis process this way one could consider the wood to consist of char that remains after pyrolysis and the volatile gases formed from the wood by pyrolysis. However this would require the assumption of a fixed amount of CHAR forming regardless of the pyrolysis temperature. This is not at all in accordance with experiments, therefore the description of Di Blasi (1993) will be followed and it is assumed that the pyrolysis process results in two gas components; a heavy TAR component and a light GAS component. Basically the solid phase is represented in the same way as the gas phase. In this case as a phase with two components (WOOD and CHAR). The solid WOOD component is assumed to pyrolyse into a solid CHAR component and the gas phase components TAR and GAS.

4.2 Rate equations

If as suggested in the previous section the solid phase reactions are represented in the same way as the gas phase reactions already given in chapter 3 the rate equations for the different species can be written down in the same way as the production terms for the gas component in equation (62). It then follows from (98) that:

$$\langle \dot{\rho}_W \rangle = -\langle \rho_W (K_1 + K_2 + K_3) \rangle = -\langle \rho_W \rangle \langle K_1 + K_2 + K_3 \rangle^W = -\epsilon_W \rho_W (K_1 + K_2 + K_3) \tag{100}$$

where the index W denotes wood. From here on $\langle f \rangle$ and $\langle f_\beta \rangle^\beta$ are noted as f and f_β to simplify the equations. For the CHAR:

$$\langle \dot{\rho}_C \rangle = \epsilon_W \rho_W K_3 \tag{101}$$

with the index C denoting CHAR. The equation for the TAR becomes:

$$\langle \dot{\rho}_T \rangle = \epsilon_W \rho_W K_2 - \epsilon_\gamma \rho_T K_4 \tag{102}$$

with the index T for TAR, while for the GAS component the result is:

$$\langle \dot{\rho}_G \rangle = \epsilon_W \rho_W K_1 + \epsilon_\gamma \rho_T K_4 \tag{103}$$

with the index G denoting the GAS component of the gas phase.

In these equations a two component solid phase i.e. unreacted wood and char was assumed and the solid components were handled in the same way as the gas phase components. An important point can be made here if these equations are compared to the rate equations obtained by Di Blasi. There is a difference since he uses phase averages for solid components and intrinsic phase averages for the gas components. While he explicitly states this fact there are

publications that do not explicitly state which average is used, e.g. Kailasanath and Zinn (1981). Since a three phase problem is considered here volume fractions have to be used while other publications on pyrolysis consider two phase problems which enable them to use the porosity ϵ which is defined as the volume fraction of the gas phase. The volume fraction of the solid phase is in that case $(1-\epsilon)$ which is clearly not the case for a three phase problem. This accounts for example for the difference between the rate equations given in this report and those given by Di Blasi (1993) and Moallemi *et al.* (1993). Since a pyrolysing (disappearing) solid phase is considered here it is not possible to assume $\epsilon_\sigma = \epsilon_W + \epsilon_C$ is constant as is done by Whitaker (1977) at some places. However the change in ϵ_σ is very slow.

4.3 Continuity equations

In order to comply with the notation that is most common in the literature about pyrolysis of wood and to get a clearer view of the equations intrinsic phase averages are replaced with the symbol itself. Some space averages equal intrinsic phase averages, so they can be replaced by the symbol itself too, so $<T> = T$ and $<\rho_\beta>^\beta = \rho_\beta$. Phase averages will either be replaced by other expressions or will be left unchanged. With the help of equations (100) to (103) the volume averaged continuity equations can be written as:

$$\frac{\partial}{\partial t}(\epsilon_\gamma \rho_G) + \nabla \cdot (\rho_G < v_\gamma >) = \epsilon_W \rho_W K_1 + \epsilon_\gamma \rho_T K_4 \tag{104}$$

for the GAS component. Here diffusion is neglected and doing the same for the TAR component results in:

$$\frac{\partial}{\partial t}(\epsilon_\gamma \rho_T) + \nabla \cdot (\rho_T < v_\gamma >) = \epsilon_W \rho_W K_2 - \epsilon_\gamma \rho_T K_4 \tag{105}$$

Using the index V to denote the vapour component leads to:

$$\frac{\partial}{\partial t}(\epsilon_\gamma \rho_V) + \nabla \cdot (\rho_V < v_\gamma >) = <\dot{\rho}_v> \tag{106}$$

Further using the index N to denote the nitrogen component and recalling that this component is not involved in any reactions results in:

$$\frac{\partial}{\partial t}(\epsilon_\gamma \rho_N) + \nabla \cdot (\rho_N < v_\gamma >) = 0 \tag{107}$$

Replacing the index N by O gives the continuity equation for oxygen. The resulting equation for oxygen is only valid if oxygen is either not taking part in the reactions occurring or has been driven off by the time reactions occur. This last point seems a reasonable assumption since the moisture has to evaporate first, thus driving off the oxygen. So by the time that the temperature is high enough for reactions with oxygen to occur it has been driven off by the moisture evaporation. This is confirmed by simulations done during this study.

Since the velocity of the solid phase is assumed to be zero the continuity equations for the solid components become:

$$\rho_W \frac{\partial}{\partial t}\epsilon_W = -(K_1 + K_2 + K_3)\epsilon_W \rho_W \tag{108}$$

for the WOOD component and

$$\rho_C \frac{\partial}{\partial t}\epsilon_C = \epsilon_W \rho_W K_3 \tag{109}$$

for the CHAR component.

A piece of dry wood consists of pores (gas phase) in a solid phase. Pyrolysis of wood into char results in a growth of pore sizes and numbers. Most pyrolysis gases leave the wood. The total weight of the piece of wood decreases, due to a reduction in total solid phase matter and a decrease in solid matter volume (so an increase in pore volume). It is assumed that the density determined by the division of the total weight of the solid phase by the total volume of the solid phase is constant. This density is the intrinsic phase averaged density of the solid phase. For both solid components the intrinsic phase averaged density can be considered separately. They are denoted by ρ_W for WOOD and by ρ_C for CHAR. Since these intrinsic phase densities are assumed to be constant and equal it is convenient to use a single intrinsic phase density ρ_s for the total solid phase. This density was studied by Kollman and Côté (1968) and turned out to be virtually constant regardless of the type of wood.

The momentum equation for the liquid phase was discussed in the previous chapter and it was there decided that in this report the phase velocity of the liquid will be neglected. This results in the continuity equation:

$$\frac{\partial}{\partial t}(\epsilon_\beta \rho_\beta) = -<\dot{\rho}_v> \tag{110}$$

with the right hand side defined as in equation (47), but still undetermined. In all these equations the reaction rate K_n is assumed to be given by the Arrhenius factor which is defined as:

$$K_n = A_n \exp[-E_{a,n}/RT] \tag{111}$$

with A_n the frequency factor for the n-th reaction and $E_{a,n}$ the activation energy for the n-th reaction. This is in line with the volume average form for $<\dot{\rho}_n>$ defined in equation (62).

4.4 Momentum equation

Since the velocity of the solid phase is zero and it is assumed that the velocity of the liquid phase is zero too the momentum equations for these two phases reduce to:

$$<\boldsymbol{v}_\beta> = <\boldsymbol{v}_\sigma> = 0 \tag{112}$$

while the Darcy equation (93) results from the gas phase momentum equation:

$$<\boldsymbol{v}_\gamma> = -\frac{1}{\mu_\gamma} K_\gamma \cdot \nabla\,(\epsilon_\gamma (p_\gamma - p_0)) \tag{113}$$

with p_0 a reference pressure for which the ambient pressure is taken.

4.5 Energy equation

Since the situation that is considered here is slightly different from that in the previous chapter, the energy source term is redefined as:

$$S(T) = -(h^0_\beta - c_{p,\beta}T^0)<\dot{\rho}_V> + (h^0_W - c_{p,W}T^0)<\dot{\rho}_W> + (h^0_C - c_{p,C}T^0)<\dot{\rho}_C> + \sum_{n=1}^{n=N}(h^0_n - c_{p,n}T^0)<\dot{\rho}_n> = -L\rho_\beta\frac{\partial \epsilon_\beta}{\partial t} - \epsilon_W\rho_W[K_1\Delta H_{WG} + K_2\Delta H_{WT} + K_3\Delta H_{WC}] - \epsilon_\gamma\rho_T K_4\Delta H_{TG} \quad (114)$$

To obtain this equation the rate equations (100), (101), (102), (103) and (110) were used.

At the start a piece of wood contains atmospheric gases in its interior. When this piece of wood is heated the moisture in the wood starts boiling well before pyrolysis sets in. Large amounts of water vapour are produced and high pressure gradients occur. This results in gas flows in the interior, which in turn rapidly flushes out the atmospheric gases present at the start. When pyrolysis sets in the only gases left in the interior of the wood are water vapour and pyrolysis gases. Therefore atmospheric gases are flushed out of the interior well before any other gases occur with which they can react. As a result the heat source terms of the atmospheric gases do not have to be considered for S(T).

The last equality in equation (114) follows after rewriting and the use of the definitions:

$$L = h_v^0 - h_\beta^0 - T^0(c_{p,v} - c_{p,\beta}) \quad (115)$$

and

$$\Delta H_{ij} = h_i^0 - h_j^0 - T^0(c_{p,i} - c_{p,j}) \quad (116)$$

where L is the latent heat of water and ΔH_{ij} the reaction heat for the reaction from substance i to substance j. Using this definition for the source term leaves the energy expression as given in (86) unchanged.

4.6 Constitutional equations

The thermodynamic relations are given in (95) and are the usual equations for ideal gases, but with intrinsic phase averages for pressure and gas density. Apart from these and equation (12) which expresses the conservation of mass the following obvious equation also applies:

$$\epsilon_\beta + \epsilon_\gamma + \epsilon_W + \epsilon_C = 1 \quad (117)$$

From these equations it follows that $p_\gamma = \rho_\gamma R_s T$ with R_s the specific gas constant defined for this gas mixture as:

$$R_s = \sum_{n=1}^{n=N} R_n\frac{\rho_n}{\rho_\gamma} \quad (118)$$

The evaporation is governed by equation (97) and after the change in notation it can be written as:

$$p_1 = p_0 \exp\left\{-\left[\frac{C_{evap}}{T} + \frac{L}{R_v}\left(\frac{1}{T} - \frac{1}{T_0}\right)\right]\right\} \quad (119)$$

As before the parameter C_{evap} was used. This parameter differs for different types of wood and it can even differ for different pieces of wood due to different origins in the tree of the pieces. However it is expected to be virtually constant for pieces of wood within one batch.

In the equations so far the effective thermal conductivity matrix k_{eff} and the gas phase permeability matrix K_y remain to be determined. Both matrices are highly anisotropic for virgin wood and almost isotropic for pure char. Most people working on wood pyrolysis and combustion do not take this anisotropy into account. Kollman and Côté (1968) discuss the heat conductivity of wood in depth. Their argument will be followed with a small change for the effect of the moisture present in the wood.

Wood consists of different phases; a solid phase, a gas phase and a liquid phase. Wood also has a highly anisotropic structure and this has its influence on the conductivity. The conductivity along the grain is much higher than the conductivity perpendicular to the grain. The grain of wood basically consists of a large number of cylinder shaped channels filled with gas and moisture and enveloped by a solid woody substance. Two cases have to be distinguished; 1) the heat flow is in the same direction as the aligned channels; and 2) the heat flow is perpendicular to the channels, see figure 3.

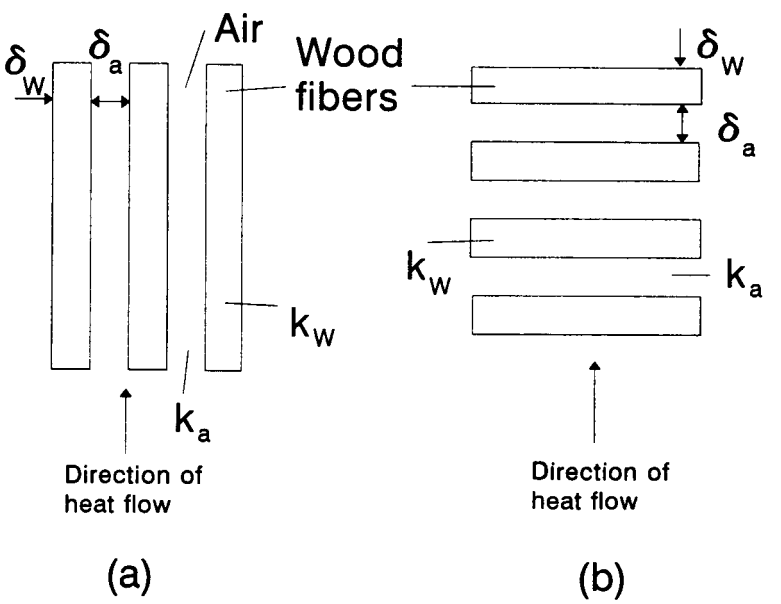

Figure 3 Directions of fibres, channels and heat flow for heat flow parallel to channels and perpendicular to channels.

Of course each of the components has its own heat conductivity. The assumption that the moisture is spread evenly along the walls of the channels makes the situation analog to parallel and serial electric resistances and the resulting conductivity in each case is easily determined. Remember that a resistance is the inverse of a conductivity. When the heat flow is in the direction of the channels the conductivity for the solid is equal to the width of the solid wall times its conductivity coefficient and the same for the gas filled channel. For parallel electric resistances the total conductivity is equal to the sum of the conductivity of the single components. Applying this to the heat conductivity results in:

$$k_{max}(\delta_W + \delta_C + \delta_\beta + \delta_\gamma) = k_W\delta_W + k_C\delta_C + k_\beta\delta_\beta + k_\gamma\delta_\gamma \tag{120}$$

where k_{max} is the total conductivity coefficient for the parallel case, δ_β is the thickness of the water filled part of the channel, δ_γ is the thickness of the gas filled part of the channel, δ_W the thickness of the unreacted solid wall and δ_C the thickness of the charred solid wall. This equation can be rewritten as:

$$k_{max} = \frac{k_\beta\delta_\beta + k_\gamma\delta_\gamma + k_W\delta_W + k_C\delta_C}{\delta_\beta + \delta_\gamma + \delta_W + \delta_C} = \epsilon_\beta k_\beta + \epsilon_\gamma k_\gamma + \epsilon_W k_W + \epsilon_C k_C \tag{121}$$

where the volume fractions follow from the thickness of the layers.

The case where the heat flow is perpendicular to the channels is analog to resistors put in series. This means that the total resistance is equal to the sum of the component resistances. Translating this to heat conduction the resistance of a solid wall is the resistance coefficient, the inverse of the conductivity coefficient, times the thickness of the wall and similar for the gas- and liquid-layers in the channel. Using conductivity coefficients results in:

$$\frac{\delta_W + \delta_C + \delta_\beta + \delta_\gamma}{k_{min}} = \frac{\delta_W}{k_W} + \frac{\delta_C}{k_C} + \frac{\delta_\beta}{k_\beta} + \frac{\delta_\gamma}{k_\gamma} \tag{122}$$

with k_{min} the total conductivity coefficient for the perpendicular case. The conductivity coefficient can be given explicitly by rewriting the previous equation and again introducing the volume fractions that follow from the thickness of the layers. The final result of this process is:

$$\frac{1}{k_{min}} = \frac{\frac{\delta_\beta}{k_\beta} + \frac{\delta_\gamma}{k_\gamma} + \frac{\delta_W}{k_W} + \frac{\delta_C}{k_C}}{\delta_\beta + \delta_\gamma + \delta_W + \delta_C} = \frac{\epsilon_\beta}{k_\beta} + \frac{\epsilon_\gamma}{k_\gamma} + \frac{\epsilon_W}{k_W} + \frac{\epsilon_C}{k_C} \tag{123}$$

In a fibrous solid the effective heat conduction can be represented as a linear combination of the heat conductivities parallel k_{max} and perpendicular k_{min} to the grain of the wood. Introducing a parameter ξ to represent the amount of mixing of the fibre directions the effective heat conductivity can be written as:

$$k_{eff} = \xi k_{max} + (1 - \xi)k_{min} \tag{124}$$

with k_{max} and k_{min} given by equations (121) and (123). For wood Kollman and Côté (1968) have gathered a large number of experimental data from the literature. This shows that in the grain direction the conductivity of wood can be represented by the previous equation with $\xi = 1$, while perpendicular to the grain the conductivity can be described with $\xi = 0.58$.

The conductivity of the solid wood phase is listed by Kollman and Côté (1968) and is:

$$k_{W,max} = 6.53\,W/m/K \quad \text{and} \quad k_{W,min} = 0.42\,W/m/K \tag{125}$$

This describes the situation for dry virgin wood, however the pyrolysis process causes a gradual change in the solid component and a movement to a more isotropic situation. This might be described by decreasing ξ in equation (124) as a function of the wood fraction, so

$$\xi_n = \xi_c + \frac{\epsilon_w}{\epsilon_{wo}} \xi_{no} \tag{126}$$

where the index n denotes either the parallel or the perpendicular case. Furthermore the index 0 refers to the value of the variable for virgin wood. The parameter ξ_c is basically the amount of mixing of parallel and perpendicular aligned fibres in the char resulting from the wood pyrolysis, it has to be determined experimentally. One axis of the coordinate system is chosen along the direction of the grain and the corresponding element on the diagonal of the effective conductivity matrix is obtained from equations (124) to (126) for the heat flow parallel to the grain ($\xi_0 = 1$). The other elements on the diagonal are obtained from the same set of equations, but for the heat flow perpendicular to the grain direction ($\xi_0 = 0.58$). The non-diagonal components for the effective conductivity matrix are all zero. Having determined the effective conductivity matrix attention is now turned to the permeability matrix.

The walls of the channels in virgin wood will block any gas flow across them and only gas flow parallel to the channels is possible. Pyrolysis leads to cracks in the channel walls through which gas can leak and this results in a higher permeability in that direction. As far as is known to us no studies have been done on the anisotropy of the permeability of wood. Moallemi *et al.* (1993) assume an isotropic permeability and approximate it with the Kozeny-Carman equation, see Cheng (1978). Strictly speaking this equation is not valid for wood, it is derived for a gas or liquid filled with spherical solid particles. Wood on the other hand is a solid medium with gas or liquid filled volumes. Since nothing better seems to be available the Kozeny-Carman equation will be used, it will be extended to an anisotropic case. The Kozeny-Carman equation gives the permeability as:

$$K_\gamma(\epsilon_\gamma) = \frac{d^2 \epsilon_\gamma^3}{175(1-\epsilon_\gamma)^2} \tag{127}$$

with d the mean diameter of the particles constituting the porous medium. This might possibly be thought of as the diameter of the channels in the wood. In that case the numerical factor in the numerator has to be changed. Both the diameter d and the numerical factor have to be determined for wood experimentally. It is quite likely that the combination of the two is constant for a given type of wood or char. The permeability for partly pyrolysed wood is written analog to the thermal conductivity as:

$$K_\gamma = \eta K_{\gamma w} + (1-\eta) K_{\gamma c} \tag{128}$$

where $K_{\gamma w}$ was given by (127) for the direction parallel to the grain of the wood and it is zero perpendicular to the grain. $K_{\gamma c}$ was used to denote the permeability of a pure char. Like the thermal conductivity matrix all non-diagonal elements are zero. The element on the diagonal corresponding to the axis parallel to the grain is given by (127) and (128), while the other two diagonal elements are given by (128) with $K_{\gamma w} = 0$. In addition to this $\eta = \epsilon_w / \epsilon_{wo}$ which is more or less analog to ξ for the thermal conductivity.

4.7 Boundary conditions

In chapter 2 boundary conditions were discussed. However due to the volume averaging that was applied to these equations the boundary conditions were incorporated in the averaged equations. Therefore new boundary conditions are needed for the equations derived in this chapter. The boundary conditions that have to be chosen depend on the geometry of the situation that has to be modeled. It is possible to choose open or closed ends and an end with or without heat flux. On open ends the boundary condition is that the pressure at the boundary is equal to the ambient pressure, while for closed ends a zero velocity at the boundary is imposed. Open ends always have a heat flux, while closed ends will usually have no heat flux. Often publications appear where a closed end is assumed to have a heat flux through it. In physical situations of wood pyrolysis a closed end only arises as a result of symmetry of the overall problem and a simulation in only half of the domain. As a result of this symmetry the temperature gradient is zero at the closed end. Open ends in wood pyrolysis usually include thermal radiation effects at the boundary. Continuity of the heat flux at the surface leads to the following boundary condition:

$$-k_{eff}\frac{\partial T}{\partial x}\Big|_{\delta V} = q_{rad} + \sigma(T_0^4 - T_{amb}^4) \qquad (129)$$

with δV the boundary of the volume of the slab of wood, q_{rad} the radiation density, σ the constant of Stefan-Boltzmann, T_{amb} the ambient temperature and T_0 the surface temperature of the wood on the boundary. The emissivity is taken as one. On the left hand side of this equation both k_{eff} and the temperature gradient have to be evaluated at the boundary. Equation (129) is written down for the left boundary, for the right boundary the minus sign has to be omitted on the left hand side of the equation. In the next chapter the implemented boundary conditions will be given.

5 Equations for a numerical simulation

The set of equations derived in chapter 4 should be put in a form that can be handled by a computer. This is done by replacing the differential equations by the corresponding difference equations. There are several ways to do this e.g. integrating over control volumes and Taylor series expansions. Anderson (1995) uses Taylor series, while Patankar (1980) gives an elaborate discussion of the control volume approach. Anderson introduces the term conservation form for the governing differential equations. A conservation form results when a control volume fixed in space is used to derive the difference equations. In that form the difference equations resulting from the Taylor expansion and the control volume approach are the same. An advantage of the difference equations resulting from the differential equations in conservation form is that they can handle discontinuities, while the difference equations resulting from the differential equations in non-conservation form usually have problems with discontinuities, see Anderson (1995). The conservation form is very useful in this model, since effects closely resembling discontinuities occur due to the moisture evaporation and pyrolysis processes. Also it should be noted that for non-Cartesian coordinates there is usually a difference in the difference equations resulting from control volume and Taylor expansion methods. Physically the control volume method is very clear, therefore it will be used to derive the difference equations.

In the control volume method a piece of wood is divided into N control volumes. Steep gradients of moisture and wood volume fractions occur. However since they move in time through the entire simulation regions only adaptive non-uniform grids might lead to faster convergence and more details compared to simple uniform grids. Therefore only uniform grids are used. The grid is chosen in such a way that the N-1 interior grid points are equally spaced with a distance of Δx between each pair of neighbouring points. The boundaries of the control volumes are chosen in such a way that each grid point lies exactly in the middle of its control volume, so the boundaries are chosen halfway between the grid points, see figure 4. For the edges of the piece of wood a grid point is put on each edge, however between a grid point on the edge and the closest interior grid point a distance $\frac{1}{2}\Delta x$ is chosen. In this way the grid points on the edge lie on the boundary of the closest interior control volume, see figure 4.
This has the advantage that boundary conditions for the piece of wood can be prescribed with some more accuracy eg. the heat flux through the surface of the particle is determined by the temperature on the surface of the particle and this temperature is now given at the grid point on the edge.

The difference equations for the rate equations can be obtained by integrating the appropriate rate equations from time t to $t+\Delta t$, leading to a rate equation for wood of:

$$\epsilon_w = \epsilon_w{}^0 \exp\left[-\int_{t-\Delta t}^{t} (K_1+K_2+K_3)\,dt'\right] \qquad (130)$$

The superscript 0 denotes the value at a previous time ie. at $t-\Delta t$. In this case ϵ_w means $\epsilon_w(t)$ and $\epsilon^0{}_w$ means $\epsilon_w(t-\Delta t)$. This notation is used to make the equations more readable. It is assumed that the time step Δt is so small that the integrand can be considered constant. Thus (130) results in:

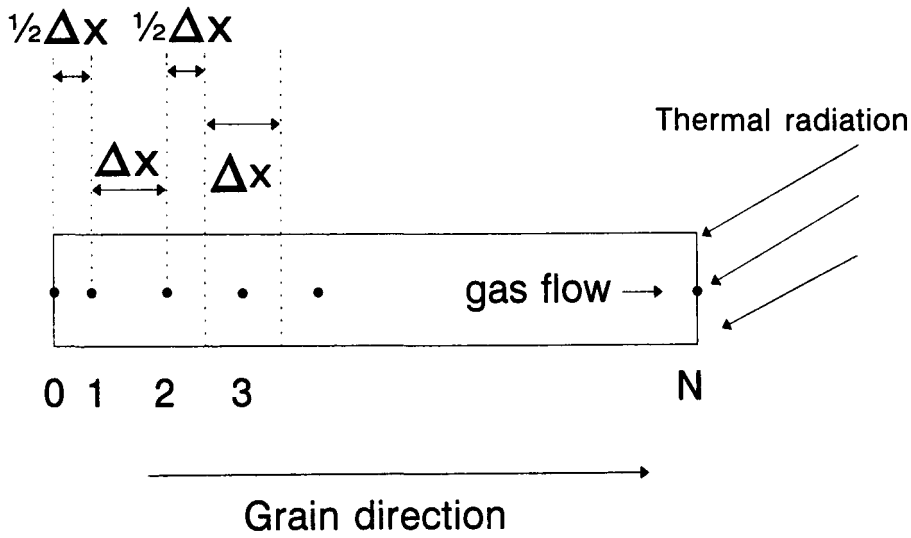

Figure 4 Control volumes in a one-dimensional piece of wood.

$$\epsilon_W = \epsilon_W{}^0 \exp[-(K_1 + K_2 + K_3)\Delta t] \tag{131}$$

For the charcoal rate equation the integration yields:

$$\epsilon_C = \epsilon_C{}^0 + \frac{\rho_W}{\rho_C}\epsilon_W K_3 \Delta t \tag{132}$$

For the gas phase components and the liquid the rate equations (102), (103) and (110) alone are insufficient for the determination of all gas densities and phase fractions and it is most convenient to insert them into the corresponding continuity equations. As an example the continuity equation for the TAR gas phase component in one dimension will be discussed. The TAR gas component shows all the problems that can occur and the other gas components are simpler cases that are easily obtained by repeating the process and making the appropriate simplifications. Higher dimensional equations and equations for non-Cartesian coordinates can be obtained in a similar

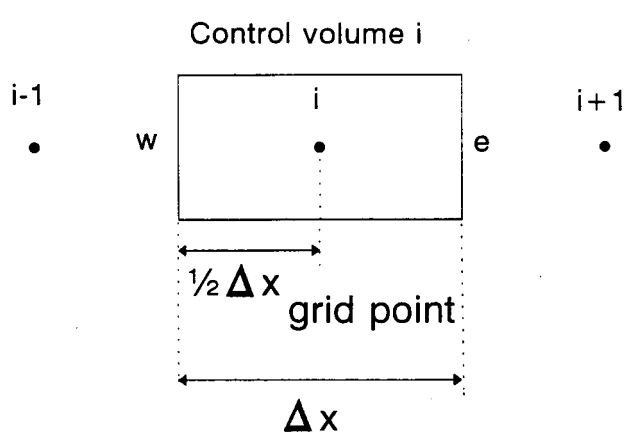

Figure 5 Detailed sketch of a single control volume and its boundaries.

way. To obtain the difference equations the TAR continuity equation (105) is integrated over the control volume i, see figure 5.
This results in:

$$\int_w^e \frac{\partial}{\partial t}(\epsilon_\gamma \rho_T)\,dx + \int_w^e \frac{\partial}{\partial x}(\rho_T < v_\gamma >)\,dx = \int_w^e < \dot{\rho}_T > dx = \int_w^e [\epsilon_W \rho_W K_2 - \epsilon_\gamma \rho_T K_4]\,dx \qquad (133)$$

with e denoting the east boundary and w the west boundary of the control volume. The second integral on the left hand side is easily calculated, while for the other integrals it is assumed that the integrand is constant over the control volume which has a length Δx. This leads to:

$$(\frac{\partial}{\partial t}(\epsilon_\gamma \rho_T))_i \Delta x + (\rho_T < v_\gamma >)_{i,e} - (\rho_T < v_\gamma >)_{i,w} = [(\epsilon_W \rho_W K_2)_i - (\epsilon_\gamma \rho_T K_4)_i]\Delta x \qquad (134)$$

here the single index i denotes the value of the variable at the centre of the control volume i and the indices i,w and i,e denote the corresponding variable at the left (west) respectively right (east) boundary of control volume i. Several sources say that combustion and pyrolysis processes are best modeled using fully time implicit equations, therefore the time derivative in the first term on the left hand side is taken as a backward time differentiation, resulting in:

$$[(\epsilon_\gamma \rho_T)_i - (\epsilon_\gamma \rho_T)_i^0]\frac{\Delta x}{\Delta t} + \tfrac{1}{2}[(\rho_{T,i} + \rho_{T,i+1}) < v_\gamma >_{i,e} - (\rho_{T,i-1} + \rho_{T,i}) < v_\gamma >_{i,w}] = [\epsilon_W \rho_W K_2 - \epsilon_\gamma \rho_T K_4]_i \Delta x \qquad (135)$$

The superscript 0 denotes the parameter value at time t-Δt, while all other parameters are given at time t. A linear interpolation was used to determine the density at the control volume boundaries. The velocities at the boundaries are most easily determined using a staggered grid. A staggered grid also has the advantage that checkerboard pressure patterns, which are un-physical, are eliminated, see also Patankar (1980) and Anderson (1995) for details. A staggered grid means that the velocities are not determined at the centre of the control volumes, but at the boundaries of the control volumes, eg. at positions e and w in figure 5. Using the Darcy equation to determine the velocities at the staggered grid points results in:

$$< v_\gamma >_i = -\frac{1}{\mu_r}\frac{K_\gamma}{\Delta x}[(\epsilon_\gamma (p_\gamma - p_0))_{i+1} - (\epsilon_\gamma (p_\gamma - p_0))_i] \qquad (136)$$

where the index i for the velocity denotes the velocity at the boundary east of control volume i. This means that the velocity at the boundary west of control volume i, which is also the velocity at the boundary east of control volume i-1, is denoted by the index i-1. Since equation (136) is a central difference expression the truncation error is of magnitude $(\Delta x)^2$ instead of Δx for forward or backward differencing, see Anderson (1995). Since backward differencing is applied to the time derivatives, their truncation errors are of magnitude Δt.

The energy equation can be calculated in a way very similar to the continuity equation. The simplified form (86) containing the source term and the effective conductivity will be used. In one dimension the equation becomes:

$$\frac{\partial}{\partial t}(C_p \rho T) + \frac{\partial}{\partial x}(c_{p,\gamma} \rho_\gamma < v_\gamma > T) + S(T) = \frac{\partial}{\partial x}(k_{eff}\frac{\partial}{\partial x}T) \qquad (137)$$

where it is assumed that the matrix k_{eff} in the original equation has only one non-zero component in the x direction, so for the first diagonal element. Also space averages were used except for the

velocity. More complicated cases are easily calculated, but involve a lot more writing. Like the continuity equation this equation is integrated over the control volume i, resulting in:

$$\frac{\Delta x}{\Delta t}[(C_p\rho T)_i-(C_p\rho T)_i^0] + (c_{p,\gamma}\rho_\gamma T)_{i,e}<\boldsymbol{v}_\gamma>_i-(c_{p,\gamma}\rho_\gamma T)_{i,w}<\boldsymbol{v}_\gamma>_{i-1} + S(T)\Delta x =$$

$$(k_{eff}\frac{\partial}{\partial x}T)_{i,e} - (k_{eff}\frac{\partial}{\partial x}T)_{i,w} = \frac{1}{\Delta x}[k_{eff,ie}(T_{i+1}-T_i)-k_{eff,iw}(T_i-T_{i-1})] \quad (138)$$

where the last equality results from using a central difference approximation for the temperature gradient at the boundaries of the control volume. This completes the set of difference equations, the equations that were not discussed here were ordinary algebraic equations and do not need further discussion.

The generalised Newton-Raphson method appears to be the only stable solution method when evaporation is included. However even that method slows down enormously with the evaporation effect included and larger permeability values (around 10^{-13} m^2). All other methods that were tried failed to converge in at least some normal circumstances. The reason that most methods fail to converge will be made plausible below.

The gas continuity equation provides an estimate for the gas density. The source term in the continuity equation is not relevant for the stability calculations, so a simple gas continuity equation is used. To simplify matters the gas component index is dropped for the remainder of this section. The continuity equation can be rewritten in the form:

$$\rho_i^{(n+1)} = \frac{1}{\epsilon_{\gamma,i}}\{(\epsilon_{\gamma,i}\rho_i^{(n)})^0+\frac{\Delta t}{2\Delta x}[(\rho_i^{(n)}+\rho_{i+1}^{(n)})<\boldsymbol{v}_\gamma>_i-(\rho_{i-1}^{(n)}+\rho_i^{(n)})<\boldsymbol{v}_\gamma>_{i-1}]\} \quad (139)$$

the superscripts of the densities denote the iteration number, so the left hand side denotes the (n + 1)-th approximation of ρ_i and it is given as a function of its n-th approximation on the right hand side. For convergence the absolute value of the derivative of the (n + 1)-th approximation to the n-th approximation should be less than 1. Since the velocities also depend on the gas densities the derivative is:

$$\frac{\partial\rho_i^{(n+1)}}{\partial\rho_i^{(n)}} = \frac{\Delta t}{\epsilon_{\gamma,i}2\Delta x}[<\boldsymbol{v}_\gamma>_i-<\boldsymbol{v}_\gamma>_{i-1}+(\rho_i^{(n)}+\rho_{i+1}^{(n)})\frac{\partial<\boldsymbol{v}_\gamma>_i}{\partial\rho_i^{(n)}}-(\rho_{i-1}^{(n)}+\rho_i^{(n)})\frac{\partial<\boldsymbol{v}_\gamma>_{i-1}}{\partial\rho_i^{(n)}}] \quad (140)$$

To calculate the derivative of the velocity to the density the derivative of the Darcy equation is all that is needed. The result of this is:

$$\frac{\partial<\boldsymbol{v}_\gamma>_i}{\partial\rho_i^{(n)}} = \frac{K_\gamma}{\mu_\gamma\Delta x M}\epsilon_{\gamma,i}RT_i \quad (141)$$

The derivative for $<\boldsymbol{v}_\gamma>_{i-1}$ is calculated in the same way. Except for the sign the result is the same as in the previous equation. Inserting the velocity derivatives into equation (140) results in:

$$\frac{\partial\rho_i^{(n+1)}}{\partial\rho_i^{(n)}} = \frac{\Delta t}{\epsilon_{\gamma,i}2\Delta x}[<\boldsymbol{v}_\gamma>_i-<\boldsymbol{v}_\gamma>_{i-1}+\frac{K_\gamma\epsilon_{\gamma,i}RT_i}{\mu_\gamma\Delta x M}(\rho_{i-1}^{(n)}+2\rho_i^{(n)}+\rho_{i+1}^{(n)})] \quad (142)$$

The combination of the first two terms is generally less than one for reasonable step sizes. Since the density is always larger or equal to zero the combination of the last three terms is obviously larger or equal to the fourth term, so just the fourth term will be considered for simplicity:

$$\frac{\partial \rho_i^{(n+1)}}{\partial \rho_i^{(n)}} = \frac{R \Delta t K_\gamma T_i}{\mu_\gamma (\Delta x)^2 M} \approx 6 \cdot 10^9 K_\gamma \frac{\Delta t}{(\Delta x)^2} \approx 600 \Delta t \qquad (143)$$

At the end several parameter estimates were used to give an estimate for the time step that should be used in order to obtain convergence. For the universal gas constant the value 8 J mole^{-1} K^{-1}, for the temperature 300 K (ambient temperature), the viscosity $2 \cdot 10^{-5}$ Pa s, the space step 10^{-3} m, the molecular weight $20 \cdot 10^{-3}$ kg and the permeability 10^{-13} m^2. The time step has to be smaller than 1/600-th of a second if convergence is required. All these values are crude estimates and were chosen to obtain a large time step, in reality the time step has to be a lot smaller than the 1/600-th second that was just calculated. It seems fair to conclude that simple iterative methods of gas densities and velocities require unacceptably small time steps; this became clear while developing the model.

A generalised Newton-Raphson method is the solution here. In some cases the convergence can still take hundreds of iterations, but at least convergence is obtained. Below these generalised Newton-Raphson equations are derived. Both the Newton-Raphson and the generalized Newton-Raphson methods can be found in several text books, see for example Hämmerlin and Hoffmann (1991). A gas continuity equation without sources is rewritten as:

$$G_i = [\epsilon_{\gamma,i}\rho_i - (\epsilon_{\gamma,i}\rho_i)^0]\frac{\Delta x}{\Delta t} + \tfrac{1}{2}(\rho_i + \rho_{i+1}) < v_\gamma >_i - \tfrac{1}{2}(\rho_{i-1} + \rho_i) < v_\gamma >_{i-1} = 0 \qquad (144)$$

with G_i the i-th component of a $N+1$ component vector with $i \neq 0$ and $i \neq N+1$. The i-th component of G represents the continuity equation for the i-th control volume. For the generalized Newton-Raphson method the $(n+1)$-th approximation is obtained by the following equation:

$$J_G(P^{(n)})(P^{(n+1)} - P^{(n)}) = -G(P^{(n)}) \qquad (145)$$

with J_G the Jacobian of the vector function G and P a vector where the i-th component is the gas density in control volume i (ρ_i) and again the superscripts indicate the number of the approximation. Equation (145) is solved using the Gauss elimination method and results in the difference between the n-th and $(n+1)$-th approximation of the vector P, so the result is $(P^{(n+1)}-P^{(n)})$. The new $(n+1)$-th approximation follows by adding this difference to the n-th approximation. The i-th component of the vector function G depends on the components i-1, i and $i+1$ of P, so the Jacobian is a tridiagonal matrix $J_G = \partial G/\partial P$ with the entries

$$J_{i,i-1} = \frac{\partial G_i}{\partial \rho_{i-1}} = -\tfrac{1}{2}\left[< v_\gamma >_{i-1} + (\rho_{i-1} + \rho_i) \frac{\partial < v_\gamma >_{i-1}}{\partial \rho_{i-1}} \right] \qquad (146)$$

and on the diagonal

$$J_{i,i} = \frac{\partial G_i}{\partial \rho_i} = \epsilon_{\gamma,i}\frac{\Delta x}{\Delta t} + \tfrac{1}{2}\left[< v_\gamma >_i - < v_\gamma >_{i-1} - (\rho_{i-1} + \rho_i) \frac{\partial < v_\gamma >_{i-1}}{\partial \rho_i} + (\rho_i + \rho_{i+1}) \frac{\partial < v_\gamma >_i}{\partial \rho_i} \right] \qquad (147)$$

and

$$J_{i,i+1} = \frac{\partial G_i}{\partial \rho_{i+1}} = \tfrac{1}{2}\left[< v_\gamma >_i + (\rho_{i+1} + \rho_i) \frac{\partial < v_\gamma >_i}{\partial \rho_{i+1}} \right] \qquad (148)$$

with $i \neq 0$ and $i \neq N+1$. To limit writing the superscripts were dropped, but they all have the index (n). For $i = 0$, for the open end, the density is determined by ideal gas law, so
with the obvious entry

$$G_0 = p_{amb} - \frac{R\rho_0 T_0}{M} \tag{149}$$

$$J_{0,0} = \frac{\partial G_0}{\partial \rho_0} = -\frac{RT_0}{M} \tag{150}$$

and 0 for $J_{0,1}$. The closed end is determined by the zero density gradient, so $\rho_N = \rho_{N+1}$ and $J_{N+1,N} = -1$ and $J_{N+1,N+1} = 1$. This completes the description of the generalized Newton-Raphson method and guarantees convergence. Of course the method should be applied to all gas components. To speed up the sometimes only linear convergence some additional strategies are recommended. Unfortunately a lack of time prohibited the search for an increased convergence. Convergence is assumed to be obtained if for all variables x with an absolute value larger than 10^{-8} the condition

$$\left| \frac{x^{(n+1)} - x^{(n)}}{x^{(n+1)}} \right| < \epsilon_{acc} \tag{151}$$

In the next chapter the value of ϵ_{acc} is listed in Table I ($\epsilon_{acc} = 10^{-4}$).

The set of energy difference equations can be represented by a tridiagonal matrix too and it can be solved using the Gauss elimination method. The complete solution method can be outlined along these lines

- ◇ Calculate the new values for the thermal conductivity (equations (121) and (123)-(124)) and permeability (equations (127) and (128) with $\eta = \epsilon_w/\epsilon_{w0}$).
- ◇ Obtain temperature from the set of energy equations (138). The resulting tridiagonal matrix is solved using Gauss elimination.
- ◇ Get the volume fractions for WOOD and CHAR from their rate equations (131) and (132).
- ◇ In volumes without moisture ($\epsilon_\beta = 0$) use the generalized Newton-Raphson equation for the vapour component to obtain the vapour density (adapt (144) to (150)).
- ◇ In volumes with moisture ($\epsilon_\beta \neq 0$) obtain the vapour density from the Clausius-Clapeyron and Kelvin equation (97). Then obtain the liquid phase volume fractions from the set of vapour continuity equations.
- ◇ Use the generalized Newton-Raphson method to obtain all other gas component densities (adapt (144) to (150)).
- ◇ $\epsilon_\gamma = 1 - \epsilon_\beta - \epsilon_w - \epsilon_c$. Equation (117).
- ◇ Calculate the total gas pressure from the partial pressures.
- ◇ Calculate the gas velocity using the Darcy equation (136).
- ◇ If the accuracy is obtained (if (151) holds) start with the next time step, else go back to the top of this list.

6 Some numerical simulations

Studies can be found that investigate the effect of several parameters on the pyrolysis of wood. The parameters studied are usually reaction rate parameters (frequency factors, activation and reaction energies for several global reactions), permeability and thermal conductivity of solid components of wood. These parameters are all material properties that are difficult to change and they are usually highly uncertain, since they depend on the type and structure of the wood. This wood structure depends among other factors on the age of the tree, position in the tree trunk, weather- and soil-conditions. The present practice is to take values for parameters from tables and vary them to see how sensitive variables like eg. gas pressure or a gas component density are for changes in the parameters. It is probably more useful to determine the values of the parameters experimentally for almost every batch of wood that is used for comparisons, thus providing a more reliable match between experiments and simulation. Even the highly uncertain global reaction rates can be more accurately estimated when permeability, heat conduction and initial wood density are experimentally determined. This determination would require a very well equipped lab indeed and most labs studying wood combustion do not have the required equipment and our lab is no exception. Even with a well equipped lab determination of reaction parameters is difficult if not impossible. This is caused by the large number of reactions occurring in the combustion of wood and the fact that not all gas concentrations can be determined with the required accuracy. Of course the highly virulent reaction zone and its high temperature do not help either.

The effect of varying reaction rate parameters and most other matter properties do not produce any surprising results and can be found in the literature anyway, see for example Kailasanath and Zinn (1981), Moallemi *et al.* (1993) and Di Blasi (1993). The effects of other parameters that are expected to vary in the field are studied. To be more precise the effects of thermal irradiation of wood, the initial density of the wood (the space averaged wood density varies with the type of wood) and the moisture content of the wood on the pyrolysis and drying processes are studied. Especially this last point has as far as we know never been studied before, while in practice wood always contains an important fraction of moisture. However in view of the stability problems, see previous chapter, and slow convergence of the simulation calculations when moisture is included it is not much of a surprise that no studies seem to exist.

6.1 Geometry

The piece of wood is irradiated from the left with radiation density q_{rad}, so the boundary condition is given by equation (129). The left end is open, so gases leave the piece of wood on the left end and $p_y = p_{amb}$ at that end. The right end is assumed to be closed so $v_y = 0$, while this end is not irradiated, so setting $q_{rad} = 0$ and dropping the minus sign on the right hand side of equation (129) gives the boundary condition for the right end. The right end is just supposed to be closed, no symmetry is assumed. The initial conditions are set to ambient values and the parameter values that are chosen for the simulation are all reasonable values for a typical case of wood pyrolysis,

see table I. Thermal conductivity for the solid phase was chosen at $k_W = 0.4$ W m^{-1} K^{-1} which is in line with most studies on wood pyrolysis. The space averaged wood density is chosen as $\rho_0 = 650$ kg m^{-3} and this is the density for beech. A moisture fraction [m] = 0.1 is chosen and this is typical for lab experiments, in the field values between 0.2 and 0.3 are more realistic.

Table I Parameter values as used in the simulations.

$\sigma = 5.78 \cdot 10^{-8}$ W m^{-2} K^{-4}	R = 8.319 J mol^{-1} K^{-1}	
$M_{O_2} = 32 \cdot 10^{-3}$ kg	$M_{N_2} = 28 \cdot 10^{-3}$ kg	$M_{H_2O} = 18 \cdot 10^{-3}$ kg
$k_\beta = 0.6$ W m^{-1} K^{-1}	$c_{p,\beta} = 4.18 \cdot 10^3$ J kg^{-1} K^{-1}	$\rho_\beta = 10^3$ kg m^{-3}
$L = 2.26 \cdot 10^6$ J kg^{-1}	$c_{p,v} = 2 \cdot 10^3$ J kg^{-1} K^{-1}	$k_\gamma = 25.77 \cdot^{-3}$ W m^{-1} K^{-1}
$k_w = 0.4$ W m^{-1} K^{-1}	$k_c = 0.42$ W m^{-1} K^{-1}	$\rho_s = 1460$ kg m^{-3}
$\rho_0 = 650$ kg m^{-3}	$c_{p,w} = 1354$ J kg^{-1} K^{-1}	$c_{p,c} = 669$ J kg^{-1} K^{-1}
$L_x = 15 \cdot 10^{-3}$ m		
$T_{amb} = 300$ K	$p_{amb} = 1.01 \cdot 10^5$ Pa	
[m] = 0.1	$q_{rad} = 3.182 \cdot 10^4$ W m^{-2}	
$\Delta t = 0.1$ s	$N_x = 31$ nodes	$\epsilon_{acc} = 10^{-4}$
$c_{p,G} = 1089$ J kg^{-1} K^{-1}	$c_{p,T} = 1089$ J kg^{-1} K^{-1}	$M_G = 30 \cdot 10^{-3}$ kg
$M_T = 60 \cdot 10^{-3}$ kg	$\mu_\gamma = 2.6 \cdot 10^{-5}$ Pa s	$C_{evap} = 100$
$K_0 = 10^{-13}$ m^2	$A_1 = 2000$ s^{-1}	$E_1 = 80/R$ kJ mole^{-1}
$A_2 = 0.5$ s^{-1}	$E_2 = 35/R$ kJ mole^{-1}	$A_3 = 1500$ s^{-1}
$E_3 = 80/R$ kJ mole^{-1}	$A_4 = 4.28 \cdot 10^6$ s^{-1}	$E_4 = 108/R$ kJ mole^{-1}
$\Delta H_{wG} = 0.5$ MJ kg^{-1}	$\Delta H_{wT} = 0.5$ MJ kg^{-1}	$\Delta H_{wc} = 0.5$ MJ kg^{-1}
$\Delta H_{TG} = -42$ kJ kg^{-1}		

Here the value of $C_{evap} = 100$ K introduced in equation (96) is given and the permeability $K_0 = 10^{-13}$m^2 in this table is for dry virgin wood. Equation (127) is used to calculate the permeability for moisture containing wood, an equivalent correction is made for the charred wood. For the initial wood density used here the permeability value is probably a little too large and should have been chosen a factor 10 or 100 smaller. Also the permeability was not adapted to the initial wood density as should have been done, instead it is kept constant in all initial conditions for the simulations in this report. This is acceptable since simulations showed that the effect of permeability is totally insignificant, except for the internal gas densities which are slightly affected and the gas pressure which changes enormously. However the positions of the pyrolysis front and the evaporation front, both of which will be explained later, will be studied and these are not affected by the permeability.

First a problem caused by the discretization of the equations will be looked into. This problem shows up clearly in the evolution of the TAR density, see figure 6. This graph shows a number of sharp peaks, which are discretization effects. In figure 7 on the other hand no peaks are visible. The difference is that for the simulation for figure 6 moisture was present, while for the simulation for figure 7 no moisture was present. This seems to suggest that the moisture volume fraction and the vapour density can lead to discretization effects. A possible explanation is given below. The evaporation process in two adjoining control volumes is considered, both still containing moisture. Assuming that the wood is irradiated from the left only the left control volume has the highest temperature. To simplify writing the indices l for the left and r for the right control volume will be used. Assumed is that T_l is smaller than the effective boiling temperature T_b, then $T_r < T_b$ too

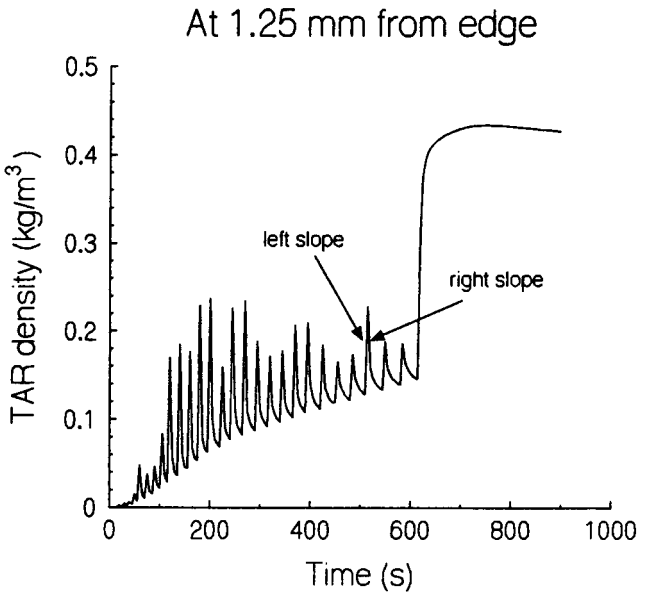

Figure 6 Discretization effects on the intrinsic phase average TAR density profile.

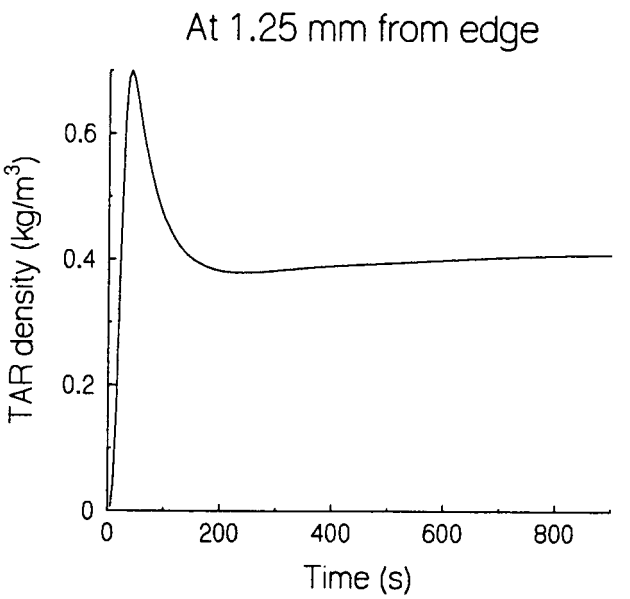

Figure 7 Intrinsic phase averaged TAR density profile. No moisture in the wood.

and the evaporation process is fastest in the left control volume. Due to heat conduction T_l increases until $T_l \geq T_b > T_r$. Assuming that both control volumes still contain a significant amount of moisture at this point the moisture in the left control volume startsboiling, thus speeding up the evaporation process enormously, resulting in a large pressure build-up. The pressure in the left control volume becomes considerably larger than in any of its neighbours, causing high velocities out of this control volume. In fact the pressure in this control volume is higher than anywhere else

in the wood. Due to the very high evaporation rate the gas phase of the left control volume contains almost exclusively water vapour. This moves to neighbouring control volumes with high velocities, thus flushing out other gas components from those control volumes. This flushing process explains the right hand slope of the peaks in figure 6. These processes continue until the moisture fraction in the left control volume becomes negligible. Usually T_r is still smaller than T_b. If this is not the case steam explosions would result inside the wood and tear it up. In fact that is what happens in a wood log fire, although only on a small scale, and the steam explosions can be heard as the popping of the burning wood. Returning to the assumption $T_r < T_b$ consider the evaporation rate again. In the left control volume there is no moisture left to evaporate, while in the right control volume $T_r < T_b$ resulting in a much slower evaporation rate. Now T_l will increase rapidly, since no energy is used for the evaporation of moisture. This rapid temperature increase causes a further albeit slower increase of pressure in the left control volume. This leads to a flushing effect that is still increasing, but at a much lower rate. In turn this leads to a reduced rate of gas component density reduction, thus explaining the shape of the valleys in Figure 6. After some time the increase in temperature is no longer sufficient for a further increase in pressure in the left control volume. In fact this pressure starts reducing quickly due to the outflow of gases while no source is present. In the right control volume the pressure is still very much lower than that in the left control volume, so all velocities reduce considerably. This in turn reduces the flushing out of gas components by vapour and as a result the concentrations of all components, except possibly the vapour, increase rapidly. This explains the left hand slope of the peaks in Figure 6. Very soon $T_r > T_b$ and flushing causes a rapid decrease in gas component density again. In fact this already starts when the gas pressure in the right control volume p_r is larger than the gas pressure in the left control volume p_l.

6.2 Evaporation and pyrolysis fronts

It is obvious that the moisture in a control volume is usually not evenly distributed. Especially in the hottest volume still containing a significant amount of liquid the moisture is distributed unevenly. In that case the left most part of the control volume contains a negligible liquid moisture fraction while for the right-most side the liquid fraction is of the same magnitude as that of the control volume on the right. Somewhere in between there would then be a region with a very sharp gradient in the moisture fraction and this region could be considered as an interface or front. It is now assumed that such a front exists and a method is given here that could be used to calculate a position of the front. To make the equations more readable the position of this evaporation front at time t will be denoted by x_e and its position at time t-Δt by x_e^0. This description would result in a zero moisture fraction on the left side of x_e and a constant moisture fraction $\epsilon_{\beta e}$ on the right side of the control volume containing x_e, see figure 8. The moisture fraction $\epsilon_{\beta n+1}$ in the control volume n + 1 is in general not constant and not equal to $\epsilon_{\beta n}$ or $\epsilon_{\beta e}$. The moisture volume fraction profile looks more like the sketch of the real profile in the graph. The bump is caused by condensation of water vapour and this is confirmed in simulations, see for example figure 9. Due to the very steep gradient of the liquid phase the bump in figure 8 is deformed to the spiky shape it has in figure 9. The moisture fraction $\epsilon_{\beta n}$ in control volume n is the average over the volume of control volume n. The value of $\epsilon_{\beta e}$ is chosen at the moment that x_e crosses the boundary

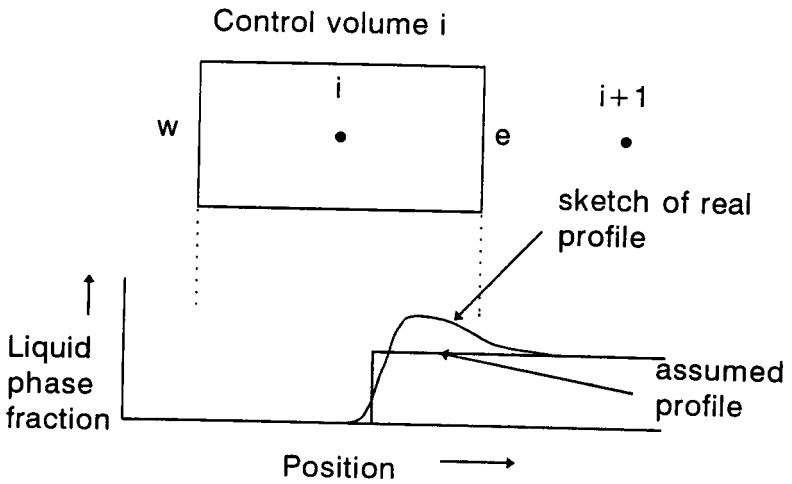

Figure 8 Sketch of the moisture profiles in drying wood.

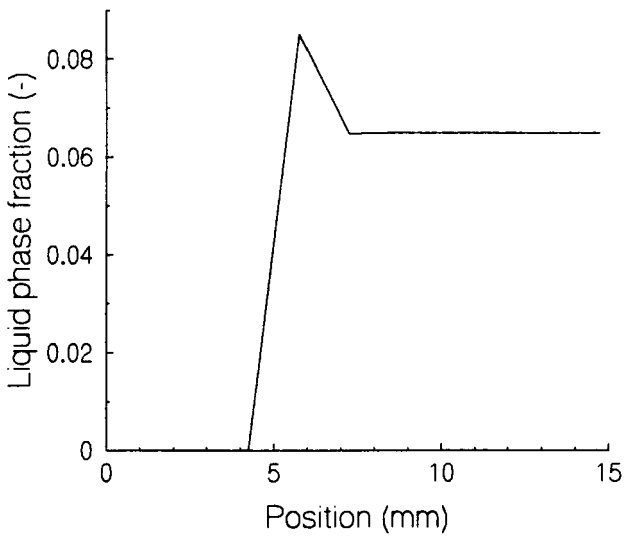

Figure 9 A moisture profile in drying wood according to a simulation.

of a control volume, so when x_e^0 is in control volume n-1 and x_e in volume n. The value of $\epsilon_{\beta e}$ is then given by:

$$\epsilon_{\beta e} = \frac{\epsilon_{\beta n}}{n-(x_e/\Delta x)} \tag{152}$$

Thus ensuring that no sudden jumps occur when x_e crosses a boundary. The position of x_e is now easy to calculate when x_e and x_e^0 are in the same control volume.

$$x_e = \Delta x(n - \frac{\epsilon_{\beta n}}{\epsilon_{\beta e}}) \tag{153}$$

Note that with $\epsilon_{\beta e}$ given by equation (152) x_e is given in a consistent manner when x_e crosses a boundary and with $\epsilon_{\beta n}=0$ x_e reaches the right boundary of the control volume as it should. Following this method closely the evaporation front would never cross a boundary, so a zero-th order estimate of x_e is used for every new time. The zero-th order approximation is used for all other variables too and is given by

$$x^{(0)}(t+\Delta t) = x(t) + [x(t)-x(t-\Delta t)] \tag{154}$$

Here $x^{(0)}$ is the zero-th order approximation of a variable x. When x_e and x_e^0 are contained in the same control volume equation (153) gives the value of x_e. However if x_e and x_e^0 are not contained in the same control volume, then x_e is obtained from its zero-th order estimate and with equation (152) a new value for $\epsilon_{\beta e}$ is calculated. In this last case the zero-order approximation of x_e is assumed to be the final result and $\epsilon_{\beta e}$ is updated as long as the required accuracy is not reached.

A similar exercise to the one for the evaporation front can be done for the pyrolysis front, however since no condensation of the solid phase is possible the pyrolysis front is calculated in a slightly different way. It is assumed that the position of the pyrolysis front is at the point where $\epsilon_w(x,t)=c$. Here c is the wood fraction that is assumed to exist at the exact position of the pyrolysis front and it is assumed to be constant. Since this is just a concept that is supposed to reduce the discretization problem and not meant to describe the pyrolysis process accurately the value of c is not that important. Of course it should meet the criteria $0<c<\epsilon_w(0)$ with $\epsilon_w(0)$ the initial solid fraction of the wood. This is obvious since the wood volume fraction can not increase and also can not become negative. The position of the pyrolysis front is taken at the point where $\epsilon_w(x,t)=c=e^{-1}\epsilon_w(0)$. Assuming a linear profile between neighbouring points for the wood fraction it is clear that

$$\epsilon_w(x,t) = \epsilon_{wn} + (\epsilon_{wn+1}-\epsilon_{wn})(\frac{x}{\Delta x} - n + \frac{1}{2}) \tag{155}$$

With n the first point left of x_p and $n+1$ the first point right of x_p, Δx the distance between points n and $n+1$ and x the point where $\epsilon_w(x,t)$ is obtained. The position of the pyrolysis front x_p is calculated by setting $\epsilon_w(x,t)$ to $e^{-1}\epsilon_w(0)$, x to x_p. Solving the resulting equation for x_p results in:

$$x_p = \Delta x[n - \frac{1}{2} + \frac{e^{-1}\epsilon_w(0)-\epsilon_{wn}}{\epsilon_{wn+1}-\epsilon_{wn}}] \tag{156}$$

Wood, char and liquid phase fractions as well as the gas densities, gas velocity and gas pressure are mainly caused by evaporation and pyrolysis. The temperature is mainly determined by the evaporation and the different phase fractions which in turn are mainly determined by evaporation and pyrolysis again. Other parameters influence the actual values of the above

mentioned variables too, but without evaporation and pyrolysis negligible changes in velocity and pressure result. Basically the piece of wood could then be described as a solid and the solution of its heat conduction equation would describe the situation quite accurately.

Since pyrolysis and evaporation affect all other variables it seems obvious to consider the effect of several parameters on these two variables only. The position of the evaporation and pyrolysis fronts in a simulation are easy to track and the effect of parameters on them is far more easy to quantify than for any of the other variables. Therefore the effect of thermal radiation q_{rad}, initial wood density ρ_0 and moisture content [m] on the position of the pyrolysis and evaporation fronts will be studied.

Using the expressions for x_e and x_p arrived at earlier in equations (153) and (156) in a simulation results in the graph in figure 10. This graph shows that the evaporation front moves much faster (steeper gradient of the curve) than the pyrolysis front. Of course this is due to the fact that the effective boiling temperature is much lower than the temperature at which pyrolysis sets in. Another important difference is that the evaporation front moves substantially virtually from the start, while the pyrolysis front hardly moves at all for quite some time. Again this is caused by the different temperatures at which the processes occur. It takes only a few seconds for the first irradiated control volume to reach the effective boiling temperature, while it takes several minutes for it to heat up to temperatures that enable pyrolysis at a reasonable rate. The fact that the pyrolysis front does not start at $x=0$ is caused by the calculation method of x_p and the fact that on the edge of the piece of wood the wood fraction is supposed to be zero. Both the graphs in figure 10 are very well described by a second order polynomial in $\sqrt{t}$, so by

$$x_i = a_0 + a_1\sqrt{t} + a_2 t \qquad (157)$$

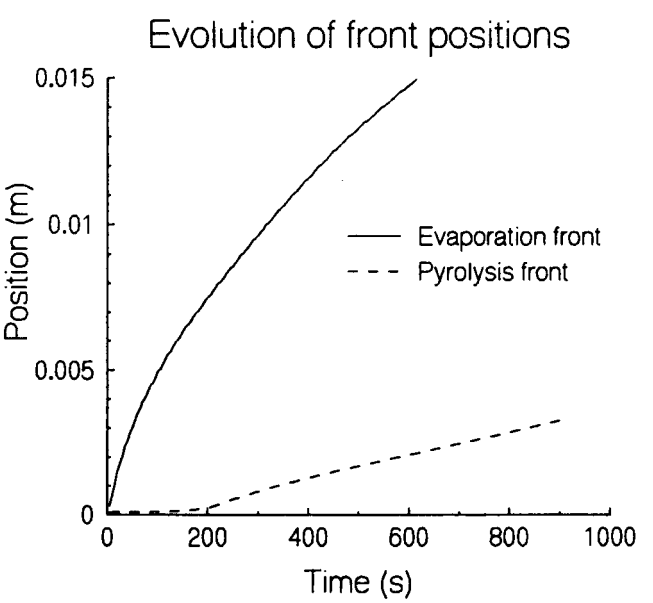

Figure 10 The position of the evaporation front x_e and the pyrolysis front x_p as a function of time in a pyrolysing piece of wood.

Here the index i can have the values e to denote the evaporation front and p to denote the pyrolysis front. Of course the coefficients differ for these two cases. Some of the simulations done in this study result in graphs that are also well described by $a_0 + a_1\sqrt{t}$ or by $a_0 + a_2 t$. For the pyrolysis front equation (157) only holds for $t > \tau$, the time when pyrolysis becomes significant. Strange enough the description $x_p = a_0 + a_1\sqrt{(t-\tau)} + a_2(t-\tau)$ is worse than that of equation (157). For $t \leq \tau$ $x_p = 0$ is taken. The way to equation (157) was really quite simple; the complementary error function is a fundamental solution of the heat equation for a homogeneous solid without heat sources or sinks. A process like moisture evaporation or wood pyrolysis occurs mainly close to some sort of process temperature which is virtually constant for the given situation. The complementary error function is equivalent to a constant process temperature for points in space and time that are determined by the equation $x = a\sqrt{t}$ and this is the second term of (157). Some of the other fundamental solutions also require $x = a\sqrt{t}$ to result in a virtually constant temperature. The first coefficient in equation (157) is needed to meet initial conditions. Due to the non-homogeneous nature of the pyrolysing moist wood and the sources and sinks in it a second order approximation is introduced to improve the description. This second order description is the last term in (157).

Since a simple equation can be easily and accurately fitted to the simulation data it becomes obvious that the effects of q_{rad}, ρ_0 and [m] on x_e and x_p can be obtained by determining their effect on the coefficients a_0, a_1 and a_2 and this is exactly what is done in the next three sections.

6.3 The effect of the initial wood density

Different types of wood have different initial wood densities ρ_0 (space averaged wood density), therefore the effect of the initial wood density on pyrolysis and evaporation has to be determined in order to determine pyrolysis and evaporation in different types of wood. Some examples for different types of wood are White Fir $\rho_0 = 410$ kg/m^3, Meranti $\rho_0 = 600$ kg/m^3, Merbau $\rho_0 = 850$ kg/m^3 and Tamarindus Indica $\rho_0 = 975$ kg/m^3, see Bussmann (1988) and Krishna Prasad (1986). Figure 11 shows the position of the evaporation front x_e for three values of the initial wood density. As can be expected the front position at a given time is further away from the irradiated edge for smaller wood densities. This can be explained easily since smaller wood densities mean smaller heat capacities which in turn lead to faster heating of the material and faster evaporation. This effect is even larger for the pyrolysis front x_p, see figure 12. The pyrolysis temperature is higher than the evaporation temperature so different heating rates occur over a longer time interval, resulting in larger differences between the different wood densities. So qualitatively the effect of the wood density can be explained, but a more quantitative description is possible. The dependence of the coefficients of x_e and x_p on ρ_0 is not very difficult. In order to better distinguish between x_e and x_p, x_e will be denoted by the coefficients a_0, a_1 and a_2 while x_p will be described by the coefficients b_0, b_1 and b_2. With an initial 0.1 fraction for the moisture content by weight on a dry matter basis ([m] = 0.1) figures 13 to 15 result describing the coefficients of x_e and figures 16 to 18 describing the coefficients of x_p. The curves are simple equations fitted to the data points obtained from simulations. For other moisture contents ([m] = 0.15 and [m] = 0.25) similar graphs could be obtained. All coefficients can be described by an equation of the form:

$$c_i = d_0 + d_1\sqrt{\rho_0} + d_2\rho_0 \qquad (158)$$

with c either a coefficient from x_e (so $c_i = a_i$) or x_p (so $c_i = b_i$) and the index i = 1, 2 or 3. The dependence of the coefficients on the initial wood density for different moisture contents is given in the table below:

Table II The initial wood density dependence of coefficients.

[m] = 0.1

$a_0 = -2.974\cdot10^{-4} - 1.813\cdot10^{-5}\sqrt{\rho_0} - 4.124\cdot10^{-7}\rho_0$
$a_1 = 10.62\cdot10^{-4} - 2.583\cdot10^{-5}\sqrt{\rho_0} + 2.197\cdot10^{-7}\rho_0$
$a_2 = -9.374\cdot10^{-6} + 6.729\cdot10^{-7}\sqrt{\rho_0} - 5.701\cdot10^{-9}\rho_0$
$b_0 = -2.958\cdot10^{-3} + 2.512\cdot10^{-4}\sqrt{\rho_0} - 7.411\cdot10^{-6}\rho_0$
$b_1 = 2.679\cdot10^{-4} - 1.905\cdot10^{-5}\sqrt{\rho_0} + 4.713\cdot10^{-7}\rho_0$
$b_2 = 2.747\cdot10^{-6} + 9.627\cdot10^{-8}\sqrt{\rho_0} - 4.7\cdot10^{-9}\rho_0$

[m] = 0.15

$a_0 = 6.146\cdot10^{-4} - 1.049\cdot10^{-4}\sqrt{\rho_0} + 1.18\cdot10^{-6}\rho_0$
$a_1 = 8.324\cdot10^{-4} - 1.184\cdot10^{-5}\sqrt{\rho_0} - 2.033\cdot10^{-8}\rho_0$
$a_2 = -5.232\cdot10^{-6} + 2.389\cdot10^{-7}\sqrt{\rho_0} + 1.442\cdot10^{-9}\rho_0$
$b_0 = -2.691\cdot10^{-3} + 2.421\cdot10^{-4}\sqrt{\rho_0} - 8.723\cdot10^{-6}\rho_0$
$b_1 = 1.864\cdot10^{-4} - 1.255\cdot10^{-5}\sqrt{\rho_0} + 4.352\cdot10^{-7}\rho_0$
$b_2 = 4.09\cdot10^{-6} - 9.228\cdot10^{-8}\sqrt{\rho_0} - 2.191\cdot10^{-9}\rho_0$

[m] = 0.25

$a_0 = -4.645\cdot10^{-3} + 4.087\cdot10^{-4}\sqrt{\rho_0} - 1.248\cdot10^{-5}\rho_0$
$a_1 = 3.462\cdot10^{-4} - 2.584\cdot10^{-5}\sqrt{\rho_0} + 7.142\cdot10^{-7}\rho_0$
$a_2 = -4.448\cdot10^{-7} + 2.244\cdot10^{-7}\sqrt{\rho_0} - 8.323\cdot10^{-9}\rho_0$
$b_0 = 6.534\cdot10^{-4} - 1.143\cdot10^{-4}\sqrt{\rho_0} + 1.499\cdot10^{-6}\rho_0$
$b_1 = 6.653\cdot10^{-4} - 5.195\cdot10^{-6}\sqrt{\rho_0} - 1.497\cdot10^{-7}\rho_0$
$b_2 = -2.708\cdot10^{-6} - 1.038\cdot10^{-8}\sqrt{\rho_0} + 6.256\cdot10^{-9}\rho_0$

The reader is given the opportunity to judge the accuracy of the curves fitted with equation (157) and the generalized equations following from the coefficients in Table II. For a representative case the best fit to the simulation of x_e is given in figure 19 and the best fit to x_p is given in figure 20. The generalized equations differ so little from the best fits that no difference can be seen on the scale of the graphs. Therefore no curves for the generalized equations are given. Especially in the graph for x_p the fit shows values $x_p < 0$. These occur since a fit is only made over the time that $x_p > \frac{1}{2}\Delta x$ or in other words for times when pyrolysis is significant. As a result the fit and the generalized equations are only valid for times when x_p (or x_e) are positive. If a negative value is calculated x_p (or x_e) is simply set to zero and pyrolysis (or evaporation) is not taking place due to an insufficiently high temperature. If this rule is followed the simple equations resulting from Table II describe the effect of initial wood density on the position of both evaporation and pyrolysis front quite accurately. So a detailed simulation is not required and x_e and x_p can even be calculated with a simple calculator.

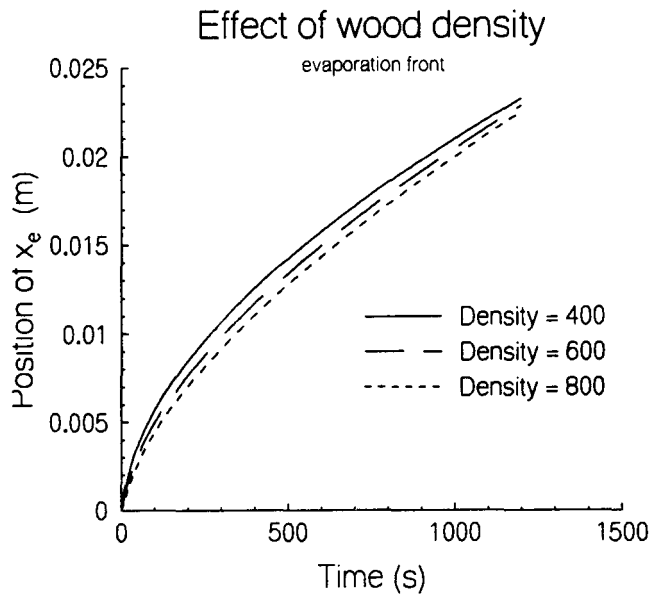

Figure 11 The evolution of the position of the evaporation front for different initial wood densities.

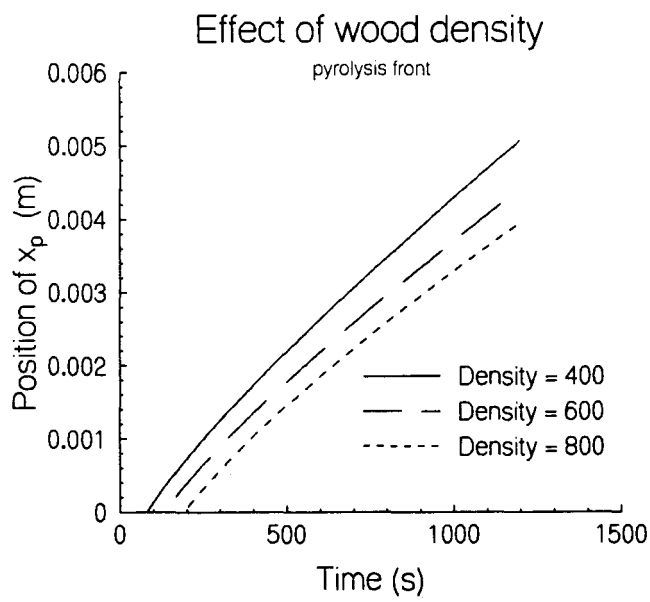

Figure 12 The evolution of the position of the pyrolysis front for different initial wood densities.

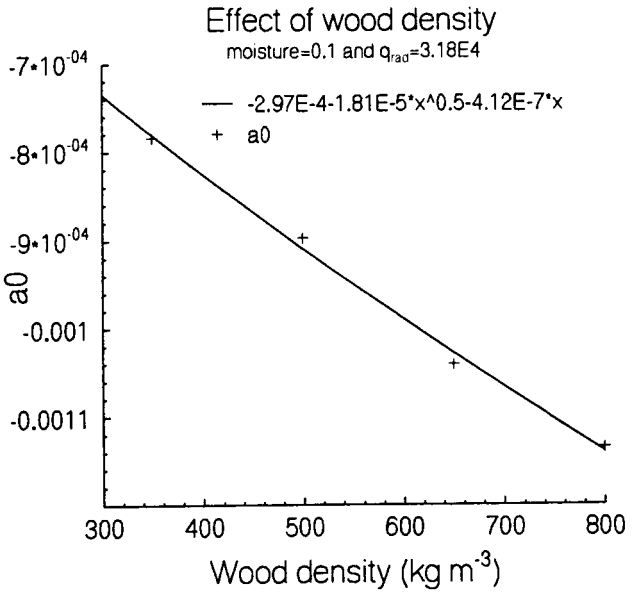

Figure 13 The effect of initial wood density of wood on the evaporation process, coefficient a_0.

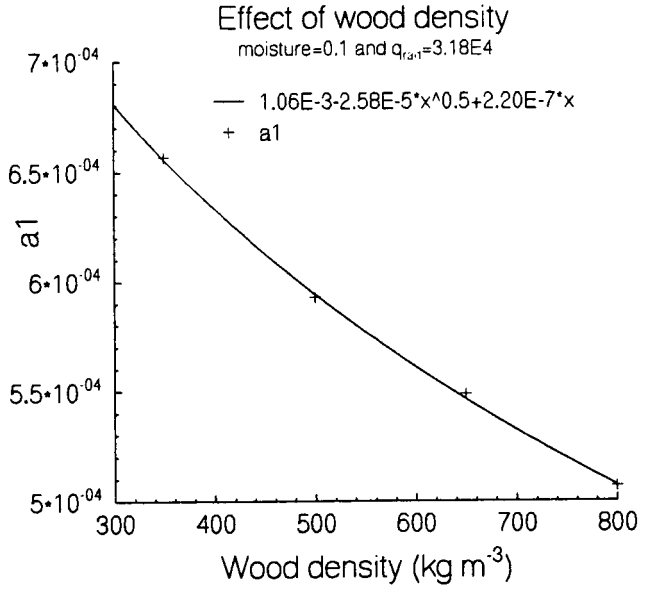

Figure 14 The effect of initial wood density of wood on the evaporation process, coefficient a_1.

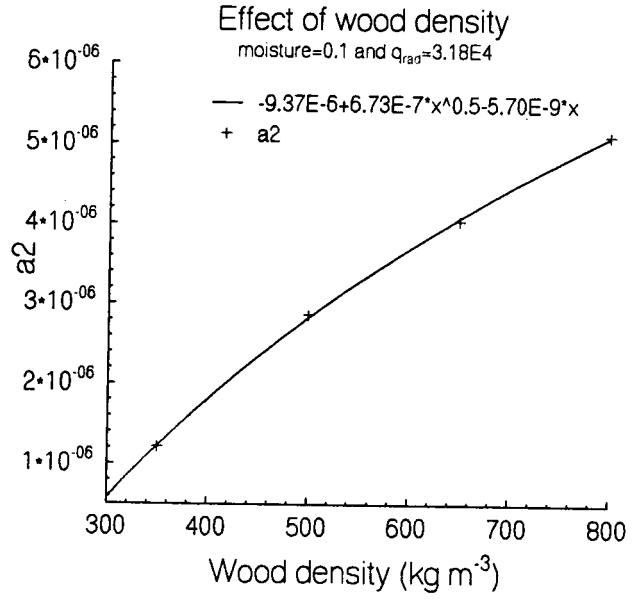

Figure 15 The effect of initial wood density of wood on the evaporation process, coefficient a_2.

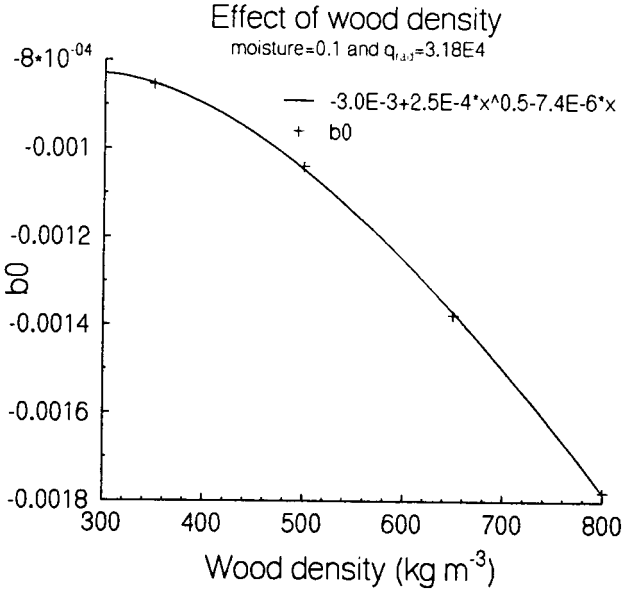

Figure 16 The effect of initial wood density of wood on the pyrolysis process, coefficient b_0.

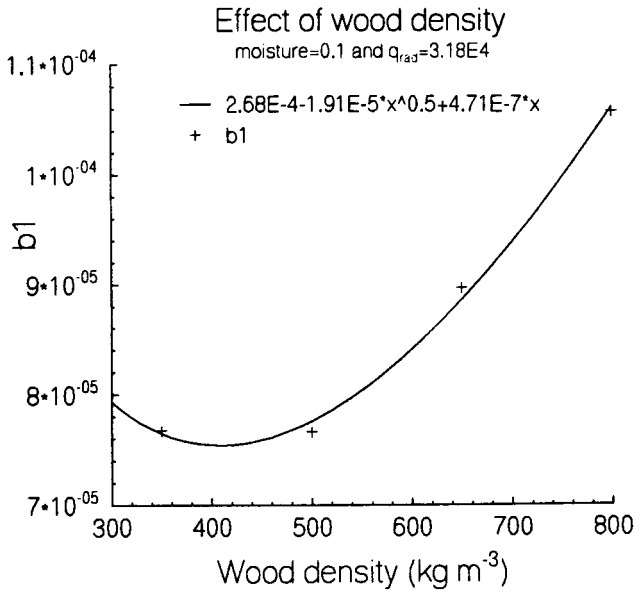

Figure 17 The effect of initial wood density of wood on the pyrolysis process, coefficient b_1.

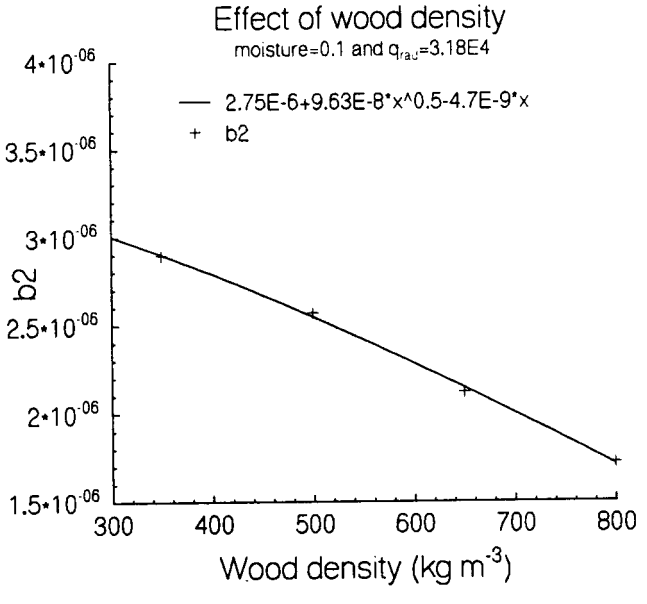

Figure 18 The effect of initial wood density of wood on the pyrolysis process, coefficient b_2.

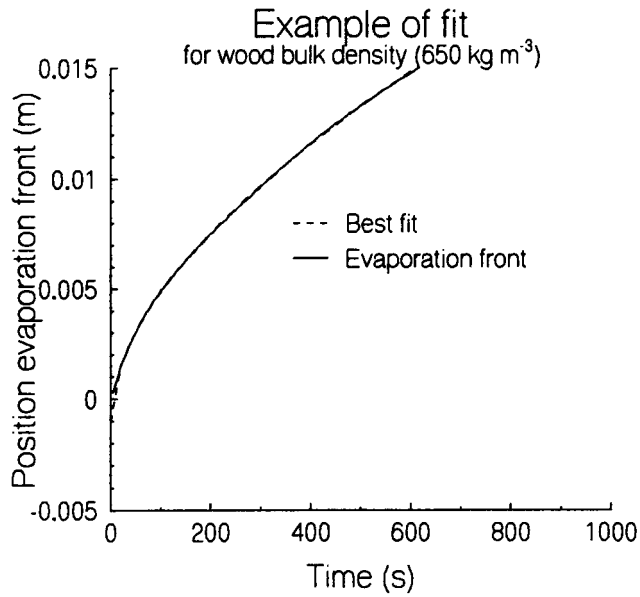

Figure 19 The position of the evaporation front for the simulation and for the best fit with (157).

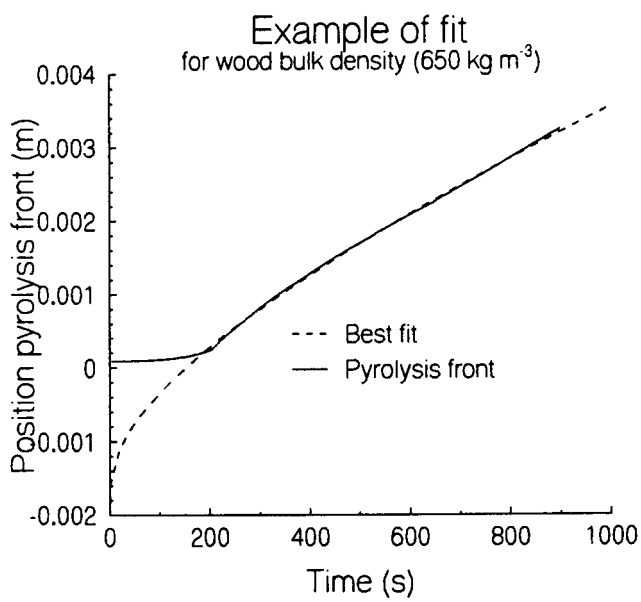

Figure 20 The position of the pyrolysis front for the simulation and for the best fit with (157).

6.4 The effect of thermal radiation

One of the most significant parameters determining the pyrolysis is arguably the thermal radiation applied to the fuel. The actual thermal radiation radiated to the fuel usually depends on the presence and distance of combustion chamber walls to a piece of wood and on other pieces of wood. This can not be determined without a detailed knowledge of stove geometry, fuel bed status, etc. Since this is not considered in this study thermal radiation levels are just chosen and set. Figure 21 shows the curves for x_e for three values of the thermal radiation q_{rad}. As can be seen a higher thermal radiation leads to a faster movement of x_e, thus to a position further away from the irradiated edge ($x = 0$) at a given time. The explanation involving the process temperature in the previous section can be repeated to explain the difference between the curves for x_e (figure 21) and the curves for x_p (figure 22). Again the qualitative explanation of the effect of thermal radiation on the front positions is quite easy and the effect is quantified by determining the thermal radiation effect on the corresponding coefficients in equation (157) Table III gives these coefficients a_i and b_i as a function of the thermal radiation q_{rad} for different moisture contents.

Table III

[m] = 0.1

$a_0 = -2.029 \cdot 10^{-3} + 3.593 \cdot 10^{-8}\, q_{rad} - 1.517 \cdot 10^{-13}\, (q_{rad})^2$

$a_1 = 7.261 \cdot 10^{-4} - 7.39 \cdot 10^{-10}\, q_{rad} - 4.946/q_{rad}$

$a_2 = -9.92 \cdot 10^{-8} + 3.752 \cdot 10^{-11}\, q_{rad} + 9.693 \cdot 10^{-2}/(q_{rad} + 1232)$

$b_0 = 4.809 \cdot 10^{-4} + 46.7/(7175 - q_{rad})$

$b_1 = -9.23 \cdot 10^{-5} + 1.27 \cdot 10^{-9}\, q_{rad} + 6.058/(q_{rad} + 10107)$

$b_2 = -1.526 \cdot 10^{-6} + 1.335 \cdot 10^{-10}\, q_{rad} - 7.041 \cdot 10^{-16}\, (q_{rad})^2$

[m] = 0.15

$a_0 = -2.235 \cdot 10^{-3} + 3.733 \cdot 10^{-8}\, q_{rad} - 1.523 \cdot 10^{-13}\, (q_{rad})^2$

$a_1 = 7.048 \cdot 10^{-4} - 9.84 \cdot 10^{-10}\, q_{rad} - 4.924/q_{rad}$

$a_2 = -2.69 \cdot 10^{-6} + 4.236 \cdot 10^{-11}\, q_{rad} + 0.1054/(q_{rad} + 1232)$

$b_0 = 5.522 \cdot 10^{-4} + 64.02/(7175 - q_{rad})$

$b_1 = -1.27 \cdot 10^{-4} + 1.446 \cdot 10^{-9}\, q_{rad} + 9.637/(q_{rad} + 10107)$

$b_2 = -3.522 \cdot 10^{-6} + 1.428 \cdot 10^{-10}\, q_{rad} - 7.201 \cdot 10^{-16}\, (q_{rad})^2$

[m] = 0.25

$a_0 = -2.122 \cdot 10^{-3} + 3.284 \cdot 10^{-8}\, q_{rad} - 1.346 \cdot 10^{-13}\, (q_{rad})^2$

$a_1 = 6.171 \cdot 10^{-4} - 6.94 \cdot 10^{-10}\, q_{rad} - 4.957/q_{rad}$

$a_2 = -3.56 \cdot 10^{-6} + 3.107 \cdot 10^{-11}\, q_{rad} + 0.1199/(q_{rad} + 1232)$

$b_0 = 1.231 \cdot 10^{-5} + 54.47/(7175 - q_{rad})$

$b_1 = -6.97 \cdot 10^{-5} + 1.587 \cdot 10^{-9}\, q_{rad} + 7.07/(q_{rad} + 10107)$

$b_2 = -2.316 \cdot 10^{-6} + 8.683 \cdot 10^{-11}\, q_{rad} - 5.237 \cdot 10^{-16}\, (q_{rad})^2$

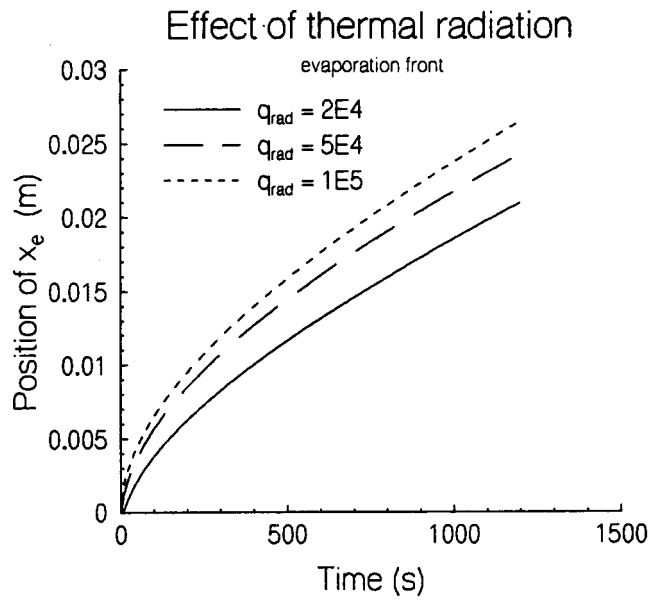

Figure 21 The effect of thermal radiation on the position of the evaporation front.

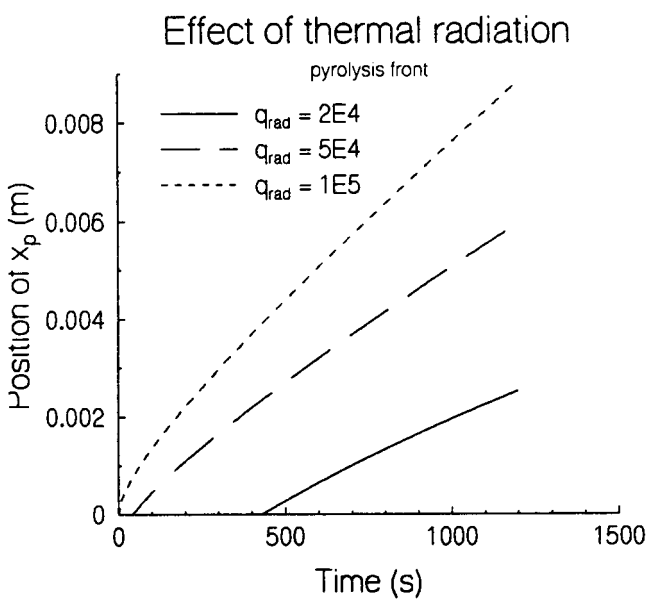

Figure 22 The effect of thermal radiation on the position of the pyrolysis front.

The effect of the thermal radiation on the coefficients of x_e and x_p is slightly more complicated than in the case of initial wood densities, however curves can be fitted to the simulation data points about as well as in the case of initial wood density. Again fits for different moisture contents were made, see Table III for the resulting coefficients. Figures 23 to 25 show the effect of the thermal radiation on the evaporation coefficients, while figures 26 to 28 show the effect on the pyrolysis coefficients.

Just as in the previous section graphs for the curves fitted with equation (157) are given so the accuracy of the fit and the generalized equations resulting from Table III can be judged. Again a representative case is taken and a best fit for the position of the evaporation front x_e can be seen in figure 29, while a best fit for the position of the pyrolysis front x_p can be seen in figure 30. Again the difference between the best fit and the generalized equations resulting from the use of Table III is too small to see on the scale of the graphs. Therefore the curves for the generalized equations are omitted.

Like the previous section $x_p < 0$ at the start, but again x_p is set to zero in those cases and no pyrolysis is assumed to occur. The generalized equations resulting from Table III describe the effect of thermal radiation on the position of the evaporation front x_e and the pyrolysis front x_p quite well. However it must be said that the thermal radiation q_{rad} should be at least 20 kW m^{-2}. The effect of lower values can not be described using equations derived from Table III. For these values of the thermal radiation the temperature increases slowly and pyrolysis sets in late at a reduced rate of pyrolysis. In fact 15 kW m^{-2} leads to some pyrolysis only after more than 900 seconds and smaller values for the thermal radiation probably do not lead to sufficiently high temperatures for significant pyrolysis. However for $q_{rad} > 20$ kW m^{-2} the effect of q_{rad} on the position of the evaporation front x_e and the pyrolysis front x_p is again well described by simple equations resulting from Table III.

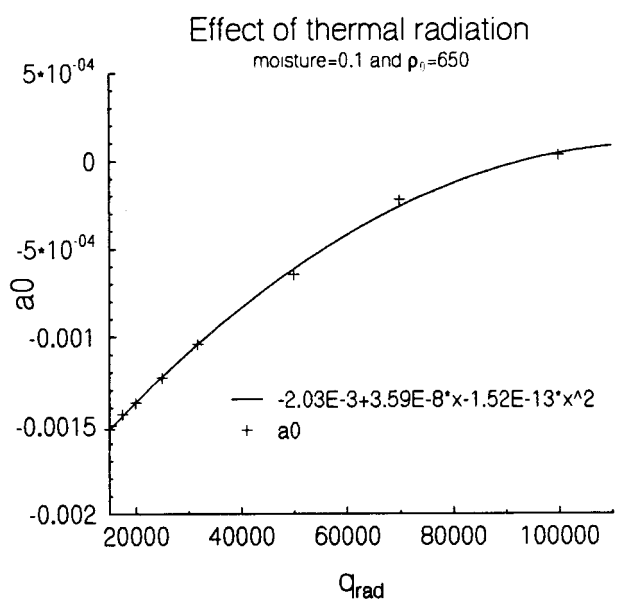

Figure 23 The effect of thermal radiation on the evaporation process, coefficients a_0.

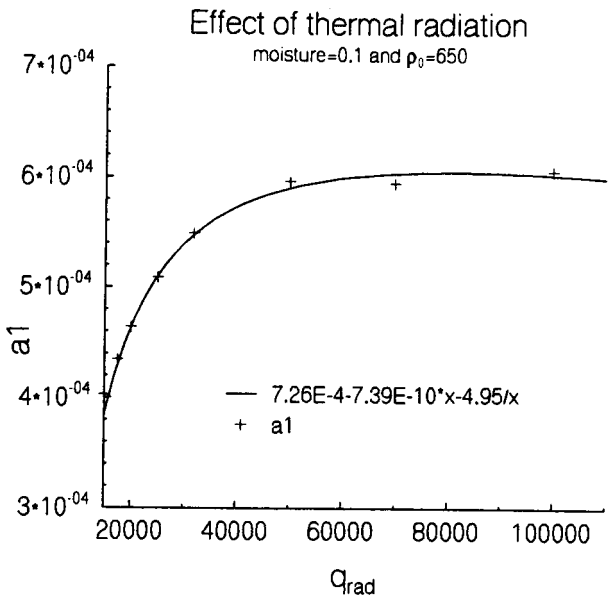

Figure 24 The effect of thermal radiation on the evaporation process, coefficient a_1.

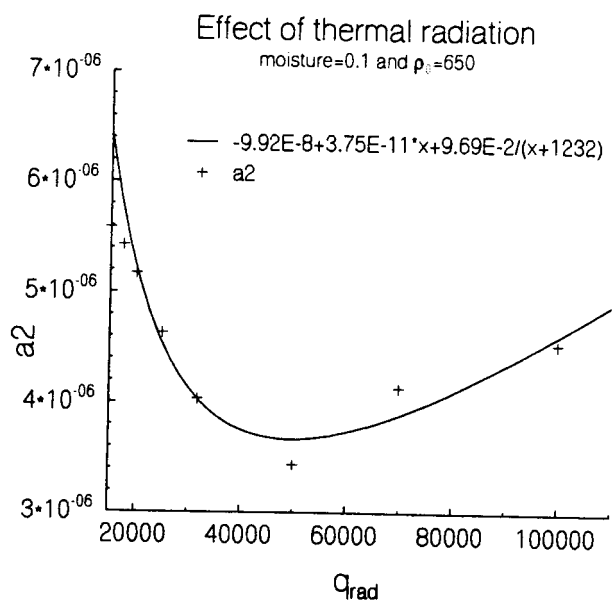

Figure 25 The effect of thermal radiation on the evaporation process, coefficient a_2.

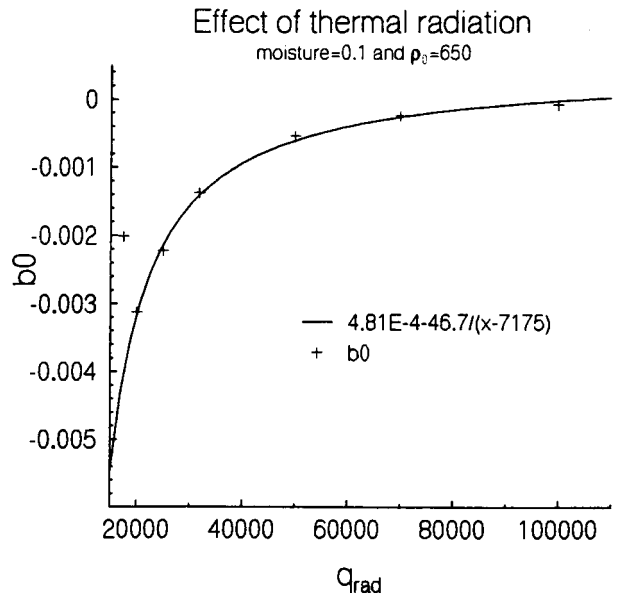

Figure 26 The effect of thermal radiation on the pyrolysis process, coefficient b_0.

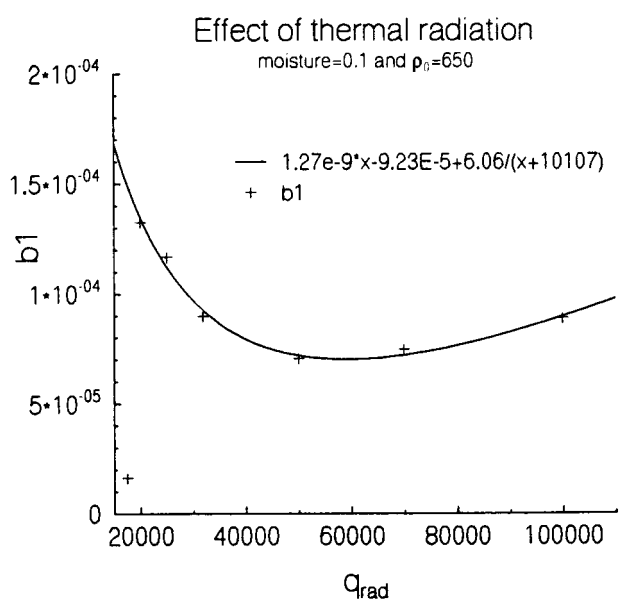

Figure 27 The effect of thermal radiation on the pyrolysis process, coefficient b_1.

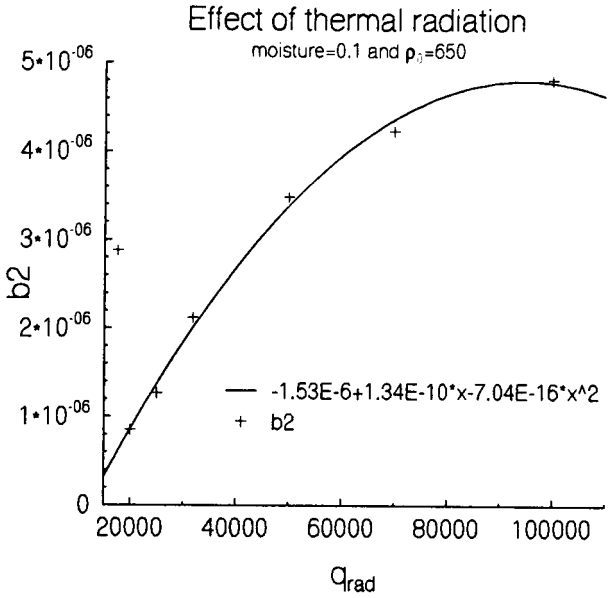

Figure 28 The effect of thermal radiation on the pyrolysis process, coefficient b_2.

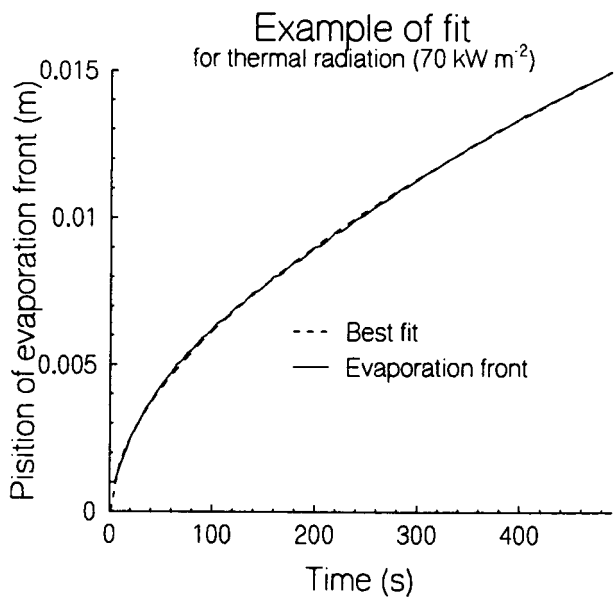

Figure 29 The position of the evaporation front for the simulation and for the best fit with (157).

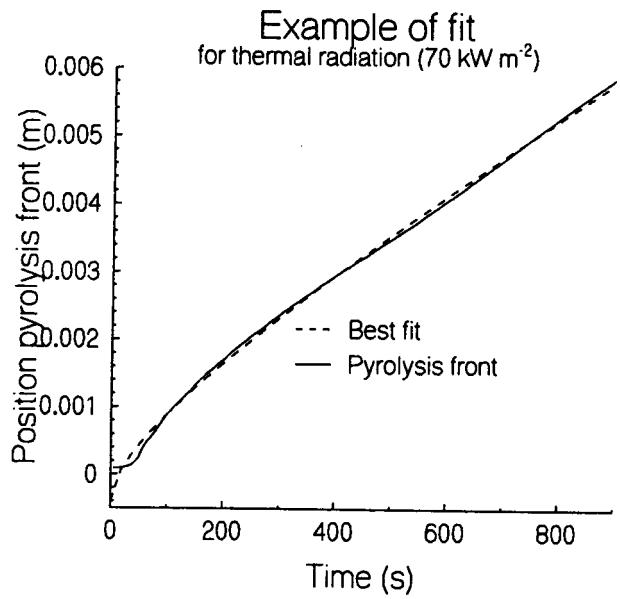

Figure 30 The position of the pyrolysis front for the simulation and for the best fit with (157).

6.5 The effect of moisture content

A parameter that can ruin the performance of wood burning systems is the moisture content of the wood. As a result it is important to know what the effect of moisture on pyrolysis and evaporation is. It is customary to express the moisture content as the weight fraction of the water on a dry matter basis, so as

$$[m] = \frac{\epsilon_\beta(0)\rho_\beta}{\rho_0} = \frac{\rho_\beta \epsilon_\beta(0)}{\rho_s \epsilon_w(0)} \tag{159}$$

with ρ_s the solid phase density (intrinsic phase average). This solid phase density is about constant between different types of wood, see Kollman and Côté (1968).

As an example figure 31 shows the curves for the position of the evaporation front for three values of the moisture content [m]. Since the moisture requires energy to evaporate it is obvious that a higher moisture content leads to a lower temperature at a given time and this leads to slower moving fronts x_e and x_p. As described in the previous sections this lower temperature results in a front which at a given time is closer to the irradiated boundary. So figure 31 and 32 are qualitatively explained since both show a front position closer to the irradiated edge ($x=0$) for higher moisture contents. As in the previous sections an attempt is made to get a quantitative expression for the effect of the moisture contents [m] on x_e and x_p, but unlike the effects of wood density and thermal radiation this one is quite complicated and it is quite difficult to get good fits for the simulation data points. The data points are more or less described by equations of the general form:

$$c_i = e_0 + (e_1[m] + e_2)\exp(-e_3[m]) \tag{160}$$

with the coefficient notation as before. In some cases the middle term does not result in a better description, so in those cases it was not included. For the moisture dependence of all the coefficients see table IV. The fits for x_e are still quite reasonable, however the fits for x_p are really unacceptable. It appears that no fit of a single parameter curve (parameter moisture content [m]) is possible. It is not at all clear what the reason for this is. One possibility is that the temperature at the pyrolysis front x_p is mainly determined by the hot part of the piece of wood. In those parts there is no moisture present anymore, thus some other parameter has a large effect on x_p. On the other hand x_p can never pass x_e, so there is still some effect of the moisture content too. Probably a two or more parameter function can be fitted to x_p. The effect of the moisture content on the

Table IV Coefficient values describing the moisture dependance.

$a_0 = -1.25\cdot10^{-3} + 1.268\cdot10^{-3}\exp(-17.94\,[m])$
$a_1 = 2.751\cdot10^{-4} + (3.2\cdot10^{-3}\,[m] + 2.406\cdot10^{-4})\exp(-7.181\,[m])$
$a_2 = 8.152\cdot10^{-7} + 2.789\cdot10^{-5}\exp(-22.14\,[m])$
$b_0 = -2.43\cdot10^{-3} + (2.173\cdot10^{-2}\,[m] - 1.6\cdot10^{-4})\exp(-10.83\,[m])$
$b_1 = 1.541\cdot10^{-4} + (-1.971\cdot10^{-3}\,[m] + 3.754\cdot10^{-5})\exp(-13.29\,[m])$
$b_2 = -6.03\cdot10^{-7} + (6.982\cdot10^{-5}\,[m] - 1.779\cdot10^{-6})\exp(-13.25\,[m])$

coefficients describing the evaporation is shown in figure 33 to 35 and the effect on the coefficients of the pyrolysis process is shown in figure 36 to 38.

Again a typical case is taken and direct simulation results, fitted results and generalized equations resulting from Table IV are compared for the front positions. Figure 39 shows the direct simulation results (solid line) and the best fit to those results using equation (157) (dashed line) for the evaporation front. Again the best fit and the generalized equations resulting from Table IV could not be distinguished on the scale of the graph, so the latter was dropped. However for the pyrolysis front a clear distinction could be made between the best fit and the curve obtained using Table IV, so both curves are presented in figure 40 together with the pyrolysis front position actually obtained from the corresponding simulation. Again the best fit describes the position of the pyrolysis front quite well, but the expressions in Table IV are not sufficiently reliable to be used for the determination of x_p. However it is possible to use the table to determine the position of the evaporation front.

The effect of moisture on pyrolysis is still not quantified very well. Therefore a closer look into the mathematical problem of a solid heat conduction equation with a moving singular heat sink is needed. Fundamental solutions or good approximate solutions to this problem can most likely be found in the literature and give a better idea of which function describes the effect of moisture.

Of course the equations describing singled out effects of initial wood density, thermal radiation and moisture are not very useful. Ideally the effects of all these parameters should be incorporated into a single equation. However this proves to be quite difficult and is left for future research. Also a large number of experiments and simulations are needed in order to determine reasonable estimates for frequency factors and activation energies. Other experiments are needed to determine permeability, thermal conductivity and the constant C_{evap} occurring in the combined Clausius-Clapeyron-Kelvin equation. This is also left for future research.

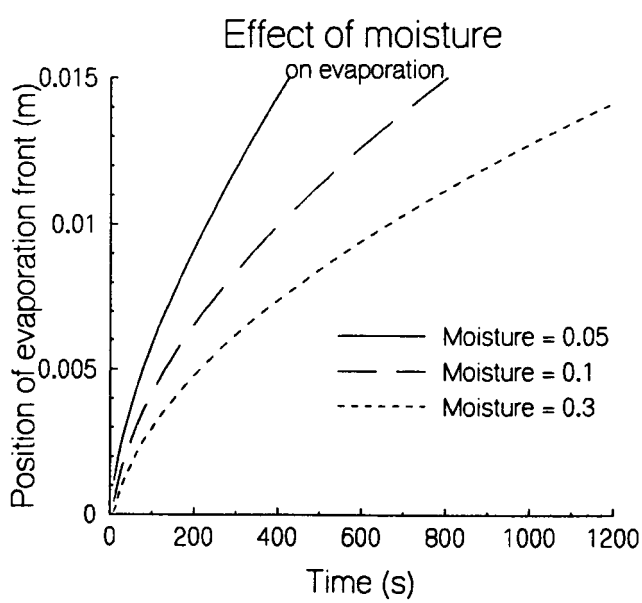

Figure 31 The effect of moisture on the position of the evaporation front.

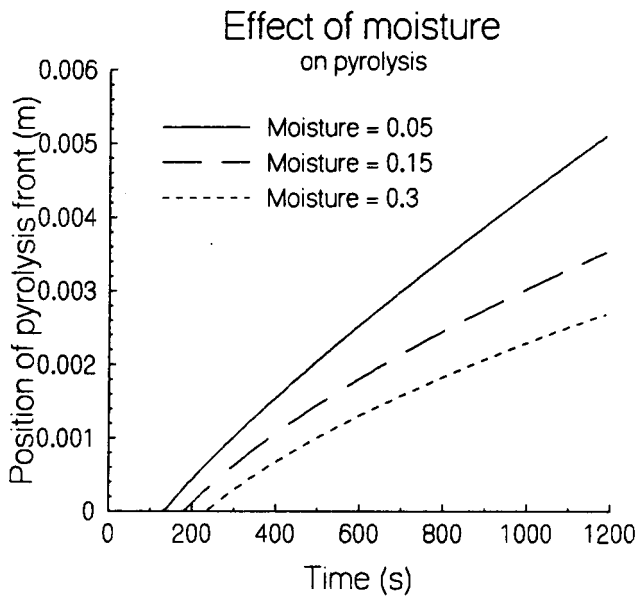

Figure 32 The effect of moisture on the position of the pyrolysis front.

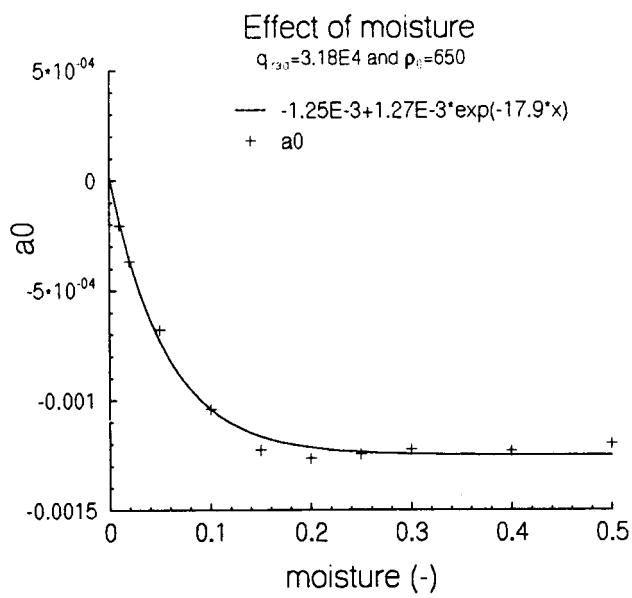

Figure 33 The effect of the moisture content on the evaporation process, coefficient a_0.

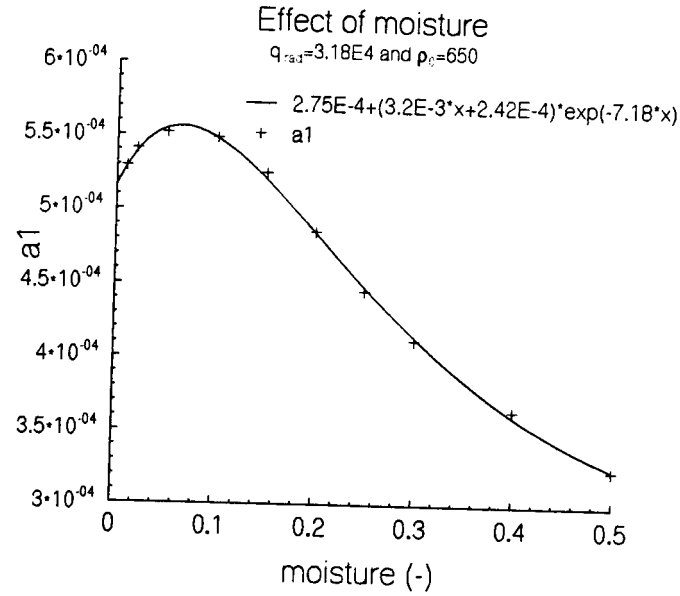

Figure 34 The effect of the moisture content on the evaporation process, coefficient a_1.

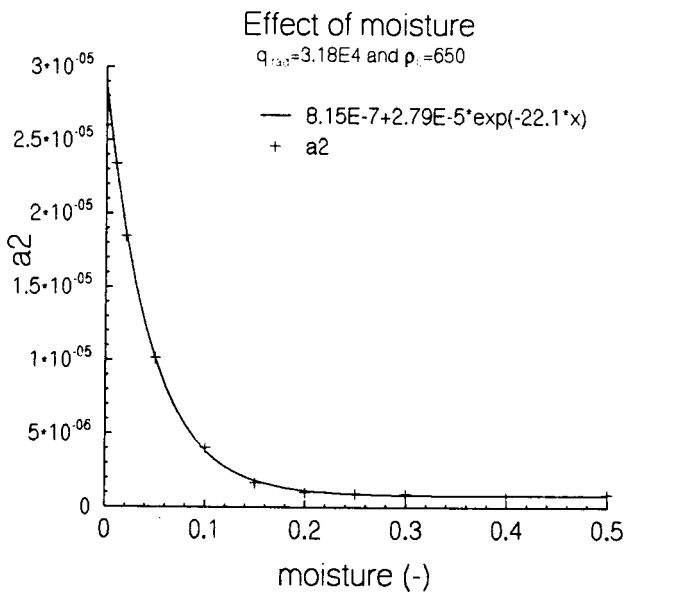

Figure 35 The effect of the moisture content on the evaporation process, coefficient a_2.

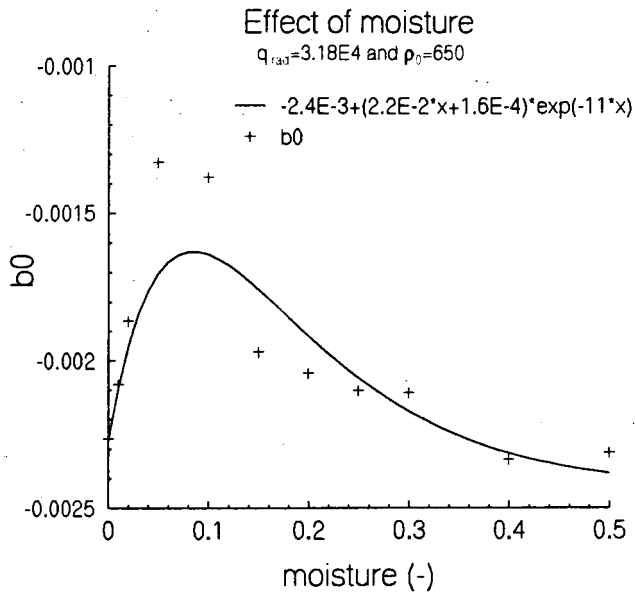

Figure 36 The effect of the moisture content on the pyrolysis process, coefficient b_0.

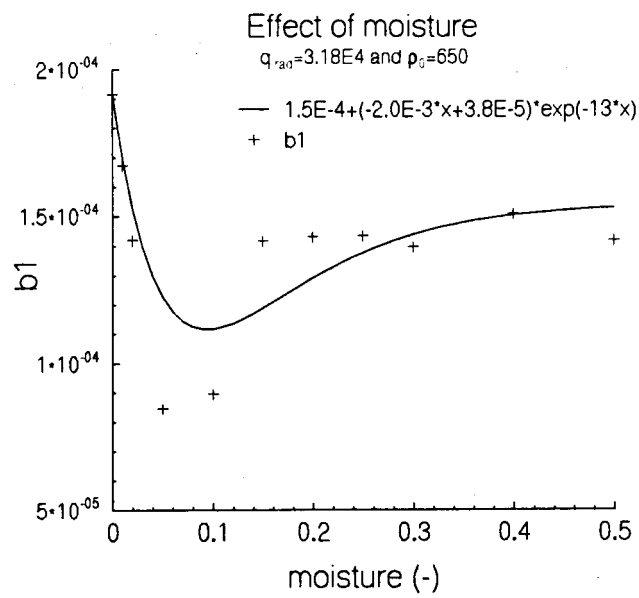

Figure 37 The effect of the moisture content on the pyrolysis process, b_1.

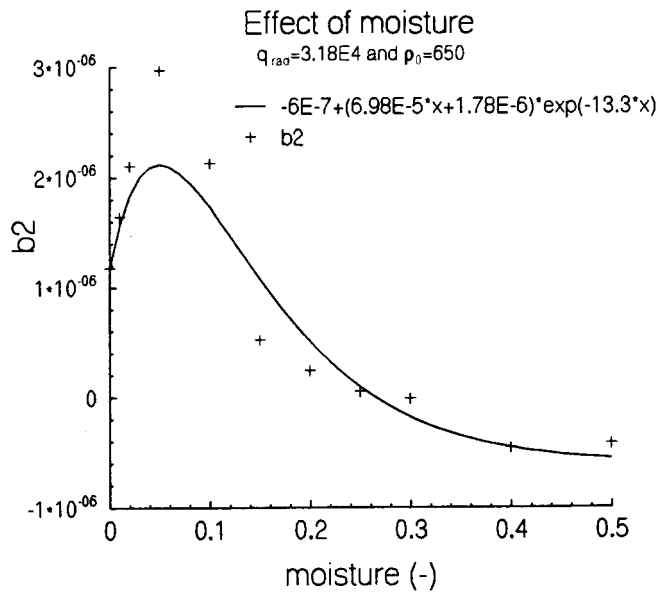

Figure 38 The effect of the moisture content on the pyrolysis process, coefficient b_2.

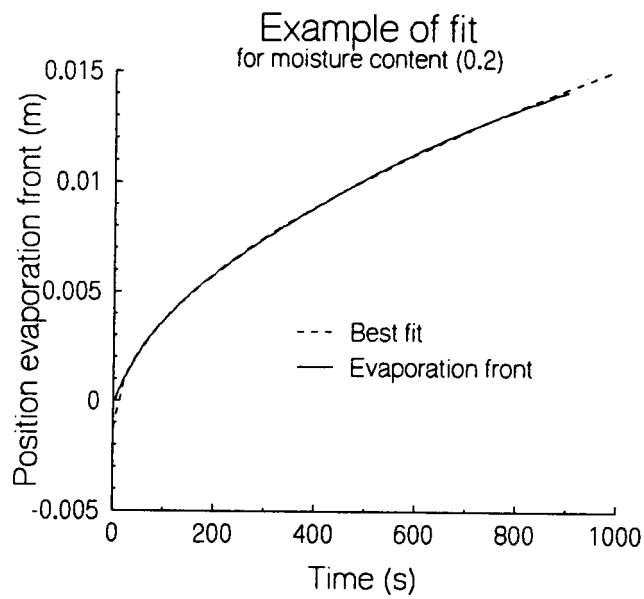

Figure 39 The position of the evaporation front for the simulation and for the best fit with (157).

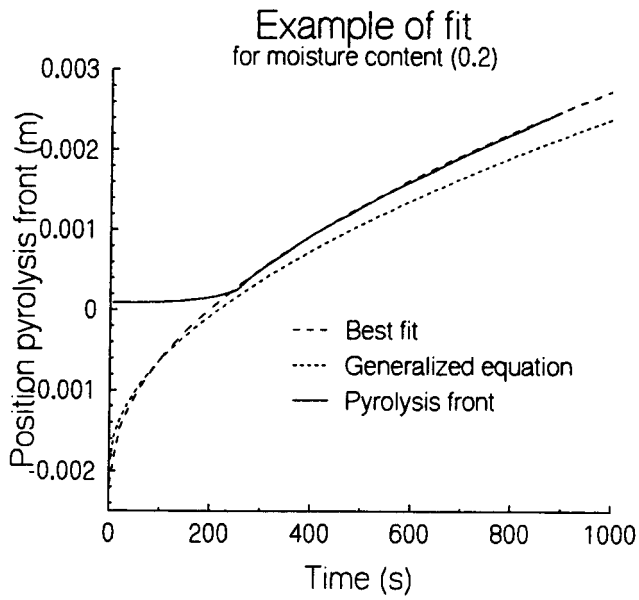

Figure 40 The position of the pyrolysis front for the simulation, for the best fit with (157) and for the curve obtianed using Table IV.

7 Context of this study

Cooking in most of the developing countries is done with wood mostly on open fires. Two problems related to the use of wood fires are health problems associated with wood smoke emitted by the fire and desertification due to fuel wood use in some sensitive areas like eg. areas around cities in sub-Saharan countries. Developing agencies and Non-Governmental Organizations are trying to reduce these problems by fuel switching and by developing improved wood stoves. As the name suggests with fuel switching other fuels like kerosene, natural gas, biogas and electricity are used for cooking. Unfortunately the supply of these fuels in developing countries is often problematic especially in rural areas and small cities. Also the cost of these fuels is often high, again especially in rural areas and small cities where fuel wood is usually free or almost free. Because of the disadvantages of fuel switching the dissemination of improved wood stoves is still popular in the fight against desertification and wood smoke induced health problems. Presently there seems to be no wood stove available that is fuel efficient, has acceptable smoke emissions and is affordable for the users in developing countries. Some people have made wild claims, but lab tests at for instance the Woodburning Stoves Group in Eindhoven always showed a failure to operate with acceptable smoke emissions and sometimes disappointing efficiencies too. Regarding smoke emission levels a notable exception is the so-called 'downdraft stove' developed and tested extensively in Eindhoven. Unfortunately its efficiency is disappointing and its cost is far too high for use in developing countries. However affordable clay and ceramic versions might be developed successfully.

Years of testing of especially the downdraft stove at the Woodburning Stove Group lead to the conclusion that the combustion quality (CO/CO_2 ratio) is very sensitive to the air supply, see Krishna Prasad and Moerman (1991) and Moerman (1991). Adding wood to the fire every minute or so is best for the combustion quality. However this is not very user friendly, so the time between two wood charges should be at least 15 minutes. In order to obtain a good combustion quality throughout such an interval requires a way of matching the air supply to the volatile and charcoal power output. An additional requirement is being able to control the pyrolysis rate, so fuel use can be reduced when less power is needed for cooking. In order to be able to determine the most fuel efficient operation of a stove configuration it is necessary to have at least some idea of the power output of a stove. Bussmann (1988) presented a model for an open fire and a model for a 'shielded fire' (as the name suggests this is basically a fire with a wind shield around it). These models enable the prediction of the stove efficiency if both the volatile and charcoal power output are known. Bussmann used a model suggested by Verhaart (1983) for the prediction of the volatile power. Verhaart assumes that all pieces of wood in a batch thrown onto a fire all ignite at once and have a constant fire penetration rate. What Verhaart calls fire penetration rate is basically what was called the velocity of the pyrolysis front in this study. A notable difference is that Verhaart does not distinguish an evaporation front. Also his model requires experimental determination of the fire penetration rate for every situation. So a change in wood type, moisture content or fuel bed temperature requires an experiment to determine the fire penetration rate. For the design of new improved stoves or the adaptation of old ones to new circumstances this is cumbersome to say the least. The study presented in this report is a marked improvement since only a few experiments

are required to determine values for some parameters like for instance activation energies and effects of other parameter values and circumstances follow from the model. Verhaart's model assumes that the fire penetration rate is constant and the moisture content is only taken into account by adjusting the caloric value of the volatile gases. Bussmann determined the fire penetration rate by measuring the maximum power output and the corresponding weight loss rate. The fire penetration rate c then follows from Verhaart's assumption of a constant fire penetration rate. In one-dimension this becomes:

$$c = \frac{P_{v,max}}{0.8\rho_w B_v w h} \tag{161}$$

The factor 0.8 in the numerator occurs since a fraction 0.8 of the original wood bulk density ρ_w is turned into volatile gases. Furthermore $P_{v,max}$ is the maximum measured power output, B_v the caloric value of the volatile gases, w the width and h the height of the piece of wood. Verhaart assumes the pyrolysis starts at the moment the piece of wood is added to the fire. This is not completely correct since it takes some time for the sides of the wood to reach the pyrolysis temperature. The simulations done as a part of this study showed that it can take several minutes before a significant pyrolysis rate is obtained. As the pyrolysis front (fire penetration) is deeper inside the piece of wood heat has to travel a longer path. Therefore it stands to reason that the actual fire penetration rate slows down with time. This could be observed in the graphs of evaporation front position x_e and pyrolysis front position x_p in the previous chapter. However Verhaart assumes it is constant, so he predicts too high a value after some time. For times close to zero the speed at which x_e and x_p travel is very high, so Verhaart's fire penetration rate c is smaller at those times. The power output depends basically linear on the fire penetration rate, and these effects can be found in the power output graphs of figure 41.

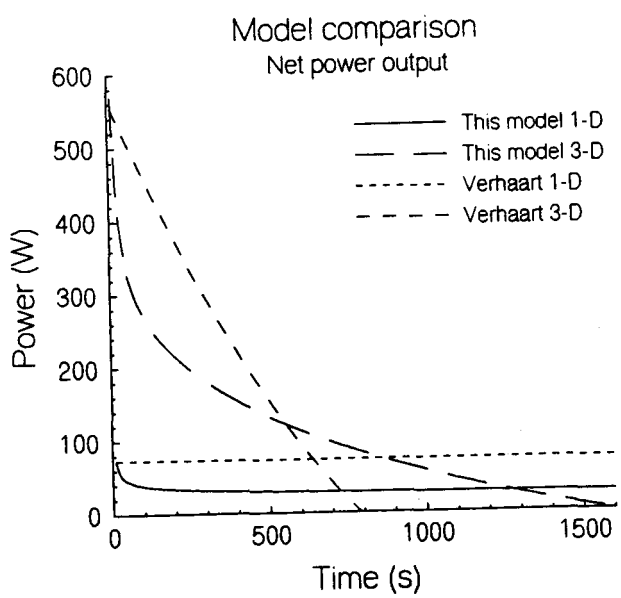

Figure 41 Power output according to this study and according to Verhaart in 1-D and 3-D.

If pyrolysis and evaporation occur in three dimensions equally in all directions then after some time the surface area of unreacted wood is much smaller for Verhaart's model than for this study, since Verhaart's fire penetration rate c is larger than the speed of x_p. Therefore there is far less wood available to pyrolyse, so at that time the power output obtained by Verhaart is less than that obtained in this study. This can be seen when the graphs for both 3-D cases in figure 41 are compared. For the one-dimensional case no surface area change occurs and the volatile power is obtained by Verhaart is larger than that from this study over the whole interval as can be seen when the graphs for both 1-D cases in figure 41 are compared.

It would seem that the model used in this study is a significant improvement on the model used by Verhaart (1983) and Bussmann (1988) since this study models processes that are discarded by the latter. For completeness figure 42 shows the separate contributions of the power needed for moisture evaporation and the power provided by the volatile gases in one-dimension. Since the moisture content is only 0.1 the power loss due to moisture evaporation is much smaller than the power output for the volatile gases. Figure 43 shows the same graph for the three-dimensional case.

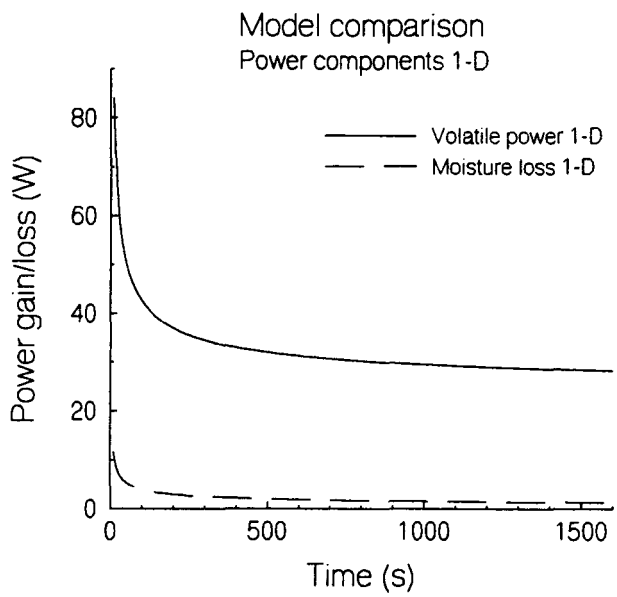

Figure 42 Volatile power and power required for moisture evaporation according to this study (1-D).

The mass evolution of a pyrolysing piece of wood is shown in figure 44. For comparability the weight of the piece of wood is made dimensionless. Again for each model 1-D and 3-D cases are distinguished. The graphs show that the mass of the wood for the model used by Bussmann and Verhaart is a little larger than for this study for the first 100 to 150 seconds. This is because the speed at which x_e and x_p travel for times close to zero is very high. This can be explained by the energy equation which can be simplified (certainly for small times) to a heat conduction equation. With the sudden switch-on of thermal radiation at $t=0$ its fundamental solutions are singular for $t=0$. Therefore for times close to $t=0$ the results are incorrect. After 150 seconds the mass according to Bussmann and Verhaart is smaller than that found with the model in this study. This is due to the over-prediction of the fire penetration rate by Verhaart for large times.

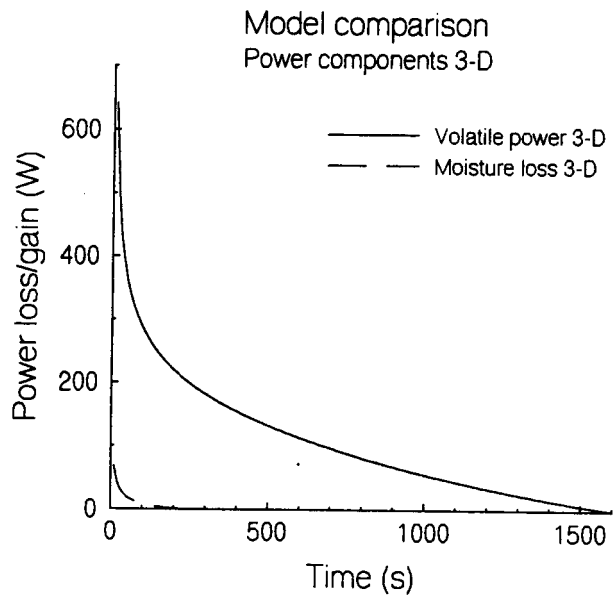

Figure 43 Volatile power and power required for moisture evaporation according to this study (3-D).

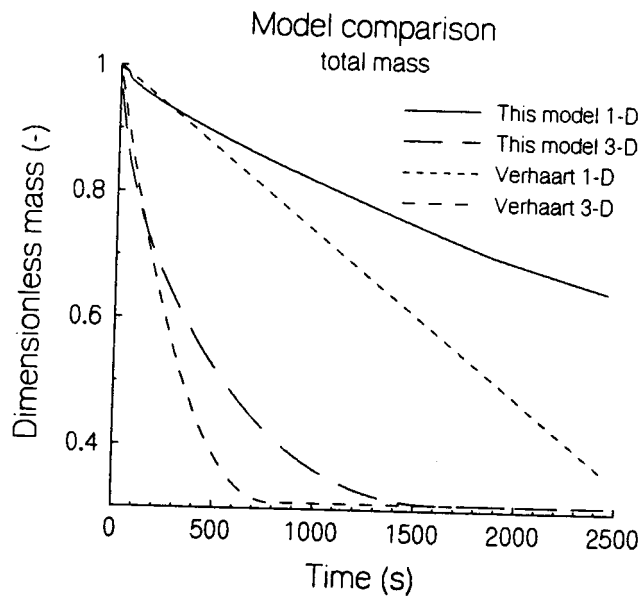

Figure 44 Mass evolution according to this study and according to Verhaart in 1-D and 3-D.

8 Conclusions and recommendations

The usual parameters that are investigated in pyrolysis studies are frequency factors, activation energies, heat of reaction and permeability. These parameters are very difficult to determine and their values are usually very uncertain. Therefore it is not very useful to study these parameters when the aim is a model to help design small wood burning devices. From that point of view it is far more useful to investigate the effects of parameters like initial wood density, thermal irradiation and moisture content. These parameters can be determined easily and accurately. In most pyrolysis studies variables like gas densities and gas pressures are studied. Unfortunately these variables are seriously affected by discretization effects when moisture is included. Temperature and phase volume fraction profiles are less sensitive for discretization effects. Capturing the pyrolysis process in a single time dependent variable and the evaporation process in another single time dependent variable makes the analysis easier. A pyrolysis front and an evaporation front were introduced in the simulation and their positions were calculated to describe the pyrolysis respectively the evaporation process. The fronts move in a manner that can be expected on the basis of the process temperatures; around 373 K for the evaporation process and 450-650 K for the pyrolysis process. The position of both fronts is very well described by a second order polynomial of the square root of time, so by $a_0 + a_1\sqrt{t} + a_2 t$. The coefficients in this equation depend on the simulation parameters e.g. initial wood density, thermal irradiation and moisture content.

The effect of the initial wood density ρ_0 on these coefficients a_i is easily and accurately described by a second order polynomial of $\sqrt{\rho_0}$, see Table II. The effect of thermal radiation q_{rad} is more complicated and less accurate. Some coefficients are given by a second order polynomial in q_{rad}. However the remaining coefficients are still described with sufficient accuracy and by simple equations, see table III. Matters get far more complicated for the effect of the moisture content. Reasonable descriptions are only possible for the evaporation process, however the effect of the moisture content on the pyrolysis coefficients is very hard to describe. The best that was managed so far were the equations in table IV, but these descriptions are quite crude, as is especially clear in figures 36 to 38.

The use of the evaporation front and pyrolysis front, especially with the use of the tables, makes it very easy to predict the power output of a piece of wood as a function of time and some other parameters. This power output can be calculated without the need of specialized computer programmes. This makes it well suited for field workers who can now access this potentially valuable information. The power output can also be used as input for the open fire and 'shielded fire' models of Bussmann (1988).

Attempts to combine the effects of initial wood density, thermal irradiation and moisture content were not successful. In order to succeed in this description more simulations are needed. Also experiments should be done in order to determine to what extent the introduced pyrolysis and evaporation fronts exist in reality and how they propagate. To do this the positions of these fronts should be determined during experiments. The usual density analysis at the end of the experiment is too cumbersome and reduces the reproducibility. In the commercial sector it is already common to measure the electric resistance of the wood to determine its moisture content. With proper

calibration procedures this might be a viable method in lab experiments too. Probably the electric resistance can also be used to determine the position of the pyrolysis front. Further research into these possibilities is recommended, since it can lead to fast, detailed data.

Di Blasi enthusiastically introduced two volatile gas components formed during the pyrolysis process in order to explain the occurrence of endothermic pyrolysis reactions in some cases and exothermic reactions in others. Another simpler method to explain the experimentally observed pyrolysis reaction energies seems to be only two pyrolysis reactions; one forming a volatile gas and one forming char. However contrary to Di Blasi's assumption the two reactions would then have different reaction energies. Their enthalpy should be chosen in such a way that the char enthalpy is equivalent to the correct combustion value of the char, which is about 33 MJ/kg. The enthalpy for the volatile gas then follows from the enthalpy of the char and the combustion value of the unreacted wood. This also makes the inclusion of char combustion a little more consistent. As long as the activation energies for the gas and the char reactions are chosen different, endothermic and exothermic reactions can result in different temperature regimes as experimentally observed. This method is a lot simpler and far more easy to analyze than the two component pyrolysis gas used by Di Blasi. Unfortunately time considerations did not permit us to try out this method, but it should be looked into if a simple and relatively accurate model is desired.

9 Literature

Anderson, J. D., 1995. Computational fluid dynamics - The basics with applications. McGraw-Hill, New York.

Bussmann, P.J.T, 1988. Woodstoves - Theory and applications in developing countries. Ph.D. thesis Eindhoven University of Technology.

Bussmann, P.J.T and Krishna Prasad, K., 1986. Parameter analysis of a woodburning cookstove. In: Proceedings 8th International Heat Transfer Conference, Hemisphere, Washington.

Cheng, P., 1978. In: *Advances in heat transfer*, Hartnett, J.P. and Irvine, T.F (Eds.). Vol. 14, Academic press, New York, pp. 1-105.

Defay, R., Prigogine, I, and Bellemans, A., 1966. Surface tension and adsorption. Wiley, New York.

Di Blasi, C., 1993. Analysis of convection and secondary reaction effects within porous solid fuels undergoing pyrolysis. In: *Combust. Sci. and Tech.*, Vol. 90, pp. 315-340.

Emmons, H.W. and Atreya, A., 1983. The science of wood combustion. In: Wood heat for cooking, Prasad, K. Krishna and Verhaart, P. (Eds.). Indian Academy of sciences, Bangalore, India, pp. 5-14.

Gray, W.G., 1975. A derivation of the equations for multi-phase transport. In: *Chem. Eng. Sci.* 30, pp. 229-233.

Hämmerlin, G and Hoffmann, K.H., 1991. Numerical mathematics. Springer-Verlag, New York.

Kailasanath, K. and Zinn, B.T., 1981. A theoretical investigation of the smoldering combustion of porous solids. In: *Fluid mechanics of combustion systems*, Morel, T., Lohmann, R.P. and Rackley, J.M (Eds.).

Krishna Prasad, K., 1986. Fuel properties and the design of multi-fuel stoves. Woodburning Stove Group, Eindhoven University of Technology, The Netherlands.

Krishna Prasad, K. and Moerman, E., 1991. Clean combustion using natural draft. Paper presented at the Third National Solar Energy Conference, Noordwijkerhout, The Netherlands, April 4-5, 1991.

Kollman, F.P.F. and Côté, W.A., 1968. Principles of wood science and technology, Springer-Verlag, Heidelberg.

Laurendeau, N.M., 1979. Heterogeneous kinetics of coal char gasification and combustion. In: *Prog. Energy Combust. Sci.*, Vol. 4, pp. 221-270.

Moallemi, M.K., Zhang, H and Kumar, S, 1993. Numerical modelling of two-dimensional smoldering processes. In: *Combustion and flame*, Vol. 95., pp. 170-182.

Moerman, E. and Krishna Prasad, K., (1991). Clean combustion and excess air factors. Paper presented at the First International Conference on Combustion Technologies for a Clean Environment, Vilamoura (Algarve), Portugal, September 3-6, 1991.

Patankar, S.V., 1980. Numerical heat transfer and fluid flow. Hemisphere publishing corporation, Washington.

Shen, J. and Smith, J.M., 1965. Diffusional effects in gas-solid reactions. In: *I&EC Fundamentals*, Vol. 4, No. 3, pp. 293-301.

Slattery, J.C., 1967. General balance equation for a single phase interface. In: *Ind. Eng. Chem. Fundam.* 6, pp. 108-118.

Slattery, J.C., 1972. Momentum, energy, and mass transfer in continua. McGraw-Hill, New York.

Verhaart, P., 1983. On designing woodstoves. In: *Wood heat for cooking*, Krishna Prasad, K. and Verhaart, P. (Eds.). Indian academy of sciences, Bangalore, pp. 33-72.

Wen, C.Y. and Wei, L.Y., 1971. Simultaneous non-isothermal non-catalytic solid-gas reactions. In: *AIChE Journal*, Vol. 17, No. 2, pp. 272-280.

Whitaker, S., 1969. Advances in the theory of fluid motion in porous media. In: *Ind. Eng. Chem.* 61, pp. 14-28.

Whitaker, S., 1977. Simultaneous heat, mass, and momentum transfer in porous media: A theory of drying. In: *Advances in heat transfer*, Hartnett, J.P. and Irvine, T.F (Eds.). Vol. 13, Academic press, New York, pp. 119-203.

List of symbols

Greek symbols

δ thickness

ϵ volume fraction (-)

ϵ_{acc} desired relative accuracy

$\epsilon_{\beta e}$ average liquid volume fraction in the control volume containing the evaporation front (-)

η indicates the amount of cracking of the channel walls

$\eta = 0$ maximum cracking, permeability is maximal = $K_{\gamma,c}$ (permeability char)

$\eta = 1$ minimum cracking, permeability is minimal = $K_{\gamma,w}$ (permeability wood)

κ_γ bulk viscosity for the gas phase (Pa s)

λ unit tangent vector along curve s

μ_γ shear viscosity for the gas phase (Pa s)

ξ parameter describing the alignment of wood fibres

$\xi = 0$ fibres mixed

$\xi = 1$ fibres aligned

ρ density (kg m^{-3})

σ Stefan-Boltzmann constant = $5.78 \cdot 10^{-8}$ W m^{-2} K^{-4}

$\sigma_{\beta\gamma}$ surface tension of the interface between the liquid β and gas γ phase

τ time at which pyrolysis becomes significant (s)

Symbols

a_i i-th coefficient of the second order polynomial in $\sqrt{t}$ describing x_e

A frequency factor (s^{-1})

A_{ij} surface area of the interface between phase i and j (m^2)

b_i i-th coefficient of the second order polynomial in $\sqrt{t}$ describing x_p

c_i coefficient denoting the coefficient a_i or b_i

c_p specific heat at constant pressure (J kg^{-1} K^{-1})

C_{evap} constant in the combined Kelvin and Clausius-Clapeyron equation (-)

C_p total specific heat over all phases (J kg^{-1} K^{-1})

d mean diameter of the particles that constitute the porous medium; in this case probably more or less equivalent to mean diameters of gas channels in the wood

d_i i-th coefficient of the second order polynomial in $\sqrt{\rho_0}$ describing the value of a coefficient c_i

E_a activation energy (J $mole^{-1}$)

f unspecified function

g gravity vector (m s^{-2})

h enthalpy (J kg^{-1})

h^0 enthalpy at reference temperature T^0 (J kg^{-1})

ΔH_{ij} reaction heat for the reaction from substance i to j (J kg^{-1})

k	thermal conductivity (tensor) (W m^{-1} K^{-1})
k_{eff}	effective heat conductivity of a fibrous material with partially aligned fibres
k_{min}	minimum total heat conductivity of a fibrous material with perfectly aligned fibres
k_{max}	maximum total heat conductivity of a fibrous material with perfectly aligned fibres
$k_{w\parallel}$	thermal conductivity parallel to the wood grain
$k_{w\perp}$	thermal conductivity perpendicular to the wood grain
K	reaction rate (s^{-1})
K_γ	gas phase permeability tensor
L	latent heat for water = 2.26 MJ kg^{-1}
L	length of the wood sample (m)
[m]	moisture content (fraction) on a dry matter basis (-)
m_γ	integral as defined in equation (91)
M	molecular mass (kg $mole^{-1}$)
M_γ	matrix that maps $<\boldsymbol{v}_\gamma>$ linear into $\boldsymbol{v}_\gamma$
$\boldsymbol{n}_{ij}$	unit vector associated with surface area A_{ij} (-)
N	total number of gas components (-)
p	pressure
$\boldsymbol{q}$	heat flux (W m^{-2})
r	length characteristic for the gas channels in wood (m)
R	universal gas constant = 8.319 J $mole^{-1}$ K^{-1}
s	arbitrary curve that doesn't pass any liquid phase regions
S	source term in the energy equation (W m^{-3})
t	time (s)
Δt	time step (s)
T	temperature (K)
T^o	reference temperature (K)
T_o	surface temperature
$\boldsymbol{v}$	velocity (m s^{-1})
V	volume (m^3)
x	position (m)
x_e	position of the evaporation front (m)
x_p	position of the pyrolysis front (m)
Δx	distance between interior grid points (m)

indices

β	liquid phase
γ	gas phase
σ	solid phase
0	initial value
amb	ambient
b	boiling
c	char
e	east

G	GAS
i	counting index
j	counting index
k	counting index
l	control volume left of considered volume
m	material
n	gas component n
N2	nitrogen
O2	oxygen
r	control volume right of considered volume
rad	radiant
T	TAR
v	vapour
w	wood

Annex

The difference equations for the simulation derived in chapter 5 are one-dimensional and are insufficient to describe realistic situations. Experiments at the Woodburning Stove Group are usually done with rectangular blocks of wood and they should obviously be described by a set of 3-dimensional difference equations in Cartesian coordinates. Outside the lab wood fuel usually consists of branches or wood logs. A branch can be thought of as a cylinder as can be a whole wood log, a split wood log can be thought of as a split cylinder. In this light it is obvious to switch to a 3-dimensional set of equations in cylinder coordinates. Generally there is little or no symmetry, since a newly added batch of wood is mostly irradiated from the bottom by glowing charcoal embers while the side and the top are irradiated only by flames. This results in different heat fluxes for different surfaces of the piece of wood.

The equations that do not change when the step to three dimensions is made are the equations for the volume fractions (117), (131) and (132), the Clausius-Clapeyron-Kelvin equation (119), the Arrhenius factor (111) and the energy source term. Of course the single index of a variable corresponding with a 1-dimensional problem should be replaced by three indices corresponding to a 3-dimensional problem eg. replace T_i by T_{ijk}. The equations that have to be adapted to the 3-dimensional case are the thermal conductivity equations (124), (126), the equations for the permeability (127) and (128), the energy equation (86), the set of continuity equations (104) to (107) and the Darcy equation (113). In the next two subsections the 3-dimensional difference equations that are changed are presented. The difference equations are first given in Cartesian coordinates and then in cylinder coordinates. Instead of the continuity equations for all the different gas components a single general equation is presented in this annex with a general source term. Inserting the correct component index and the correct source term results in the correct continuity equation.

Cartesian coordinates

For the general continuity equation the index n will be used, so in three dimensions and for Cartesian coordinates a continuity equation is written as:

$$\frac{\partial}{\partial t}(\epsilon_v \rho_n) + \frac{\partial}{\partial x}(\rho_n V^x) + \frac{\partial}{\partial y}(\rho_n V^y) + \frac{\partial}{\partial z}(\rho_n V^z) = <\dot{\rho}_n>$$

where V^x is the velocity component along the x-direction, V^y is the velocity component in the y-direction and V^z the velocity component in the z-direction. The finite volume method can be used to obtain the difference equation just as was done before for the one-dimensional case in chapter 5. This results in the following difference equation:

$$\frac{1}{\Delta t}[(\epsilon_\gamma \rho_n)_{klm} - (\epsilon_\gamma \rho_n)^0_{klm}] + \frac{1}{2\Delta x}[(\rho_{n,klm} + \rho_{n,k+1lm}) V^x_{klm} - (\rho_{n,klm} + \rho_{n,k-1lm}) V^x_{k-1lm}]$$

$$+ \frac{1}{2\Delta y}[(\rho_{n,klm} + \rho_{n,kl+1m}) V^y_{klm} - (\rho_{n,klm} + \rho_{n,kl-1m}) V^y_{kl-1m}] +$$

$$\frac{1}{2\Delta z}[(\rho_{n,klm} + \rho_{n,klm+1}) V^z_{klm} - (\rho_{n,klm} + \rho_{n,klm-1}) V^z_{klm-1}] = <\dot{\rho}_n>$$

with V^i_{klm} the velocity component in the i-direction and k the index of the control volume along the x-direction, l the index along the y direction and m the index along the z direction. In analogy with chapter 5 V^i_{klm} denotes the velocity V^x at $k\Delta x$ if $i=x$, V^y at $l\Delta y$ if $i=y$ and V^z at $m\Delta z$ if $i=z$. Assuming of course that the coordinates are chosen such that the origin coincides with a corner of the wood block and that all positive axes are each positioned along an edge of the block.

Next the velocity components have to be obtained from the Darcy equation. For a 3-dimensional case the Darcy equation leads to three equations; one for each velocity component and they are given by

$$V^x = -\frac{1}{\mu_r} K^{xx}{}_\gamma \frac{\partial}{\partial x}(\epsilon_\gamma (p_\gamma - p_0))$$

for the x velocity component

$$V^y = -\frac{1}{\mu_r} K^{yy}{}_\gamma \frac{\partial}{\partial y}(\epsilon_\gamma (p_\gamma - p_0))$$

for the y component of the velocity, and

$$V^z = -\frac{1}{\mu_r} K^{zz}{}_\gamma \frac{\partial}{\partial z}(\epsilon_\gamma (p_\gamma - p_0))$$

for the velocity in the z-direction. Introducing indices and interpolating to obtain variable values at boundaries, just as in chapter 5 results in:

$$V^x_{klm} = -\frac{1}{2\Delta x \mu_r}(K^{xx}_{klm} + K^{xx}_{k+1lm})[\epsilon_{\gamma,k+1lm}(p_{\gamma,k+1lm} - p_0) - \epsilon_{\gamma,klm}(p_{\gamma,klm} - p_0)]$$

for the x-component,

$$V^y_{klm} = -\frac{1}{2\Delta y \mu_r}(K^{yy}_{klm} + K^{yy}_{kl+1m})[\epsilon_{\gamma,kl+1m}(p_{\gamma,kl+1m} - p_0) - \epsilon_{\gamma,klm}(p_{\gamma,klm} - p_0)]$$

for the y-component and

$$V^z_{klm} = -\frac{1}{2\Delta z \mu_r}(K^{zz}_{klm} + K^{zz}_{klm+1})[\epsilon_{\gamma,klm+1}(p_{\gamma,klm+1} - p_0) - \epsilon_{\gamma,klm}(p_{\gamma,klm} - p_0)]$$

for the z-component, which completes the velocity equations.

The energy equation can be expressed in three dimensions as:

$$\frac{\partial}{\partial t}(C_p \rho T) + \frac{\partial}{\partial x}(c_{p,\gamma} \rho_\gamma T V^x) + \frac{\partial}{\partial y}(c_{p,\gamma} \rho_\gamma T V^y) + \frac{\partial}{\partial z}(c_{p,\gamma} \rho_\gamma T V^z) + S(T) =$$

$$\frac{\partial}{\partial x}(k^{xx}_{eff} \frac{\partial T}{\partial x}) + \frac{\partial}{\partial y}(k^{yy}_{eff} \frac{\partial T}{\partial y}) + \frac{\partial}{\partial z}(k^{zz}_{eff} \frac{\partial T}{\partial z})$$

which leads to the difference equation:

$$\frac{1}{\Delta t}[(C_p\rho T)_{klm}-(C_p\rho T)^0_{klm}]+\frac{1}{2\Delta x}\{[(c_{p,\gamma}\rho_\gamma T)_{klm}+(c_{p,\gamma}\rho_\gamma T)_{k+1lm}]V^x_{klm}-$$

$$[(c_{p,\gamma}\rho_\gamma T)_{klm}+(c_{p,\gamma}\rho_\gamma T)_{k-1lm}]V^x_{k-1lm}\}+\frac{1}{2\Delta y}\{[(c_{p,\gamma}\rho_\gamma T)_{klm}+(c_{p,\gamma}\rho_\gamma T)_{kl+1m}]V^y_{klm}-$$

$$[(c_{p,\gamma}\rho_\gamma T)_{klm}+(c_{p,\gamma}\rho_\gamma T)_{kl-1m}]V^y_{kl-1m}\}+\frac{1}{2\Delta z}\{[(c_{p,\gamma}\rho_\gamma T)_{klm}+(c_{p,\gamma}\rho_\gamma T)_{klm+1}]V^z_{klm}-$$

$$[(c_{p,\gamma}\rho_\gamma T)_{klm}+(c_{p,\gamma}\rho_\gamma T)_{klm-1}]V^z_{klm-1}\}+S(T)\ =$$

$$\frac{1}{2(\Delta x)^2}\{(k^{xx}_{klm}+k^{xx}_{k+1lm})(T_{k+1lm}-T_{klm})-(k^{xx}_{klm}+k^{xx}_{k-1lm})(T_{klm}-T_{k-1lm})\}+$$

$$\frac{1}{2(\Delta y)^2}\{(k^{yy}_{klm}+k^{yy}_{kl+1m})(T_{kl+1m}-T_{klm})-(k^{yy}_{klm}+k^{yy}_{kl-1m})(T_{klm}-T_{kl-1m})\}+$$

$$\frac{1}{2(\Delta z)^2}\{(k^{zz}_{klm}+k^{zz}_{klm+1})(T_{klm+1}-T_{klm})-(k^{zz}_{klm}+k^{zz}_{klm-1})(T_{klm}-T_{klm-1})\}$$

where the subscript eff was dropped from the thermal conductivity k_{eff} in order to reduce writing.

In the Darcy equation the permeability is used and it should be converted to three dimensions too. The z-axis is chosen along the length of the branch or wood log which is also the grain direction of the wood. This makes the comparisons with cylinder coordinates which are introduced in the next subsection easier. Assume for simplicity that permeability and thermal conductivity in the grain direction are independent of the permeability and thermal conductivity perpendicular to the grain direction. This was used to obtain the Darcy and energy difference equations presented here. Obviously there does exist a link between the two cases since pyrolysis occurs in the solid walls of the channels in the wood and a breakdown in these walls influences permeability and thermal conductivity both along the grain and perpendicular to it at the same time. See also equations (124), (126), (127) and (128) which are used to model permeability and thermal conductivity in different directions. Darcy and energy equations would become very lengthy and rather complicated, so the simple case of

$$K^{xx}_\gamma = K^{yy}_\gamma = K_{\gamma,\perp} \quad \wedge \quad K^{zz}_\gamma = K_{\gamma,\parallel} \quad \wedge \quad K^{ij}_\gamma = 0$$

for the permeability is chosen and

$$k^{xx}_{eff} = k^{yy}_{eff} = k_{min} \quad \wedge \quad k^{zz}_{eff} = k_{max} \quad \wedge \quad k^{ij}_{eff} = 0$$

for the thermal conductivity. In both cases i and j can have the index value x, y or z with $i \neq j$.

Cylinder coordinates

As was done in the previous section the index n is used for the general continuity equation, so in cylinder coordinates a continuity equation can be written as:

$$\frac{\partial}{\partial t}(\epsilon_\gamma\rho_n)+\frac{1}{r}\frac{\partial}{\partial r}(r\rho_n V^r)+\frac{\partial}{\partial\varphi}(\rho_n V^\varphi)+\frac{\partial}{\partial z}(\rho_n V^z) = <\dot{\rho}_n>$$

where r, ϕ and z are the usual cylinder coordinates, V^r is the radial velocity component, V^φ is the tangential velocity component and V^z the velocity component in the z-direction. The finite volume method can be used to obtain the difference equation just as was done before for the 1-dimensional case in chapter 5 and for the 3-dimensional case in the previous section. This results in the following difference equation:

$$\frac{1}{\Delta t}[(\epsilon_\gamma\rho_n)_{klm}-(\epsilon_\gamma\rho_n)^0_{klm}]+\frac{1}{((k+1)^2-k^2)\Delta r}[(k+1)(\rho_{n,klm}+\rho_{n,k+1lm})V^r_{klm}-k(\rho_{n,klm}+\rho_{n,k-1lm})V^r_{k-1lm}]$$

$$+\frac{1}{2\Delta\varphi}[(\rho_{n,klm}+\rho_{n,kl+1m})V^\varphi_{klm}-(\rho_{n,klm}+\rho_{n,kl-1m})V^\varphi_{kl-1m}]+$$

$$\frac{1}{2\Delta z}[(\rho_{n,klm}+\rho_{n,klm+1})V^z_{klm}-(\rho_{n,klm}+\rho_{n,klm-1})V^z_{klm-1}]=<\dot{\rho}_n>$$

with V^i_{klm} the component in the i-direction and k the index of control volume along the r-direction, l the index along the ϕ direction and m the index along the z direction. As in the previous section for Cartesian coordinates in cylinder coordinates V^i_{klm} denotes the velocity V^r at $k\Delta r$ if $i=r$, V^ϕ at $l\Delta\phi$ if $i=\phi$ and V^z at $m\Delta z$ if $i=z$.

For 3-dimensional cylinder coordinates the Darcy equation leads to three equations; one for each velocity component. They are given by

$$V^r=-\frac{1}{\mu_r}K^{rr}_\gamma\frac{\partial}{\partial r}(\epsilon_\gamma(p_\gamma-p_0))$$

for the radial velocity

$$V^\varphi=-\frac{1}{\mu_r}K^{\varphi\varphi}_\gamma\frac{\partial}{\partial\varphi}(\epsilon_\gamma(p_\gamma-p_0))$$

for the tangential velocity, and

$$V^z=-\frac{1}{\mu_r}K^{zz}_\gamma\frac{\partial}{\partial z}(\epsilon_\gamma(p_\gamma-p_0))$$

for the velocity in the z-direction. Introducing indices and interpolating using linear profiles to obtain variable values at boundaries results in:

$$V^r_{klm}=-\frac{1}{2\Delta r\mu_r}(K^{rr}_{klm}+K^{rr}_{k+1lm})[\epsilon_{\gamma,k+1lm}(p_{\gamma,k+1lm}-p_0)-\epsilon_{\gamma,klm}(p_{\gamma,klm}-p_0)]$$

for the r-component,

$$V^\varphi_{klm}=-\frac{1}{2\Delta\varphi\mu_r}(K^{\varphi\varphi}_{klm}+K^{\varphi\varphi}_{kl+1m})[\epsilon_{\gamma,kl+1m}(p_{\gamma,kl+1m}-p_0)-\epsilon_{\gamma,klm}(p_{\gamma,klm}-p_0)]$$

for the ϕ-component and

$$V^z_{klm}=-\frac{1}{2\Delta z\mu_r}(K^{zz}_{klm}+K^{zz}_{klm+1})[\epsilon_{\gamma,klm+1}(p_{\gamma,klm+1}-p_0)-\epsilon_{\gamma,klm}(p_{\gamma,klm}-p_0)]$$

for the z-component.

The energy equation can be expressed in cylinder coordinates as:

$$\frac{\partial}{\partial t}(C_p\rho T)+\frac{1}{r}\frac{\partial}{\partial r}(rc_{p,\gamma}\rho_\gamma TV^r)+\frac{\partial}{\partial\varphi}(c_{p,\gamma}\rho_\gamma TV^\varphi)+\frac{\partial}{\partial z}(c_{p,\gamma}\rho_\gamma TV^z)+S(T)=$$

$$\frac{1}{r}\frac{\partial}{\partial r}(rk^{rr}_{eff}\frac{\partial T}{\partial r})+\frac{1}{r^2}\frac{\partial}{\partial\varphi}(k^{\varphi\varphi}_{eff}\frac{\partial T}{\partial\varphi})+\frac{\partial}{\partial z}(k^{zz}_{eff}\frac{\partial T}{\partial z})$$

which leads to the difference equation:

$$\frac{1}{\Delta t}[(C_p\rho T)_{klm}-(C_p\rho T)^0_{klm}]+\frac{1}{(k^2-(k-1)^2)\Delta r}\{k[(c_{p,\gamma}\rho_\gamma T)_{klm}+(c_{p,\gamma}\rho_\gamma T)_{k+1lm}]V^r_{klm}$$

$$-(k-1)[(c_{p,\gamma}\rho_\gamma T)_{klm}+(c_{p,\gamma}\rho_\gamma T)_{k-1lm}]V^r_{k-1lm}\}+\frac{1}{2\Delta\varphi}\{[(c_{p,\gamma}\rho_\gamma T)_{klm}+(c_{p,\gamma}\rho_\gamma T)_{kl+1m}]V^\varphi_{klm}-$$

$$[(c_{p,\gamma}\rho_\gamma T)_{klm}+(c_{p,\gamma}\rho_\gamma T)_{kl-1m}]V^\varphi_{kl-1m}\}+\frac{1}{2\Delta z}\{[(c_{p,\gamma}\rho_\gamma T)_{klm}+(c_{p,\gamma}\rho_\gamma T)_{klm+1}]V^z_{klm}-$$

$$[(c_{p,\gamma}\rho_\gamma T)_{klm}+(c_{p,\gamma}\rho_\gamma T)_{klm-1}]V^z_{klm-1}\}+S(T)=$$

$$\frac{1}{(k^2-(k-1)^2)(\Delta r)^2}\{k(k^{rr}_{klm}+k^{rr}_{k+1lm})(T_{k+1lm}-T_{klm})-(k-1)(k^{rr}_{klm}+k^{rr}_{k-1lm})(T_{klm}-T_{k-1lm})\}+$$

$$\frac{1}{2(\Delta\varphi)^2}\frac{\ln(\frac{k}{k-1})}{(k^2-(k-1)^2)(\Delta r)^2}\{(k^{\varphi\varphi}_{klm}+k^{\varphi\varphi}_{kl+1m})(T_{kl+1m}-T_{klm})-(k^{\varphi\varphi}_{klm}+k^{\varphi\varphi}_{kl-1m})(T_{klm}-T_{kl-1m})\}+$$

$$\frac{1}{4(\Delta z)^2}\{(k^{zz}_{klm}+k^{zz}_{klm+1})(T_{klm+1}-T_{klm})-(k^{zz}_{klm}+k^{zz}_{klm-1})(T_{klm}-T_{klm-1})\}$$

again the subscript eff was dropped from the thermal conductivity k_{eff} in order to reduce writing.

The permeability and thermal conductivity are used and should be converted to cylindrical coordinates too. To make optimal use of the cylinder coordinates the z-axis has to be chosen along the length direction of the branch or wood log which is also the grain direction of the wood. As in the previous section permeability and thermal conductivity in the grain direction are supposed to be independent of the permeability and thermal conductivity perpendicular to the grain direction. This was used to obtain the Darcy and energy equations presented in this subsection.

$$K^{rr}_\gamma = K^{\varphi\varphi}_\gamma = K_{\gamma,\perp} \quad \wedge \quad K^{zz}_\gamma = K_{\gamma,\parallel} \quad \wedge \quad K^{ij}_\gamma = 0$$

is chosen for the permeability and

$$k^{rr}_{eff} = k^{\varphi\varphi}_{eff} = k_{min} \quad \wedge \quad k^{zz}_{eff} = k_{max} \quad \wedge \quad k^{ij}_{eff} = 0$$

for the thermal conductivity. In both cases i and j can have the index value r, ϕ or z with $i \neq j$. This completes the adaptations needed for the cylindrical case.